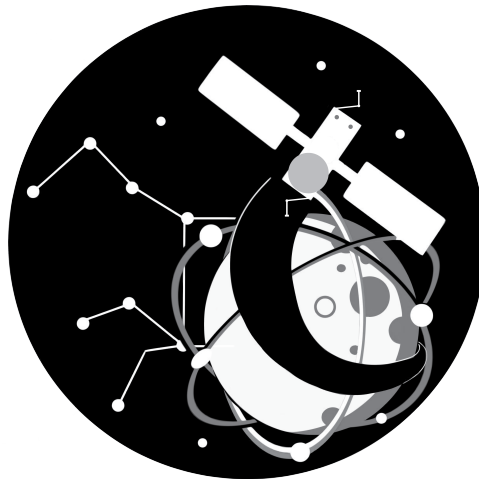


# Technical Report

Project Pegasus Navigation

Demeillers Thomas  
Dowding Nicolas  
Fillol Florian  
Mouchel Roman  
Serna Elsa  
Valentin Baptiste  
Vinière Benoit



Under the supervision of  
Stéphanie LIZY-DESTREZ, Didier ALARY and Vincent GUERMONPREZ

ISAE-SUPAERO  
Toulouse

## Abstract

This paper is a theoretical study about the implementation of a Global Navigation Satellite System around the Moon. The objective of the study is to investigate from the feasibility to the implementation of such a system within the framework of a broader project which aims to see humans activities back on the Moon in the next decade. In that order, the system is complying with technical specifications as defined by a client. The rationale behind the system is that to reach a satisfying level of performance - and therefore meet the client's requirements - a constellation of twenty-one satellites spread out on three orbits around the Moon at a constant semi-major axis of 10,000 [km] is needed. The constellation is named after the Greek divinity Pegasus and in reference to the star constellation. Each orbit is set at an 80 [°] inclination and respectively spaced at 120 [°] from one another with regard to their Right Ascension of Ascending Node. There are seven satellites per orbit. Every Pegasus's satellites carry on-board four atomic clocks, three Emergency Broadcast System antennas, two Tracking, Telecommand and Control antennas and one navigation antenna. Maneuvers for station-keeping and end-of-life are ensured by four 1500 [W] hall effect thrusters mounted on two robotic arms with six degrees of freedom. 150 [kg] of Xenon will be used as propellant so that the mission can be carried out for at least ten years. A Pegasus satellite has a dry mass of 711.04 [kg] and a wet mass of 860.64 [kg]. Regarding the service provided on the lunar surface and its low orbit, the Pegasus constellation guarantees a 100% GNSS and Emergency broadcast availability with a 6.80 [m] global precision at  $3\sigma$  and a 33 [ns] time precision. All the subsystems are powered by a 50 [V] Power Conditioning Unit and 165 [Wh/kg] Li-on battery which will be recharged by 15 [m<sup>2</sup>] of solar panels and used during eclipses. The overall dimensions of one Pegasus spacecraft are 2.34 [m] × 1.480[m] × 1.284[m]. One full orbital plane of the constellation can be launched by one Ariane 64, which guarantees its implementation with only three launches, fulfilling a deployment time span inferior to a year.

## List of symbols - Glossary

Symbol	Meaning	Unit
ACK	Acknowledgement	
AoP	Argument of Perigee	[°]
BER	Bit Error Rate	
BPSK	Binary Phase Shift Keying	
CCR	Corner Cube Reflectors	
COG	Centre of gravity	
COM	Centre of mass	
DSSS	Direct Sequence Spread Spectrum	
e	eccentricity	
EBS	Emergency Broadcast System	
EIRP	Effective Isotropic Radiated	
EoL	End of Life	
E/P	Electrical Power	
FGUU	Frequency Generator and Upconverter Unit	
FSPL	Free Space Path Loss	
FU	Filter Unit	
GDoP	Geometric Dilution of Precision	
GNSS	Global Navigation Satellite System	
GS	Ground Station	
G/T	Gain over Noise Temperature Ratio	
i	inclination	[°]
I	Moment of inertia	[kg.m <sup>2</sup> ]
LELT	Low-Energy Low-Thrust	
LM	Link Margin	
LRR	Laser Retro Reflector	
NS	Navigation System	
NSGU	Navigation Signal Generation Unit	
NFSGUU	Navigation Signal Frequency Generator and Up-conversion Units	
P	Power	W
$m_p$	Propellant mass	[kg]
PCDU	Power Conditioning and Distribution Unit	
PCU	Power Conditioning Unit	
PDoP	Position Dilution of Precision	
PDU	Power Distribution Unit	
P/L	Payload	
PRN	Pseudo-Random Noise	
PPU	Power Processing Unit	
RAAN	Right Ascension of the Ascending Node	[°]
RF	Radio Frequency	
$\alpha$	Rotation acceleration	[rad/s <sup>2</sup> ]
$\theta$	Rotation angle	[rad]
$\omega$	Rotation speed	[rad/s]

SADM	Solar Array Drive Mechanism	
$P_{SP}$	Solar radiation pressure	[Pa]
SAFS	Space Atomic Frequency Standards	
SAR	Search and Rescue	
S/C	Spacecraft	
SLR	Satellite Laser Ranging	
SMA	Semi-Major Axis	[m]
SMS	Short Message Service	
SNR	Signal over Noise Ratio	
SSPA	Solid State Power Amplifier	
$\Delta V$	Spacecraft speed change	[m/s]
$I_{sp}$	Specific impulse	[s]
T	Torque	[N.m]
T <sup>o</sup>	Temperature	[°C]
T/C	Thermal Control	
TWTA	Travelling Tube Amplifier	
UERE	User Equivalent Range Error	[m]

# Contents

<b>1</b>	<b>Introduction</b>	<b>1</b>
<b>2</b>	<b>Mission and Environment Analysis</b>	<b>3</b>
2.1	Introduction . . . . .	3
2.2	Lunar Orbit Design and Analysis . . . . .	4
2.2.1	Methodology . . . . .	4
2.2.2	Constellation Performance . . . . .	5
2.2.3	Orbit Stability . . . . .	7
2.2.4	Quality . . . . .	11
2.2.5	Synthesis . . . . .	12
2.3	Trajectories Analysis . . . . .	14
2.3.1	Low-Energy Low-Thrust Deployment . . . . .	14
2.3.2	End of Life . . . . .	14
2.4	Environment Analysis . . . . .	15
2.4.1	Thermal Fluxes . . . . .	15
2.4.2	Eclipses . . . . .	17
2.4.3	Radiation Environment . . . . .	18
2.4.4	Disturbing Torques . . . . .	21
<b>3</b>	<b>Payload</b>	<b>22</b>
3.1	Navigation System . . . . .	23
3.1.1	Introduction . . . . .	23
3.1.2	NS Service Level . . . . .	23
3.1.3	On-Board Atomic Clocks . . . . .	28
3.1.4	Ephemeris and Clock Corrections . . . . .	31
3.1.5	Navigation Signals . . . . .	32
3.1.6	NS Antenna . . . . .	35
3.2	Emergency Broadcast System . . . . .	41
3.2.1	Introduction . . . . .	41
3.2.2	EBS Signals . . . . .	41
3.2.3	EBS Antennas . . . . .	44
3.2.4	Portable EBS User Specifications . . . . .	52
3.3	Payload Synthesis . . . . .	53
<b>4</b>	<b>Platform</b>	<b>54</b>
4.1	Telemetry, Tracking and Command . . . . .	55
4.1.1	Link Budget . . . . .	55
4.1.2	Required Transmitting Power Simulation . . . . .	58
4.1.3	TTC Equipment . . . . .	59
4.2	Propulsion . . . . .	60

4.2.1	Introduction . . . . .	60
4.2.2	Propulsion system choice . . . . .	60
4.2.3	Xenon mass estimation . . . . .	61
4.2.4	Electrical Propulsion System . . . . .	65
4.3	Attitude and Orbit Control System . . . . .	69
4.3.1	Introduction . . . . .	69
4.3.2	AOCS Modes . . . . .	70
4.3.3	Yaw Steering Law . . . . .	71
4.3.4	Reaction wheel desaturation: solar sailing . . . . .	72
4.3.5	AOCS Equipment . . . . .	73
4.4	Electrical Power . . . . .	76
4.4.1	Introduction . . . . .	76
4.4.2	Power Budget . . . . .	76
4.4.3	Architecture Definition . . . . .	78
4.4.4	Electrical Power Equipment . . . . .	80
4.4.5	Battery Sizing . . . . .	81
4.4.6	Solar Arrays Sizing . . . . .	83
4.4.7	Synthesis . . . . .	86
4.5	On-Board Data Handling and Software . . . . .	87
4.5.1	Introduction . . . . .	87
4.5.2	OBDH Equipment & Tasks . . . . .	87
4.5.3	Global Redundancy . . . . .	90
4.5.4	Modes Transitions . . . . .	92
4.6	Thermal Control . . . . .	93
4.6.1	Introduction . . . . .	93
4.6.2	Equipment Temperature Ranges . . . . .	93
4.6.3	Yaw Law and Incoming Heat Fluxes Simulation . . . . .	94
4.6.4	Thermal Budget . . . . .	96
4.6.5	First model: global study . . . . .	97
4.6.6	Second model: local study . . . . .	98
4.6.7	Synthesis . . . . .	104
4.7	Structure . . . . .	107
4.7.1	Introduction . . . . .	107
4.7.2	Satellite Platform . . . . .	107
4.7.3	Mass budget . . . . .	110
4.7.4	Satellite Design . . . . .	110
<b>5</b>	<b>Conclusion</b>	<b>115</b>
<b>A</b>	<b>Appendix</b>	<b>117</b>
A.1	Navigation data sheets . . . . .	117
A.2	SMS data sheets . . . . .	119
A.3	TTC data sheets . . . . .	123
A.4	Propulsion data sheets . . . . .	125
A.5	AOCS data sheets . . . . .	127
A.6	Power subsystem data sheets . . . . .	131
A.7	Thermal data sheets . . . . .	135
A.8	OBDH data sheets . . . . .	136
A.9	Structure data sheets . . . . .	137

# List of Figures

2.1	Tools used to propagate and visualize orbits . . . . .	4
2.2	Global GDoP obtained for each configuration. . . . .	6
2.3	Position error obtained @ $3\sigma$ at the lunar base for each configuration. . . . .	6
2.4	Observation of the orbit stability over a period of 20 days. . . . .	7
2.5	Effects of the SMA and the inclination on the relative standard deviations (normalized) of the different osculating Keplerian elements . . . . .	9
2.6	Stability indicator for the different configurations. . . . .	10
2.7	Quality indicator of the different configurations and selected orbit in red circle. . . . .	11
2.8	Formation configuration of the Pegasus constellation. . . . .	13
2.9	Visualization of the Pegasus constellation. . . . .	13
2.10	LELT solution from LEO to reach elliptic lunar orbit [2]. . . . .	14
2.11	Direct fluxes on the six spacecraft sides. . . . .	16
2.12	Worst-case eclipses. . . . .	17
2.13	Solar particles fluences. . . . .	19
2.14	Cosmic rays fluxes . . . . .	20
3.1	Tetrahedron volume example . . . . .	23
3.2	Pegasus GNSS performance on lunar surface at $10^\circ$ minimum elevation. . . . .	26
3.3	Pegasus GNSS performance on LLO ( $22^\circ$ aperture beam) . . . . .	26
3.4	Pegasus GNSS performance on lunar surface $22^\circ$ aperture beam. . . . .	27
3.5	Constellation performance with 20 satellites. . . . .	27
3.6	A comparison of standard space atomic clock technologies and the Hg Ion Clock. . . . .	28
3.7	Space atomic clock standards sent into orbit. [4] . . . . .	29
3.8	Clock equipment . . . . .	30
3.9	Satellite Laser Ranging equipment. . . . .	31
3.10	Navigation data modulated by the PRN code and carrier. . . . .	32
3.11	Super-frame structure. [11] . . . . .	34
3.12	BER in function of SNR for DSSS. [11] . . . . .	35
3.13	Galileo group delay variation over the coverage in high band. [12]. . . . .	37
3.14	Galileo phase dispersion optimizing BFN amplitude excitation. [12]. . . . .	38
3.15	Gain radiation patterns in high band: for a carrier frequency of 1575 MHz. [12] . . . . .	38
3.16	Galileo navigation antenna NAVANT [13] . . . . .	39
3.17	NSFGUU module photos. [14] . . . . .	40
3.18	EBS Down-link Solid State Power Amplifier. . . . .	40
3.19	Chronological operation for the Emergency Broadcast System. . . . .	42
3.20	EBS eclipse availability. . . . .	44
3.21	BPSK BER abacus [16] . . . . .	45
3.22	EBS Anywaves antenna . . . . .	47
3.23	Emergency Broadcast Anywaves Down-link . . . . .	47
3.24	EBS up-link Helix antenna photos of deployment. [18] . . . . .	51

3.25	Kongsberg Search And Rescue Transponder used for the EBS. [14]	51
3.26	Example of a Galileo SAR beacon	52
3.27	Synthesis of the carrier frequencies used by Pegasus antennas.	53
4.1	Screenshot of Pegasus constellation simulated.	58
4.2	Required transmitting power simulated.	58
4.3	Transceiver Honeywell chosen for TTC Link.	59
4.4	End of life simulation to estimate $m_p$ .	62
4.5	Keplerian parameters drift over 200 days.	62
4.6	Station-keeping simulation over 10 years.	63
4.7	Flow regulation loop of the electrical propulsion system.	65
4.8	PPS 1350-G thruster [19].	66
4.9	Eutelsat-172B robotic arm [20].	66
4.10	XPRF System. [21]	67
4.11	Xenon density variation depending on P and $T^\circ$	67
4.12	ETS VIII xenon tank.	68
4.13	Equipment of the power system.	68
4.14	Satellite Axis convention.	69
4.15	Representation of the yaw steering law [26].	71
4.16	Desaturation around the Z axis	73
4.17	Desaturation around the X axis	73
4.18	NFSS-411 Sun Sensor [28].	74
4.19	AA-STR Star tracker [29].	74
4.20	Actuators.	75
4.21	Schematic of the power subsystem.	78
4.22	SAFT VES180 battery cell [33].	80
4.23	Chosen PCU and solar cells.	80
4.24	Design of the battery.	82
4.25	Equivalent Fluxes versus depth in the Azur 3G30 solar cell simulation.	83
4.26	Design of the solar array.	86
4.27	OBDH top level diagram.	88
4.28	Modes switching diagram.	92
4.29	Thermal fluxes on the six surfaces (with yaw steering law).	95
4.30	Temperature evolution of the spacecraft over one year.	97
4.31	Thermal model of the clocks.	100
4.32	Nodal representation of the local thermal model.	101
4.33	System of louvers used to reduce the heat rejection during eclipses [38]	105
4.34	Several heat pipes profile.	105
4.35	A conventional frame type structure – Science and Technology Satellite II, [40]	107
4.36	Material chosen for the monocoque structure configuration of Pegasus' satellites.	108
4.37	Evolution of Aluminium coating's thickness with received dose	109
4.38	Perspective CAD view of a Pegasus spacecraft.	111
4.39	External Pegasus configurations.	111
4.40	In orbit configuration, of a Pegasus satellite.	111
4.41	Inside configuration of a Pegasus satellite.	112
4.42	Final dimension of a Pegasus satellite in mm.	113
4.43	Configuration of a one of the three launch of the Pegasus constellation.	114



# List of Tables

2.1	Availability obtained for each configuration. . . . .	5
2.2	Reference constellation orbital and technical parameters. . . . .	12
2.3	Order of magnitude of disturbing torques in Pegasus orbit. . . . .	21
3.1	Synthesis of the navigation units. . . . .	23
3.2	State of the art of GNSS atomic clocks. . . . .	29
3.3	Data size of the navigation message. . . . .	33
3.4	Navigation signal baseline data. . . . .	36
3.5	Navigation signal calculated data. . . . .	36
3.6	Power budget with depointing using a patch model . . . . .	37
3.7	Galileo model antenna satellite data . . . . .	39
3.8	Power Budget computed with Galileo Antenna Model Navigation Signal . . . . .	39
3.9	Synthesis of the emergency broadcast units. . . . .	41
3.10	Emergency Broadcast Signal Down-link Baseline Data . . . . .	45
3.11	Emergency Broadcast Signal Down-link Calculated Data . . . . .	46
3.12	Emergency Broadcast Down-link Power Budget with Depointing . . . . .	46
3.13	Emergency Broadcast signal up-link baseline data . . . . .	48
3.14	Emergency Broadcast signal up-link calculated data . . . . .	49
3.15	Emergency Broadcast signal up-link parabolic and helical antennas calculated data . . . . .	49
3.16	Emergency Broadcast signal up-link multi helical antenna calculated data . . . . .	50
3.17	Emergency Broadcast signal up-link emitter power budget comparison . . . . .	50
3.18	Synthesis of the payload units. . . . .	53
3.19	Synthesis of the payload performance (lunar surface, errors @ $3\sigma$ ). . . . .	53
4.1	TTC down-link baseline data. . . . .	56
4.2	Navigation Signal calculated data. . . . .	57
4.3	TTC down-link power budget with pointing error. . . . .	57
4.4	TTC Up-link power budget with pointing error. . . . .	57
4.5	Synthesis of the TTC units. . . . .	59
4.6	Xenon mass estimation for nominal tasks. . . . .	61
4.7	Synthesis of propulsion units. . . . .	65
4.8	AOCS modes description . . . . .	70
4.9	Synthesis of the AOCS units . . . . .	74
4.10	Spacecraft modes and their subsystem configuration. . . . .	76
4.11	Power consumption in <i>Orbit Correction Mode</i> . . . . .	77
4.12	Power consumption in <i>Eclipse Mode</i> . . . . .	77
4.13	Voltage properties of the battery. . . . .	81
4.14	Main properties of the designed battery. . . . .	82
4.15	Main properties of the designed solar panel. . . . .	85
4.16	Synthesis of electrical power units. . . . .	86

4.17	Synthesis of the OBDH units. . . . .	87
4.18	Temperature tolerances of the main equipment of the satellite (operating conditions)	93
4.19	Components of the thermal budget equation. . . . .	96
4.20	Synthesis of the design yielded by the global model. . . . .	98
4.21	Synthesis of the design yielded by the nodal model. . . . .	103
4.22	Calculated temperature ranges for each node . . . . .	103
4.23	Synthesis of the optical properties of the radiative surfaces. . . . .	106
4.24	Summary of the thermal covering areas in $[m^2]$ for the satellite external faces. . .	106
4.25	Properties of the Thermal subsystem. . . . .	106
4.26	Satellite Mass Budget. . . . .	110

# Chapter 1

## Introduction

Being the closest celestial body to Earth, the Moon is a natural place to study and consider the feasibility of extraterrestrial human activities. Recently, there has been renewed enthusiasm in the exploration of the Moon and Mars. The public is more and more interested in space exploration thanks to the new achievements accomplished by the companies and start-ups disrupting the space market. Moreover, space agencies like ESA or NASA are showing a growing interest on new ideas to have a permanent and sustainable presence on the Moon on the prospect to make it a hub for future Mars missions. It is in that regard that ISAE Supaero and Airbus Defense & Space entrusted the 2021 Advanced Master TAS ASTRO class to investigate the feasibility of a long-term Moon Exploration program.

This expedition, called Omega, shall feature six distinct services performed by three satellite constellations, namely Telecommunication, Moon Observation, Global Navigation, and three on-ground operations involving an in-situ Human Base, Rover Capacity and a LLO Shuttle Service. The subject of this paper is the Technical Preliminary Design of the Global Navigation Satellite System "Pegasus" around the Moon.

Pegasus GNSS objective is to broadcast a Navigation Message throughout the Moon surface and LLO. To do so, each S/C requires its own ephemeris provided by tracking ground facilities on Earth and an on board atomic clock. Subsequently the constellation provides the receiver its position and time reference.

Furthermore, Pegasus will supply an Emergency Broadcast Service by taking advantage of the full coverage provided by the GNSS requirements. It is possible to receive and transmit a message through an additional emergency telecommunication link that could supplement the adjacent Telecommunication Mission.

This study will not cover deeply the launch and transfer orbit towards the Moon since these were deemed out of scope. This report will not be focusing on developing software or hardware solutions for the user. The control of the spacecraft and the positioning algorithm for GNSS and time signals will not be studied in this project.

Setting up a constellation around the Moon poses new challenges that have never been met before. The objective of this report is to address the different technical challenges about implementing a GNSS constellation around the Moon. More precisely, this study will focus on the constellation and its S/C's architecture.



This report is going to be segmented into three major sections. The first consideration will be focus on the *Mission and Environment Analysis* of the project where the structure of the Pegasus constellation will be determined, and the environment in which the S/Cs are going to evolve is defined. Secondly, the focus will be on the Payload definition where both the Navigation System and Emergency Broadcast System will be established, and their user service level discussed. Finally, the focus will be put on the Platform of the satellite, in which all the subsystems necessary to the spacecraft survival and functioning will be characterized.

## Chapter 2

# Mission and Environment Analysis

### 2.1 Introduction

The objective of the mission analysis part is to define the structure of the GNSS constellation, that is to say the number and characteristics of the orbital planes as well as the number of satellites per plane. The method for the orbit choice is explained in the next section *Lunar Orbit Design and Analysis*. The system requirements set up for the constellation on the lunar surface and on LLO are:

- At least 4 satellites shall be visible at all time from all points.
- Availability shall be  $\geq 0.95$ .
- Position error @ $3\sigma$  shall be  $\leq 16$  [m] in the worst case<sup>1</sup>, should be as smaller as possible.
- Time error @ $3\sigma$  shall be  $\leq 100$  [ $\mu$ s].

At the same time, it has to be considered to minimize:

- Number of satellites in orbit, to limit the system cost.
- $\Delta V$  used for station-keeping by picking the most stable orbit possible.

The deployment and End of Life (EoL) phases have also been discussed in this section. The output is used in section *Propulsion* 4.2 to estimate the propellant needed for these phases. The system requirements set up for the deployment phase and the EoL are:

- The deployment shall be done is less than one year.
- The strategy of the EoL shall be selected in order to limit lunar orbit debris.

In the last part, the environment of the selected constellation is further analyzed. Thermal fluxes, radiation environment, and disturbing torques are successively studied.

---

<sup>1</sup>The initial client requirement of 1m has been adjusted as it cannot be achieved without Augmented GNSS, see deliverable *System Engineering Report*

## 2.2 Lunar Orbit Design and Analysis

### 2.2.1 Methodology

Two main constraints drive the choice of the constellation. The first one is the quality of the positioning service. The second one is the stability of the orbits, which imposes the amount of  $\Delta V$  required for the station-keeping.

Different constellation configurations have been propagated with the General Mission Analysis Tool (GMAT): circular orbits with SMA values from 9000 [km] to 15000 [km] and  $i$  from 30 [°] to 90 [°] have been tested. At first, the position and attitude ephemeris data from GMAT have been exported and modified by a MATLAB program to be readable by the VTS software. The latter has been used to visualize the constellation and the visibility of each satellite (qualitative analysis). In a second step, a self-developed MATLAB program was used to evaluate, for each point of the Moon surface, the number of visible satellites and the quality of the positioning (quantitative analysis). One output example of this algorithm can be seen on figure 3.4 in section *Payload 3*. The software *Freeflyer* has also been used to propagate orbits, in particular for station keeping and the TM/TC studies.

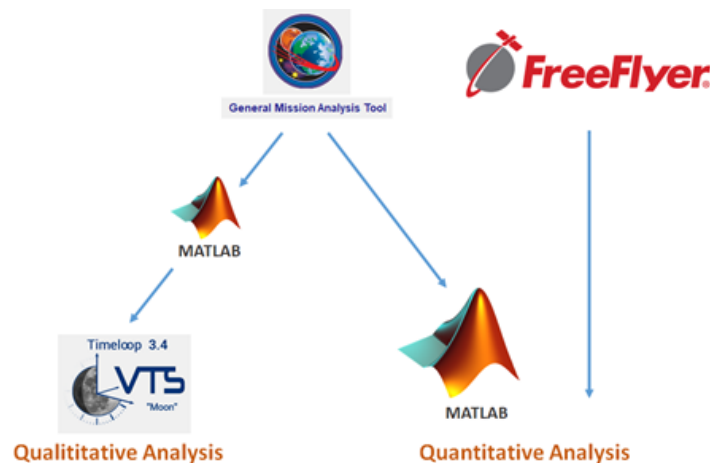


Figure 2.1: Tools used to propagate and visualize orbits

After preliminary studies with this method, it has been decided to use 21 satellites for the constellation, the section is more deeply focused on the SMA and inclination choice. The best GNSS performance was obtained with:

- 3 circular planes system (also facilitating the deployment).
- 7 satellites per plane (limiting the system cost, since adding more satellites does not improve significantly the positioning quality).

In order to make a constellation choice, four criteria have been taken into account to calculate a quality value for each configuration (Section 2.2.4): the availability, the GDoP, the lunar base position error, and the orbit stability. These criteria are quantified by means of indicators ranging from 0 to 1, 1 being excellent. Also, each of them has been assigned a certain weight, depending on the importance.

## 2.2.2 Constellation Performance

The quality of the positioning service is depending on 3 criteria:

- GDoP, linked to the tetrahedron volume formed by the 4 best satellites visible to the receiver. For this first study, it has been supposed that a satellite is visible for an elevation angle above 10 [°] to take in consideration the lunar relief such as craters.
- Availability of the service (the system is considered available if  $GDoP \leq 6$ ).
- Position error, which depends on the UERE and PDoP.

More details on these parameters can be found in the section *Navigation System 3.1.2*. Finally, the performance quality is defined by:

$$\begin{aligned}
 Q_{performance} &= 0.5 \times Q_{availability} + 0.5 \times Q_{accuracy} \\
 Q_{performance} &= 0.5 \times Q_{availability} + 0.5 \times (0.4 \times Q_{GDoP} + 0.6 \times Q_{error}) \\
 Q_{performance} &= 0.5 \times Q_{availability} + 0.2 \times Q_{GDoP} + 0.3 \times Q_{error}
 \end{aligned} \tag{2.1}$$

**Availability** The requirement imposed on the availability is  $\geq 0.95$  as a minimum during the mission, worst-case conditions. To have a small margin in case of a performance loss during the mission, a minimum availability value of  $\geq 0.96$  is chosen. As it can be seen on the table 2.1, most of the configuration with a SMA below 10000 [km] can be removed from the choice, as well as  $i \leq 30$  [°]. The higher the altitude, the better the availability and the availability quality of the configuration since it is defined as:  $Q_{availability} = \frac{Availability}{max(Availability)}$ .

Inclination[°]	SMA [km]							
	8000	9000	10000	11000	12000	13000	14000	15000
30	0.774	0.834	0.877	0.905	0.925	0.940	0.950	0.957
40	0.909	0.935	0.951	0.960	0.968	0.975	0.979	0.983
50	0.937	0.956	0.968	0.972	0.976	0.980	0.983	0.986
60	0.941	0.960	0.971	0.977	0.981	0.984	0.987	0.990
70	0.947	0.956	0.967	0.974	0.980	0.984	0.988	0.991
80	0.929	0.952	0.966	0.975	0.981	0.986	0.990	0.992
90	0.935	0.954	0.967	0.975	0.978	0.986	0.990	0.992

Table 2.1: Availability obtained for each configuration.

**Global GDoP** The requirement imposed on the GDoP is an average  $\leq 4$  during the whole mission, worst-case conditions. As it can be seen on the figure 2.1, an inclination below 50[°] does not seem to provide good enough performance and can be removed. The higher the altitude, the better is the GDoP and the GDoP quality of the configuration:  $Q_{GDoP} = 1 - \frac{GDoP}{max(GDoP)}$ .

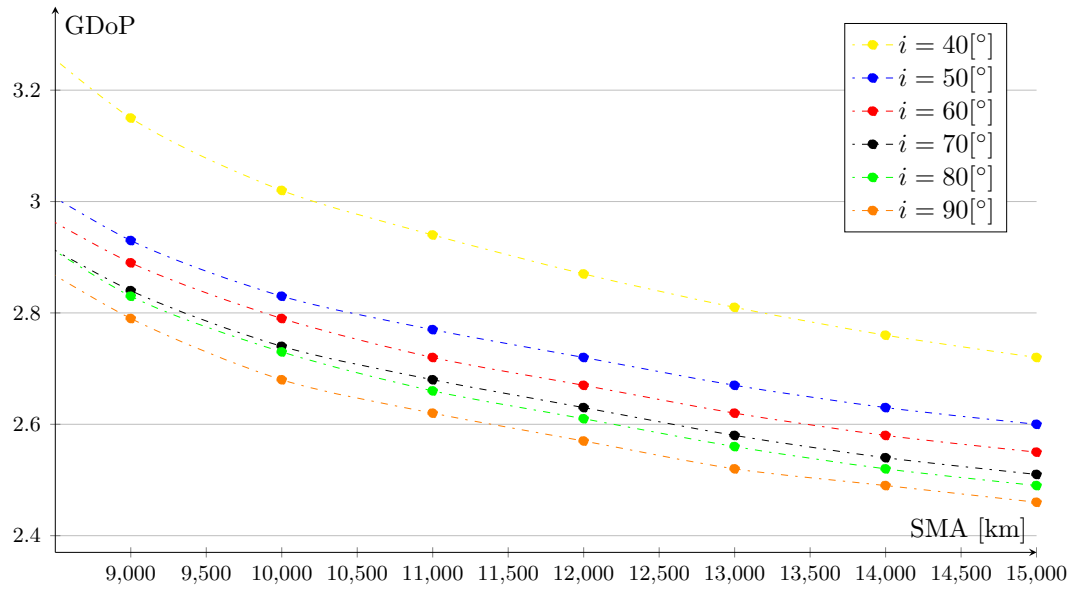


Figure 2.2: Global GDoP obtained for each configuration.

**Lunar Base Position Error** Specific pole's performance has been studied as well. The lunar base outpost previewed location is close to Schackleton crater, on the South pole. It is necessary to provide better performance on this location as most of the users will be there initially. This criterion is then chosen to add a lunar pole performance weigh on the performance. As it can be seen in the figure 2.3,  $i = 80^\circ$  seems to be the minimum value to get the best performance at the poles no matter the SMA. The higher the inclination, the lower is the error position and the error quality of the configuration  $Q_{error} = 1 - \frac{error}{max(error)}$ .

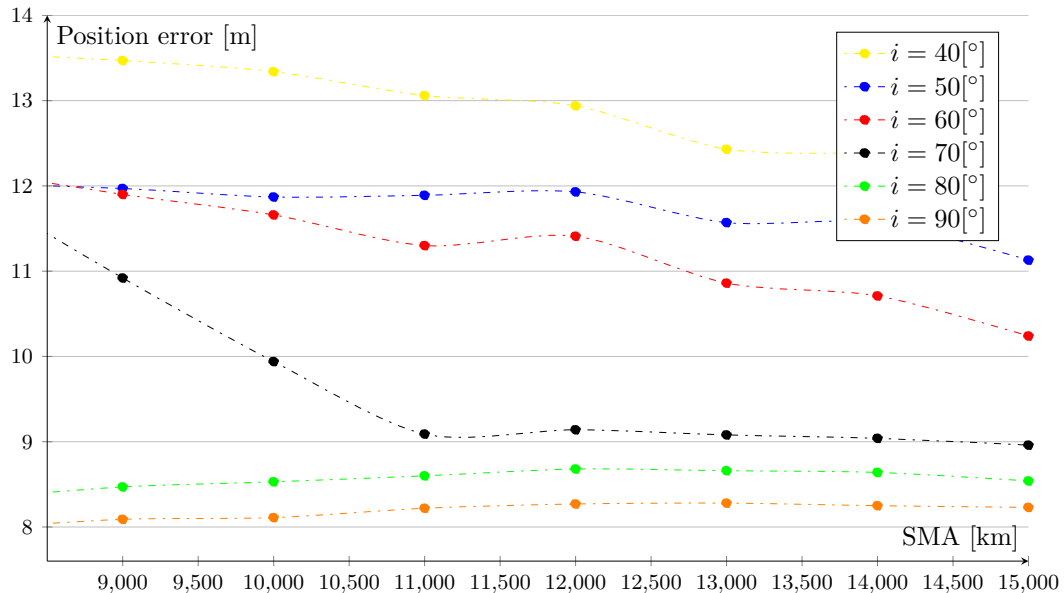


Figure 2.3: Position error obtained @3σ at the lunar base for each configuration.



### 2.2.3 Orbit Stability

Due to the influence of the Sun and the Earth (main perturbation for altitudes above 6000[km]) and mass concentrations under the Moon surface that induce a variable gravity field, most of the lunar orbits are unstable. The difficulty is to identify which orbits can be suitable for a GNSS application by remaining the most stable possible during the mission, to limit the  $\Delta V$  required for station-keeping.

#### Observation

Some lunar orbits called "frozen orbits" are characterized by good stability. In order to know if a given orbit is effectively a frozen orbit (or at least more stable than the majority of the other orbits), one can study the variations of the osculating Keplerian elements of the satellite over the time. Indeed, a higher stability will induce fewer variations of the Keplerian elements. Plotting combination of Keplerian parameters, as for example the polar plot of the eccentricity versus the Argument of Perigee is an interesting way to identify drifts of the orbit. As illustrated in the figure 2.4 obtained after propagating different orbits with *GMAT*, whereas stable orbits remain in the same location of the polar plot (blue and red crosses), less stable orbits move in different areas of the plot (black crosses). However, this methodology based only on observations is not adapted when the number of configurations to test is high (which is the case here with more than 50 different configurations to test).

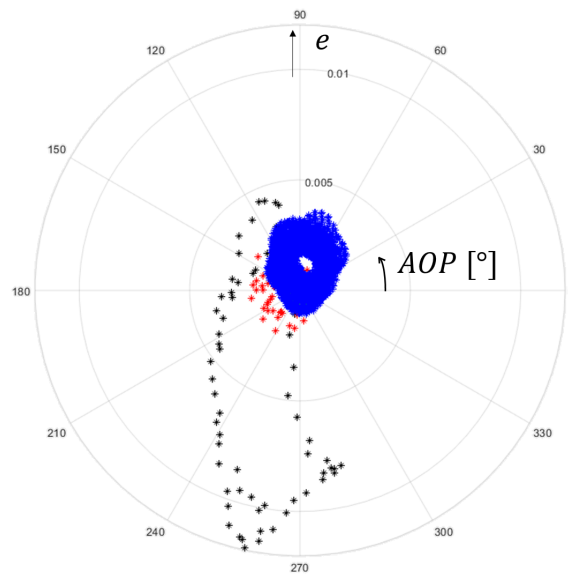


Figure 2.4: Observation of the orbit stability over a period of 20 days.

## Quantification

An easy way to quantify the stability of a particular orbit is to compute the relative standard deviations of the following Keplerian elements: (a, e, i, AoP, RAAN). Indeed, drifts or oscillations with large amplitudes of these parameters increase the standard deviations. As stable orbits are characterized by limited variations of the Keplerian elements, they are logically associated with small standard deviations.

The definition of the relative standard deviation noted  $RSD_i$  is recalled below,  $x_i$  being the Keplerian Element studied,  $\mu$  the average of  $x_i$  over the time and  $N$  the number of time steps (the time is considered as discretized).

$$\sigma_{x_i} = \sqrt{\frac{1}{N} \sum_{n=1}^N (x_i(n) - \mu)^2} \quad (2.2)$$

$$RSD_i = \frac{\sigma_{x_i}}{\mu}$$

The different constellations evaluated regarding the quality of the positioning service (Section 2.2.2) are now assessed regarding the stability of their orbital planes. As the constellations with an inclination of  $30^\circ$  and the ones with a SMA lower than  $9000 [km]$  have been discarded in the performance analysis, only inclinations between  $40^\circ$  and  $90^\circ$  and SMA between  $9000 [km]$  and  $15000 [km]$  are tested here. A total of 42 configurations are therefore studied here.

Each orbit is propagated with the software *GMAT* during 120 days and the relative standard deviation of each osculating Keplerian element is calculated. It is noted that the propagation model takes into consideration the main sources of disturbance (effect of the Sun and the Earth, irregular gravity field of the Moon, solar radiation pressure). The results obtained are shown in the figure 2.5 (the relative standard deviations have been normalized during the process). The following observations are made:

- Increasing the altitude increases the standard deviations of all Keplerian elements. This is explained by the fact that at this altitude, the main perturbation is the effect of the Sun and the Earth. Increasing the altitude increases therefore the perturbation of the Earth and thus the dispersion of the Keplerian elements.
- Increasing the inclination has antagonist effects depending on the Keplerian element considered: increasing the inclination reduces the standard deviations of i, RAAN, and SMA. On the other hand, increasing i leads to an increase in the dispersion of the eccentricity. To explain the reason for these effects, the way the Earth attracts the satellite must be analyzed in order to understand what are the perturbed accelerations induced on the satellite. This study is out of scope.

This first analysis shows that it is difficult to assess the orbit stability by using all standard deviations. Therefore, it is decided to create a unique indicator of the stability, noted  $Q_{stab}$ , based on a Weighted Sum Model (WSM) used in the decision theory. The relative standard deviation of the Keplerian element  $x_i$  calculated for one specific constellation is noted  $RSD_{i,c}$ ,  $i$  being the index of the Keplerian element and  $c$  the index of the constellation ( $1 \leq i \leq 5$ ,  $1 \leq c \leq 42$ ).

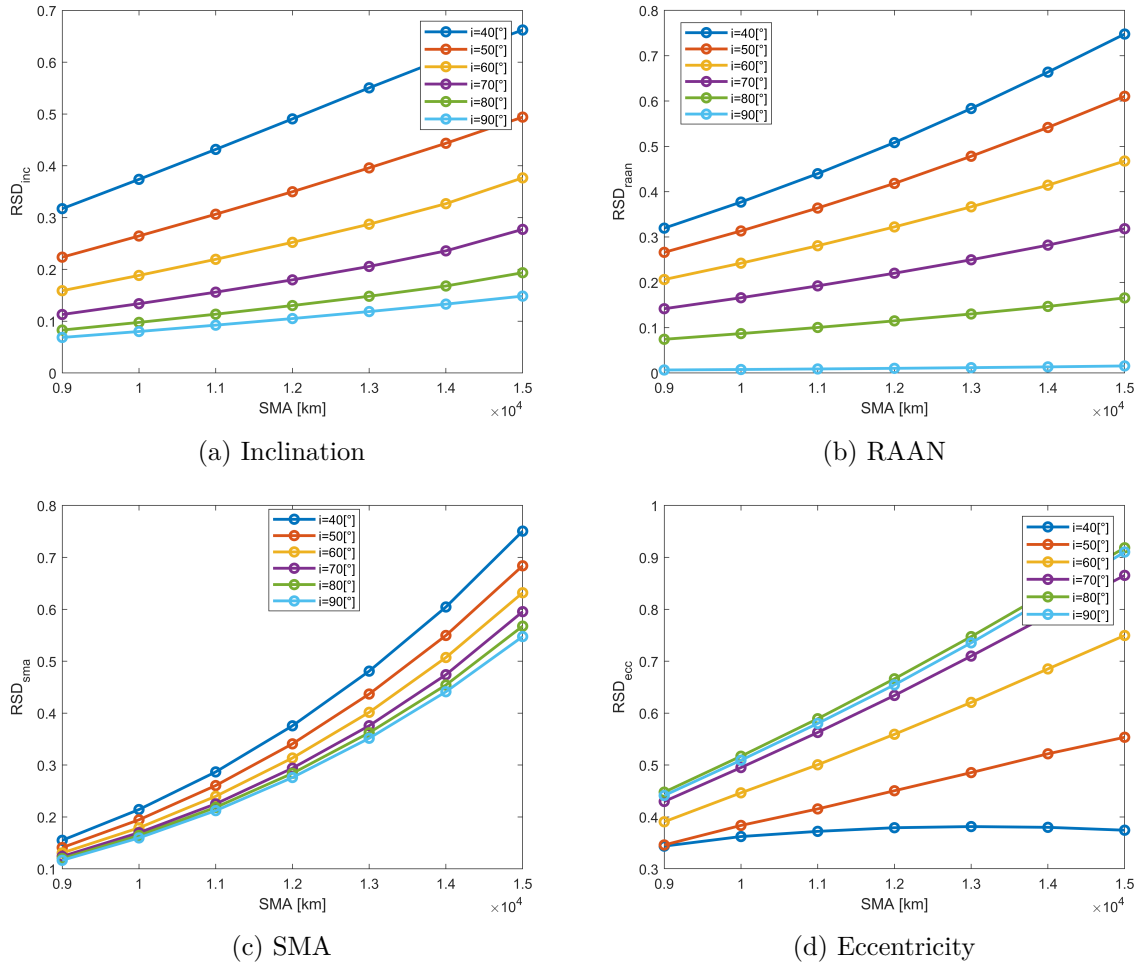


Figure 2.5: Effects of the SMA and the inclination on the relative standard deviations (normalized) of the different osculating Keplerian elements

The stability indicator of the constellation  $c$  is given by the following formula:

$$Q_{stab_c} = 1 - \left( \frac{1}{\sum_{i=1}^5 \alpha_i} \cdot \sum_{i=1}^5 \alpha_i \cdot \frac{RSD_{i,c}}{\max_c RSD_{i,c}} \right) \quad (2.3)$$

The final indicators are then normalized to obtain indicators between 0 and 1, 1 meaning that the constellation is the most stable among all configurations tested.

The weights  $\alpha_i$  are chosen according to the constraints of the maneuvers necessary to correct the drift of the corresponding Keplerian element: since that out-of-the plane maneuvers are way more expensive than in-the-plane maneuvers, a weight equal to 5 is used for the inclination and a weight equal to 2 is used for both the eccentricity and the semi-major axis. Since it is expected that the eccentricity remains low, the variation of the argument of perigee is not a problem, a weight equal to 1 is chosen. As explained later in this report (Section 4.2.3), the

RAAN variations will not be corrected and therefore will not participate in the  $\Delta V$  required for the maneuvers. Consequently, a weight equal to 0 is given to the RAAN.

The final stability indicators obtained for all constellations are presented in figure 2.6. As more weights are given to the inclination, and due to the fact that higher inclinations reduce the variations of inclination, it is logical that constellations with higher inclinations have a better stability indicator. Moreover, the negative effects of altitude on global stability are clearly noticeable.

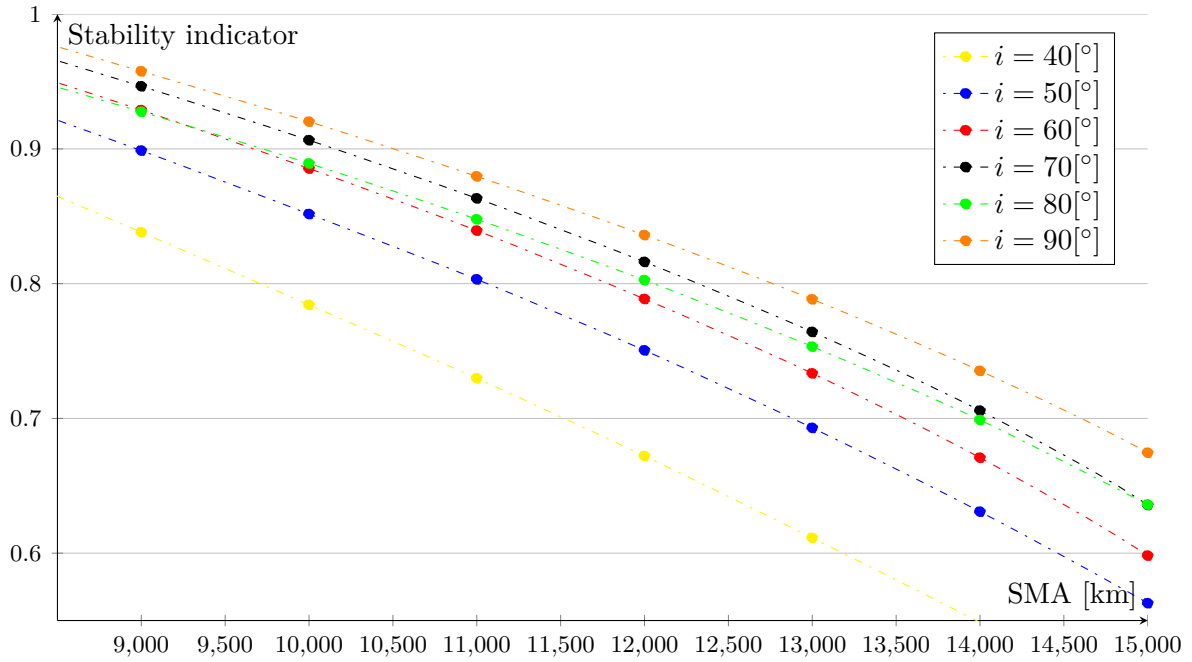


Figure 2.6: Stability indicator for the different configurations.

### 2.2.4 Quality

The choice of the final orbit is made according to the performance and stability, a quality value  $Q_{tot}$  is calculated for each of them:

$$Q_{tot} = 0.7 \times Q_{perfo} + 0.3 \times Q_{stab}$$

More weight is put on the performance than the stability. Indeed, the project requirements are mainly related to the performance of the service offered by the constellation. The stability will have an effect on the technical aspects (and especially on the station-keeping strategy) but is considered as less important than the performance. The result is presented on the figure 2.7, the best inclination option is clearly either  $i = 80 [^\circ]$  or  $i = 90 [^\circ]$ . To avoid to have collisions maneuvers issues at the poles  $i = 90 [^\circ]$  orbits are removed from the choice. At last,  $SMA = 10000[\text{km}]$  is picked instead of  $SMA = 9000[\text{km}]$  as it reduces almost of  $0.7 [\text{m}]$  the global error position, while keeping an acceptable stability indicator. The quality of the chosen constellation is  $Q_{tot} = 0.973$ .

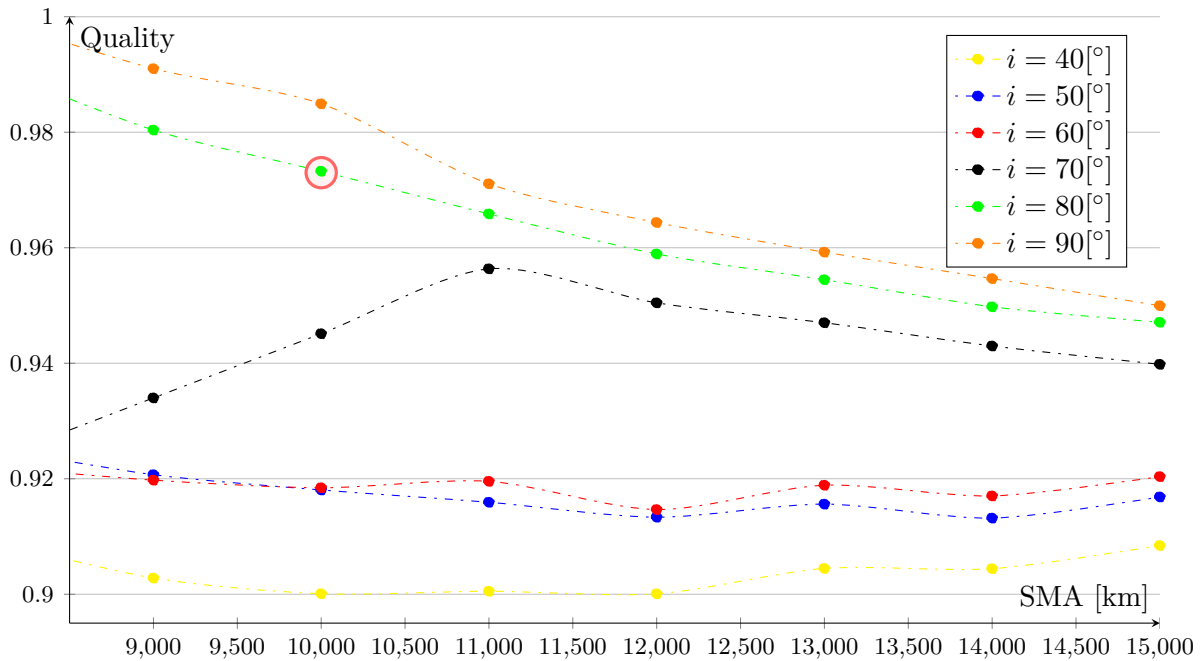


Figure 2.7: Quality indicator of the different configurations and selected orbit in red circle.

### 2.2.5 Synthesis

The final choice made is 3 orbital planes consisting of 7 satellites each. The planes, at the beginning of the operations, are characterized by the following orbital parameters:

- $a = 10\,000[\text{km}]$
- $e = 0.003$
- $i = 80[^\circ]$
- $\text{RAAN} = 0/120/240[^\circ]$
- $\text{AoP} = 270[^\circ]$

The Pegasus reference constellation is thus a Walker 80  $[^\circ]$ : 21/3/1 constellation. As such, it implies that the system consists of 21 satellites homogeneously distributed in 3 orbital planes and separated in the equatorial plane by 120  $[^\circ]$  as Galileo [1]. As observed Table 2.2, in each orbital plane, each satellite is separated with an angular distance of 51.4  $[^\circ]$ . The relative phase shift factor between satellites in adjacent planes is 1, leading to an offset of 17.1  $[^\circ]$  between satellites in adjacent planes. A two-dimensional visualization of the system configuration can be seen in Fig. 2.8, while a three-dimensional view is depicted on figure 2.9.

Reference constellation orbital and technical parameters								
Satellite	ID	Slot	SMA[km]	e	i $[^\circ]$	RAAN $[^\circ]$	AoP $[^\circ]$	TA $[^\circ]$
Pegasus01	01	A01	10000	0.003	80	0	270	0
Pegasus02	02	A02	10000	0.003	80	0	270	51.4
Pegasus03	03	A03	10000	0.003	80	0	270	102.8
Pegasus04	04	A04	10000	0.003	80	0	270	154.2
Pegasus05	05	A05	10000	0.003	80	0	270	205.7
Pegasus06	06	A06	10000	0.003	80	0	270	257.1
Pegasus07	07	A07	10000	0.003	80	0	270	308.5
Pegasus08	08	B01	10000	0.003	80	120	270	17.1
Pegasus09	09	B02	10000	0.003	80	120	270	68.5
Pegasus10	10	B03	10000	0.003	80	120	270	120
Pegasus11	11	B04	10000	0.003	80	120	270	171.4
Pegasus12	12	B05	10000	0.003	80	120	270	222.8
Pegasus13	13	B06	10000	0.003	80	120	270	274.2
Pegasus14	14	B07	10000	0.003	80	120	270	325.7
Pegasus15	15	C01	10000	0.003	80	240	270	34.2
Pegasus16	16	C02	10000	0.003	80	240	270	85.7
Pegasus17	17	C03	10000	0.003	80	240	270	137.1
Pegasus18	18	C04	10000	0.003	80	240	270	188.5
Pegasus19	19	C05	10000	0.003	80	240	270	240
Pegasus20	20	C06	10000	0.003	80	240	270	291.4
Pegasus21	21	C07	10000	0.003	80	240	270	342.8

Table 2.2: Reference constellation orbital and technical parameters.

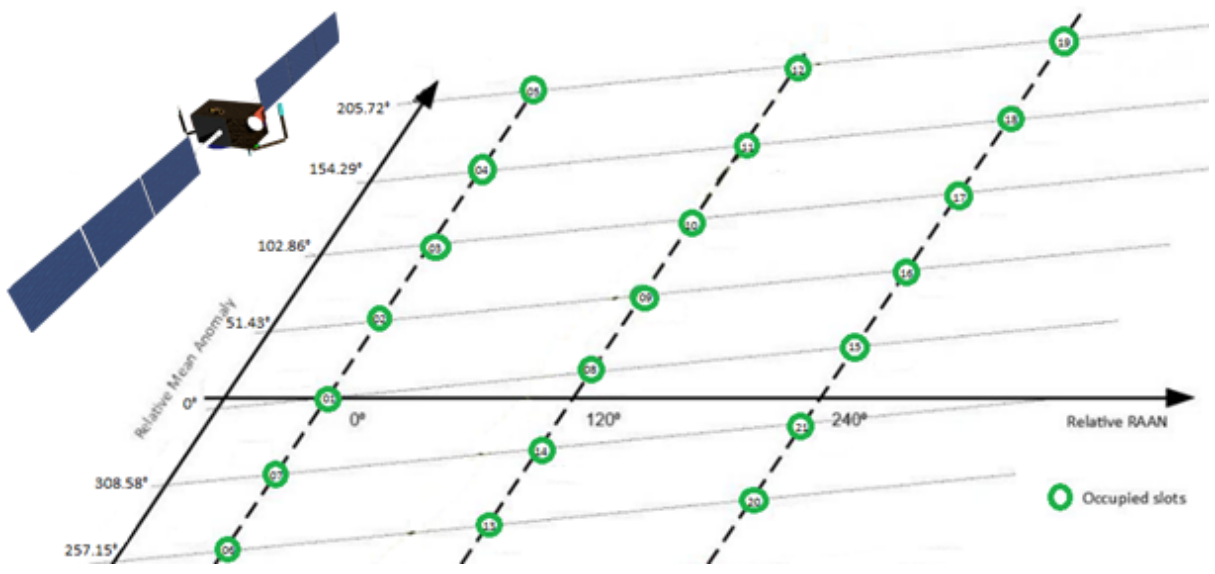


Figure 2.8: Formation configuration of the Pegasus constellation.

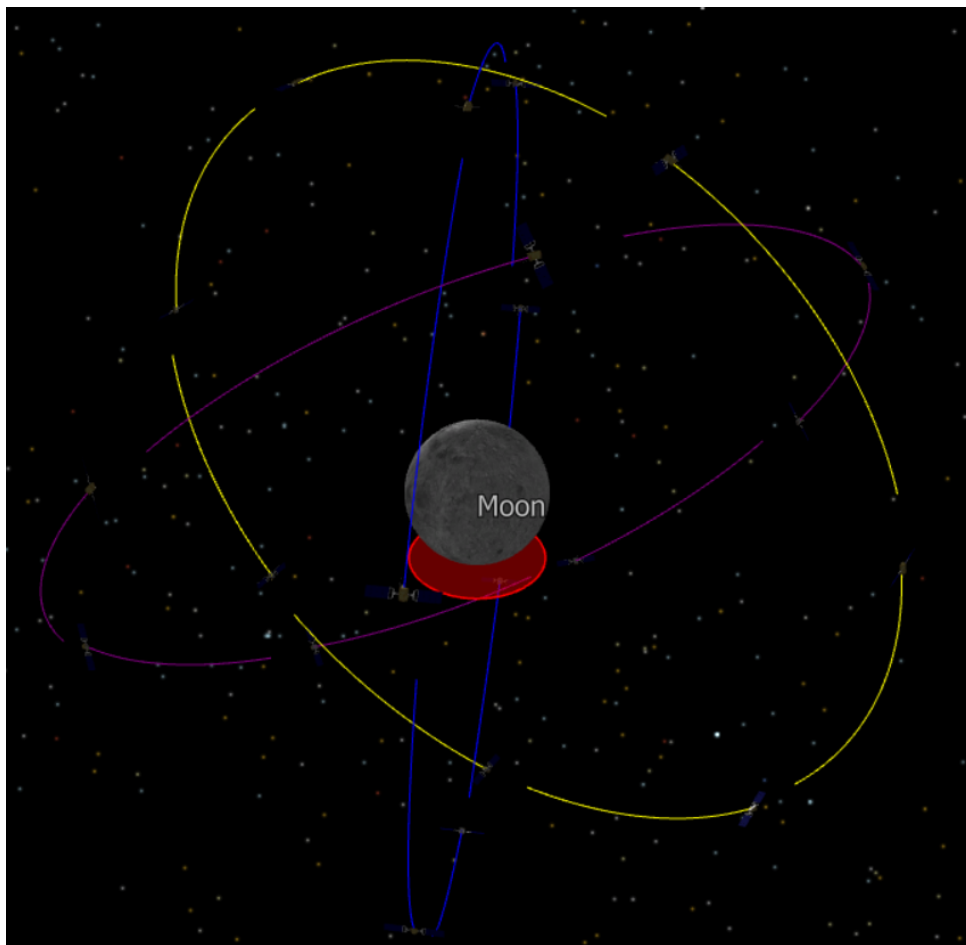


Figure 2.9: Visualization of the Pegasus constellation.

## 2.3 Trajectories Analysis

### 2.3.1 Low-Energy Low-Thrust Deployment

A low-energy Earth-Moon transfer is considered for the deployment as it is an interesting alternative to Hohmann-like transfers. Low-energy transfers are characterized by a long flight duration but their fuel consumption is making them suitable for unmanned missions. A LELET (Low-Energy Low-Thrust) method executing ballistic lunar capture is chosen for the constellation deployment [2]. The main idea is to exploit Lagrange point orbits, gravitational attractions of the Sun, the Earth, and the Moon, and the high  $I_{sp}$  of low-thrust thrusters.

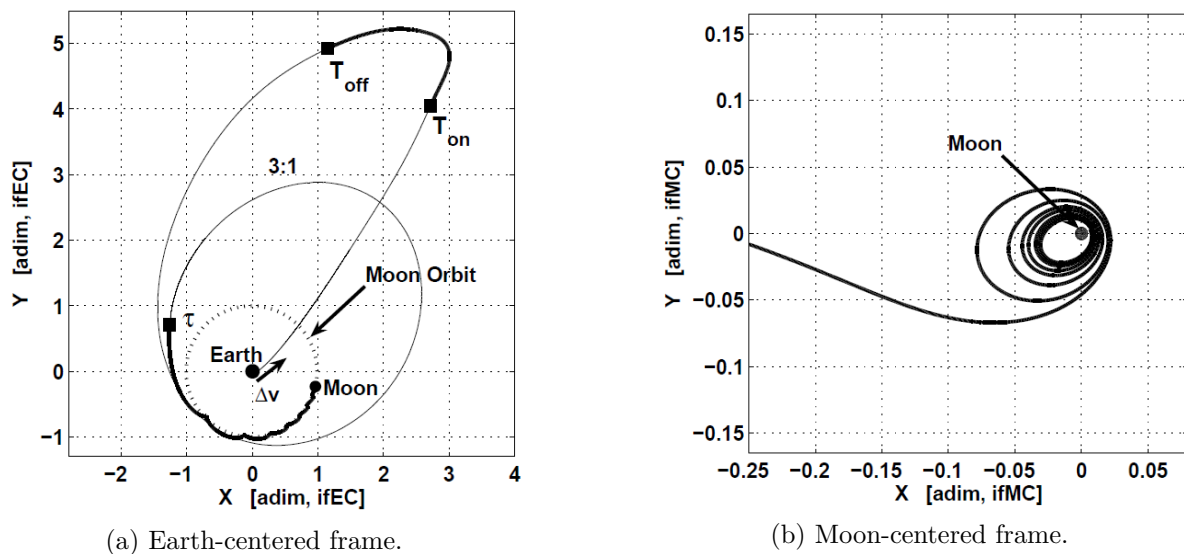


Figure 2.10: LELET solution from LEO to reach elliptic lunar orbit [2].

The transfer orbit presented in the Earth-centered frame shows a Moon gravity assist placing the spacecraft into a 3:1 resonant orbit with the Moon, leading to the low-thrust Moon capture. Across the region six times the Earth-Moon distance, a first maneuver using very low-thrust arc is performed (Fig. 2.10a [2]) with  $T_{on}$  to  $T_{off}$ . The Moon-centered frame (Fig. 2.10b) shows a second long maneuver when approaching the Moon, proceeding to the lunar capture and eccentricity/perigee altitude correction<sup>2</sup>. The complete interplanetary travel computed is less than 360 days, which fits the requirements of 1 year of deployment.

### 2.3.2 End of Life

To follow space agencies' standards and protocols, a legal EOL protocol had to be ensured in order to limit lunar orbit debris. Usually on Earth, atmospheric reentry maneuvers are performed for LEO satellites, and graveyard orbits are used for higher altitude ones such as S/C in geostationary orbit. As the lunar base "HOME" is projected to be on the South pole, a common strategy has been decided with the other constellation projects. It implicates to crash on the lunar surface close to the North pole for lunar base safety reasons. To do so, Pegasus satellites have to perform maneuvers from 10000 [km] to reach a perigee altitude smaller than 1737.1 [km] (Moon radius).

<sup>2</sup>The figure does not show the current trajectory proposal as final orbit is elliptical, the deployment phase is further discussed in section *Propulsion* 4.2.3.



## 2.4 Environment Analysis

The purpose of this section is to briefly explain the consequences of the chosen orbits for the Pegasus constellation on the environment that the satellites will face. As it has been explained in section 2.2, the spacecraft will be located on three different orbital planes, with the following properties:  $a = 10000$  [km],  $e = 0.003$ ,  $i = 80$  [°]. The consequences of this choice in terms of thermal environment, eclipses, radiative environment, and disturbing torques will be detailed in the next sections.

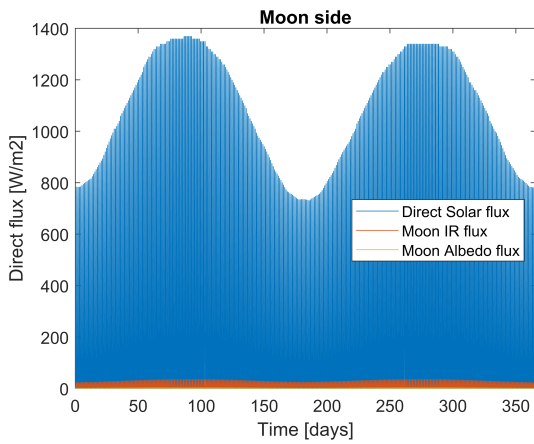
### 2.4.1 Thermal Fluxes

The plug-in *Thermica* from the software *Systema* is used to compute the incoming fluxes received by the six faces of the satellite. In this preliminary study, one spacecraft's side is imposed to point to the Moon (*Moon side*), whereas the normal of another side (*Velocity side*) coincides with the velocity vector. The results obtained for one satellite located on an orbital plane with  $\Omega(t_0) = 0$  [°] are depicted on figure 2.11. It should be noted that the fluxes taken into account in this analysis are: the direct solar flux, the Albedo fluxes originating from the Moon and the Earth, and the IR-fluxes generated by the Earth and the Moon.

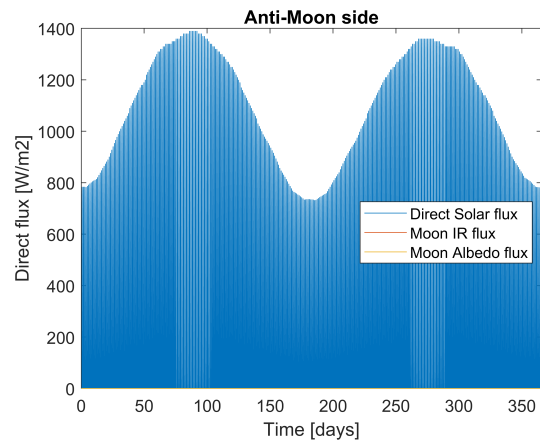
Here is a short summary of the comments yielded by this preliminary thermal analysis.

- It has been noticed that Earth Albedo and IR fluxes are negligible due to the large distance between the Earth and the Moon. Hence, they won't be considered in the following anymore and they are not plotted on the graphs of figure 2.11.
- From figure 2.11, one can conclude that the Moon Albedo and IR fluxes are negligible on all faces except on the "Moon Side". Hence, in the future, they will only be taken into account for this side.
- Looking at figure 2.11 more closely, an interesting property regarding the direct solar flux can be seen: one can notice that the phase of the solar fluxes of two opposing sides is shifted by 180 [°]. This means that a hot case for one face corresponds to a cold case for the opposite one.
- Moreover, figure 2.11 exhibits variations of the fluxes at very different frequencies.
  - A low-frequency variation of the envelope of the fluxes is observed, which is related to variations of the relative position and orientation of the Moon with respect to the Sun and can be interpreted as "seasonal effects".
  - High-frequency oscillations of the fluxes due to the rotation of the spacecraft with respect to the Sun along its orbit, are also discovered.

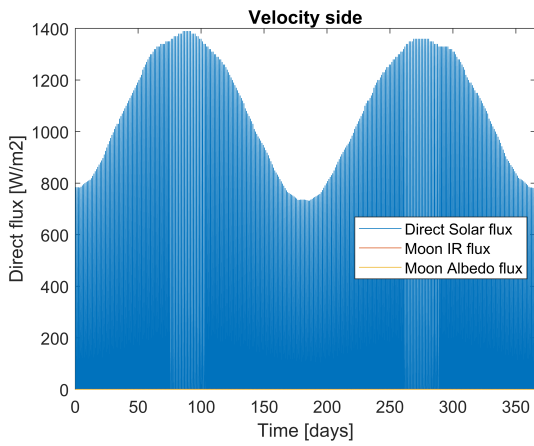
Large variations of incident fluxes on the six sides of the spacecraft were found with this preliminary study of the thermal fluxes. They indeed vary from 0 [W/m<sup>2</sup>] to more than 1000 [W/m<sup>2</sup>] on all faces. As it will be seen later in the section *Thermal control* 4.6, this behavior will require problem-solving for the Pegasus satellites.



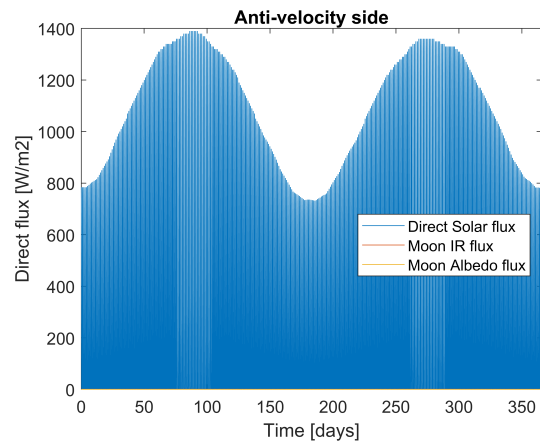
(a) Moon side.



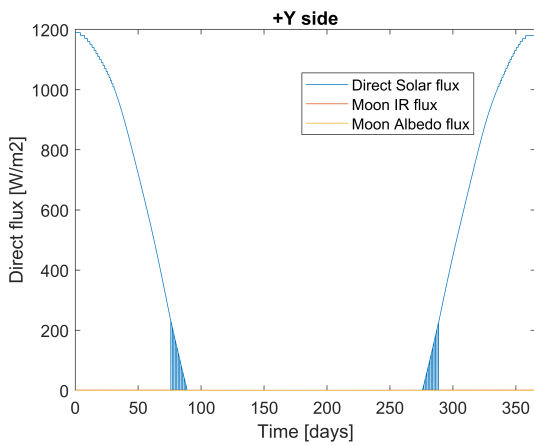
(b) Anti-Moon side.



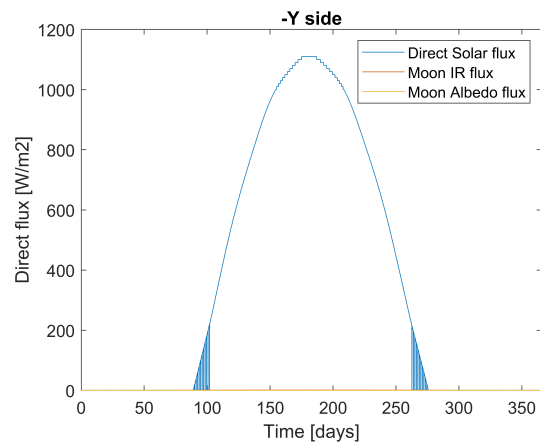
(c) Velocity side.



(d) Anti-Velocity side.



(e) +Y side.



(f) -Y side.

Figure 2.11: Direct fluxes on the six spacecraft sides.

## 2.4.2 Eclipses

Another important element of the environment faced by the satellites is the eclipses. These periods of time where the spacecraft lies in the obscurity of another celestial body are design drivers for both the power and the thermal subsystems.

In the case of lunar orbits, two kinds of eclipses should be considered. The first one, and most frequent one, arises in the case of an alignment Sun-Moon-Satellite and is called *lunar eclipse* since from the satellite perspective they are created by the Moon. For the chosen orbits, these eclipses occur two times a year for several consecutive orbits. Moreover, their maximum duration (worst-case) can be computed by means of simple geometric reasoning depicted in figure 2.12a, the result is depicted in equation 2.4.

The second type of eclipses that will be faced by the Pegasus satellites are the so-called *Earth eclipse* that result from an alignment Sun-Earth-Satellite. This kind of eclipse occurs between two and three times a year only but should be taken into consideration. Their maximum duration can be computed thanks to figure 2.12b, the result is depicted in equation 2.4.

$$\begin{aligned}
 T_{Eclipse, Moon} &= \frac{2\pi}{T} \cdot 2\alpha = \frac{2\pi}{T} \cdot 2 \cdot \text{asin} \left( \frac{R_M}{SMA} \cdot \sin\left(\frac{\pi}{2}\right) \right) \approx 1 \text{ [h]} 23 \text{ [min]} \\
 T_{Eclipse, Earth} &= \frac{2\pi}{T} \cdot 2\alpha = \frac{2\pi}{T} \cdot 2 \cdot \text{asin} \left( \frac{R_E}{SMA} \cdot \sin\left(\frac{\pi}{2}\right) \right) \approx 2 \text{ [h]} 35 \text{ [min]}
 \end{aligned} \tag{2.4}$$

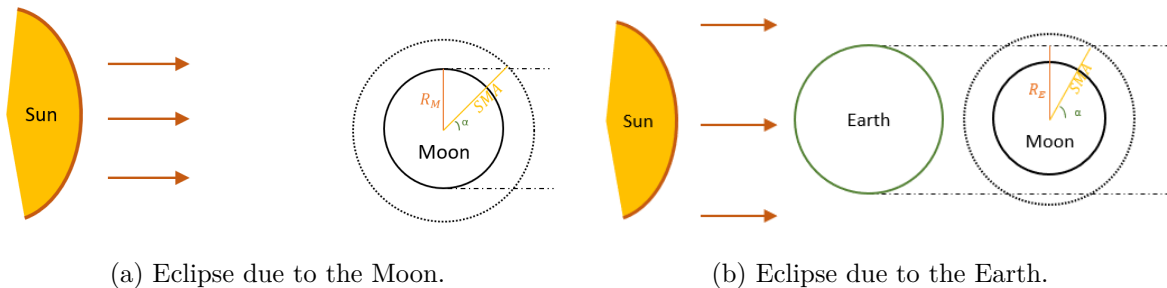


Figure 2.12: Worst-case eclipses.

Based on the results of equation 2.4, one can conclude that Earth eclipses will be driving the sizing for the power and thermal subsystems since their duration is longer. The results of this section will be used in the design of the power subsystem (Section 4.4) and the thermal subsystem (Section 4.6), where the effect of the eclipses on the spacecraft temperature will also be clarified.

### 2.4.3 Radiation Environment

Assessing the radiation environment in which the satellites will evolve is important for evaluating the risk of single event effects (SEE) and cumulative effects that can occur in electronic components, and to estimate the performance decrease of solar arrays. Results obtained are then used during the mechanical design, for the definition of shielding to protect sensitive equipment (Section 4.7), and during the solar arrays sizing (Section 4.4).

In order to obtain an estimation of the particle fluxes, two different software are used (to cross-check the results): the software *Omere*, developed by the company TRAD in cooperation with the CNES and *SPENVIS*, a WWW interface developed by a consortium led by the Royal Belgian Institute for Space Aeronomy (BIRA-IASB), especially for ESA's activities.

#### Generalities

Energetic waves and particles exist in space. Some of them are generated by solar activity, others, known as cosmic rays can have different origins.

Regarding the solar radiations, 3 main categories can be differentiated:

- **Photons:** The Sun emits electromagnetic waves at different frequencies. The solar flux is very stable in the visible domain (400-750 [nm]) and contains cyclical fluctuations in other frequency domains (gamma, X, UV). The power received from the Moon is about  $1.37 [kW/m^2]$ .
- **Low energy electrons and protons:** Ejected during the solar activity, their energy can be up to a few keV. A continuous solar wind is generated by the Sun, with some sporadic and periodic phenomena due to Coronal Holes and some random ejections called Coronal Mass Ejection.
- **High Energy electrons, protons, and heavy ions:** Random events called Solar Flares generate these particles that have an energy of up to 100 [MeV].

Cosmic rays are composed of high-energy protons and atomic nuclei that originate from the Milky Way or from other galaxies, and that have an energy of up to 100 [MeV]

Due to the Earth's magnetic field, incoming particles are trapped and accumulated in specific areas in the vicinity of the Earth called Radiation Belts or Van-Allen belts. These regions can represent a danger for spacecraft as it is more likely that high energetic particles collide with them and damage sensitive units. However, the belts do not extend more than approximately 10 times the Earth's radius, which is much smaller than the distance Moon/Earth (6 times greater). Therefore, trapped particles will not be a problem during the operating life of the constellation.

During the deployment, the satellites will cross the Van-Allen Belt. However, the time spent in this region is expected to low. Thus, it is assumed that this will not be the major factor for the sizing of the shielding or for the solar array degradation. Trapped particles are therefore neglected in the present study, which will focus on the radiation particles in the vicinity of the Moon, i.e. solar particles and cosmic rays (photons are also not considered here).

### Solar Particles Fluences

A first simulation is performed with *OMERE* to assess the solar particle fluences received by satellite during a 10 years mission (that corresponds to the lifetime of the Pegasus constellation), considering that the satellite is on the Moon orbit. This orbit is selected because the main factor that will influence the particle's flux is the distance from the Sun. Indeed, the Moon is far away from the radiation belts and we neglect all shadowing effects due to the Moon or the Earth. The results of this simulation are depicted in the figure 2.13.

It is recalled that the Flux is the number of particles per unit area and the Fluence is the time integration of the Flux. The Flux can be expressed either in integral form (number of particles per unit area and per unit time) or in differential form (differential with respect to the energy). In the framework of this analysis, only integral forms of Fluence and Flux are considered.

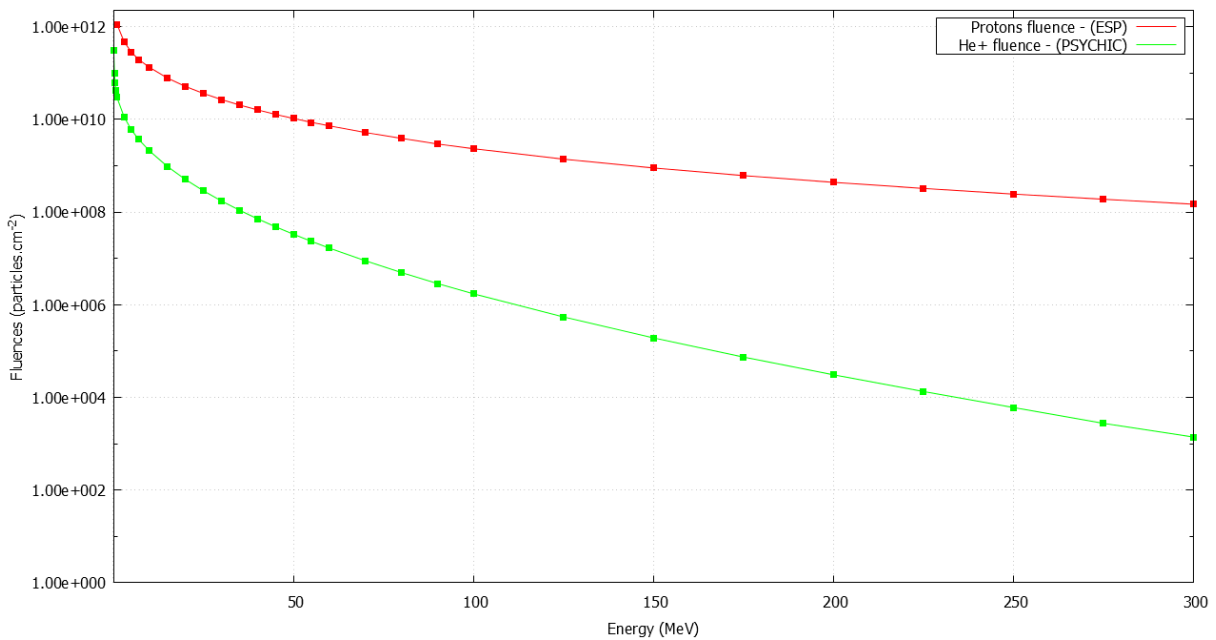


Figure 2.13: Solar particles fluences.

The results show that the heavy ions and high energy electrons fluences are way lower than the solar protons fluence. For this reason, only the He+ ions fluence has been displayed on the figure, as they have the highest fluence among all other ions. In conclusion, concerning the solar particles, solar protons will have major participation in the total fluence. This first result will be used later, when the radiation dose received by satellite will be computed in the section 4.37.

### Cosmic Rays Fluxes

A second simulation is done to compute the cosmic rays fluxes received by satellites during the mission. Results are depicted on the figure 2.14.

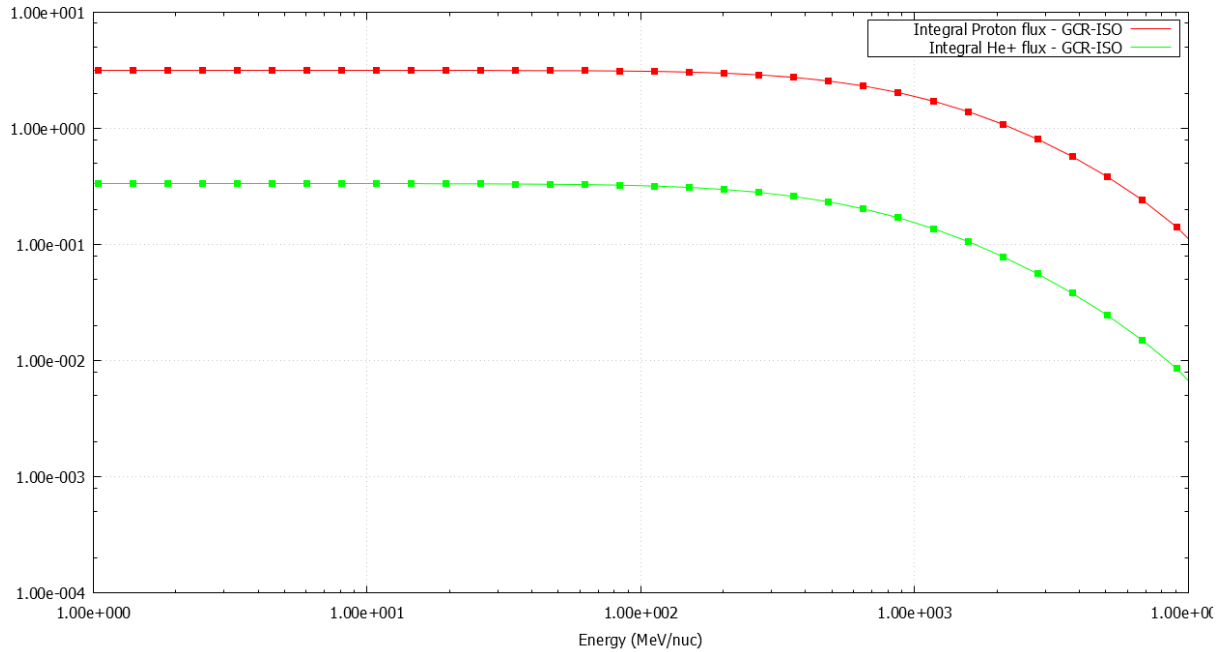


Figure 2.14: Cosmic rays fluxes

Concerning the cosmic rays, the maximum fluxes are obtained for the protons and the He+ ions. Associated fluences can be computed by multiplying fluxes by the duration of the mission (assuming a constant flux over time). The order of magnitude of the fluences for the lowest energetic cosmic particles is  $1e9 [particle.cm^{-2}]$ , which is lower than the solar particles fluences. The fluence of the cosmic particles with an energy between 300 [MeV] and 1000 [MeV] remains around  $1e9 [particle.cm^{-2}]$ , which is comparable or even higher than the fluence of solar protons with the same energy. It is concluded that the impact of the cosmic rays on the dose received by satellite will be negligible for the lowest energetic cosmic particles but not for the high energetic ones.

#### 2.4.4 Disturbing Torques

The order of magnitude of the external disturbance torques that apply at the altitude of the Pegasus orbits must be assessed since it is one of the drivers for the design of the AOCS subsystem. Generally, the main external torques to take into account have four origins: (a) the aerodynamic pressure, (b) the solar radiation pressure, (c) magnetic fields, (d) gravity fields.

In the case of lunar orbits, the situation can be simplified since two perturbations aren't present: the aerodynamic pressure (since there is no atmosphere around the Moon), and the magnetic field (since the Moon doesn't have one). Hence, the only two perturbations remaining are the solar radiation pressure and the lunar gravity field. As it will be seen, they have a very different order of magnitude in the case of the Pegasus orbits.

The solar pressure is due to incident solar radiation that plies pressure on all surfaces that cross its way. This pressure depends on the distance to the Sun, approximately  $4.5 \cdot 10^{-6}$  [N/m<sup>2</sup>] around the Moon [3]. It should be noted that another pressure exists due to the Moon albedo (the reflection of solar radiation on the Moon surface), but it is negligible at the high altitudes of the Pegasus orbits. The disturbing torques created by solar pressure are highly dependent on the spacecraft geometry, but generally reach the order of magnitude of  $10^{-5}$  [N.m].

The gravity gradient torques are created due to the distance between the center of gravity (COG) and the center of mass (COM) of the spacecraft. This distance depends again on the spacecraft geometry. However, due to Moon gravity being smaller than Earth's (approximately 16.6 %) and due to the choice of high orbits for the Pegasus satellites, the gravity gradient torques are expected to be (at least) one order of magnitude smaller than the disturbing torques originating from solar pressure.

All in all, the order of magnitude of the different disturbing torques is summarized in table 2.3. The main disturbing torques to take into account in the design of the AOCS subsystem (Section 4.3) are the torques due to solar radiation pressure and have an order of magnitude of  $10^{-5}$  [N/m<sup>2</sup>].

Disturbing torques	Order of magnitude [N.m]
Solar radiation pressure	$10^{-5}$
Gravity gradient	$< 10^{-6}$
Magnetic field	No
Aerodynamic pressure	No

Table 2.3: Order of magnitude of disturbing torques in Pegasus orbit.

## Chapter 3

# Payload

After the choice of the Pegasus orbits and the thorough analysis of the influence of this choice on their environment (Chapter 2), the payload of the satellites will be described in this chapter. As it has been explained in the *System Engineering Report*, the payload of the Pegasus satellites consists in two different systems providing several services on Low Lunar Orbit (LLO) and lunar surface:

- The *Navigation System* (NS) providing both localisation and time services.
- The *Emergency Broadcast System* (EBS) providing a short message service (SMS).

These systems will be described in more detail respectively in the sections 3.1 and 3.2 where their level of service (accuracy and availability), required equipment, and way of working will be specified. Here, it should be noted that the localization and time services are inseparable since they are inextricably linked.



## 3.1 Navigation System

### 3.1.1 Introduction

This first part of the payload intends to explain the choices made regarding the Navigation System (NS) of the Pegasus satellites. This system aims to provide localization and timing services on the lunar surface and in LLO. In the following sections, the description of the onboard atomic clocks, which are the heart of GNSS satellites, the corrections to be applied, the navigation signals, and the antennas will be studied, reaching the computed performance of the Pegasus constellation.

A synthesis of the units used for this system is presented in the following table 3.1. Their role and description can be found in the next sections.

Part	Unit	Quantity	Mass [kg]	Power [W]	T [°C]
Atomic clock	RAFS	2	3.4	60	-5/10
	Passive H-masers	2	12	54	-5/10
Corrections	LRR & CCR	2	4.85	0	N/A
Antenna	NS Antenna	1	15	50	-120/120
	FGUU	2	7.6	22	N/A
	NSGU	2	1.2	20	-20/70
	Amplificator	1	20	2.5	-55
	Total	12	93.1	364.5	N/A

Table 3.1: Synthesis of the navigation units.

### 3.1.2 NS Service Level

#### Parameters

**Visibility** The first consideration to take into account when trying to design a GNSS constellation is that a user must be in direct visibility of at least four satellites to be able to use the localization and time services. The visibility of the Antennas bandwidth is considered large enough to cover all the points under it, with an elevation higher than 10 [°] to consider the slopes, craters, and hills on the Moon.

**Geometric Dilution of Precision** The most important performance indicator is a dimensionless number that measures the satellite geometry. The geometric arrangement of satellites, as they are presented to the receiver, affects the accuracy of position and time calculations. Satellites that are close together cannot provide as much information as satellites that are widely separated. Thus, GDoP analysis can be based on the volume of the tetrahedron, which is formed closing off the unit vectors from the four best satellites visible to the receiver (Fig. 3.1).

A large volume of the tetrahedron, means a smaller GDoP. For Pegasus the objective is  $GDoP \leq 4$ .

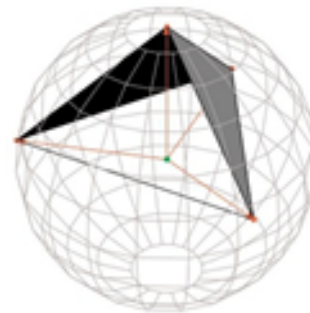


Figure 3.1: Tetrahedron volume example

The GDOP takes into account both the 3D position error  $d_x$ ,  $d_y$ ,  $d_z$  Position Dilution of Precision (PDoP), and the time error  $d_t$  Time Dilution of Precision (TDoP). However, it can be computed based only on geometrical properties, as depicted in equations 3.1.

$$GDOP = \text{trace}(Q) = \sqrt{PDoP^2 + TDoP^2} = \sqrt{d_x^2 + d_y^2 + d_z^2 + d_t^2} \quad (3.1)$$

with

$$Q = (A^T A)^{-1} = \begin{bmatrix} d_x^2 & d_{xy}^2 & d_{xz}^2 & d_{xt}^2 \\ d_{xy}^2 & d_y^2 & d_{yz}^2 & d_{yt}^2 \\ d_{xz}^2 & d_{yz}^2 & d_z^2 & d_{zt}^2 \\ d_{xt}^2 & d_{xy}^2 & d_{zt}^2 & d_t^2 \end{bmatrix}, A = \begin{bmatrix} \frac{x_1-x}{R_1} & \frac{y_1-x}{R_1} & \frac{z_1-x}{R_1} & 1 \\ \frac{x_2-x}{R_2} & \frac{y_2-x}{R_2} & \frac{z_2-x}{R_2} & 1 \\ \frac{x_3-x}{R_3} & \frac{y_3-x}{R_3} & \frac{z_3-x}{R_3} & 1 \\ \frac{x_4-x}{R_4} & \frac{y_4-x}{R_4} & \frac{z_4-x}{R_4} & 1 \end{bmatrix}$$

Matrix A depends only on the geometry of the satellites around the receiver. As such, no accurate satellite positions are needed to calculate it and it can be computed from the almanac. The first three columns are linked to the  $PDoP = \sqrt{d_x^2 + d_y^2 + d_z^2}$ , whereas the last one is linked to the  $TDoP = \sqrt{d_t^2}$ .

**Availability** Another indicator is availability, which provides an assessment of the usability at a specific user location. A GDoP above 6 generally results in unacceptable accuracy for GNSS operations, this threshold is taken to calculate the availability.

**Position error** GNSS constellations do not offer accurate positioning services by themselves. Signal propagation can be disrupted on several levels and errors need to be corrected to achieve accepted positioning and navigational accuracy. These errors can be split into three different groups: spacecraft, signal travel, and GNSS receiver. It is important to be able to estimate the error position and inform the user of this data.

**Spacecraft** Is composed of Ephemeris & Clock Drift Corrections (Section 3.1.4), and the satellite group delay error, which is the total amount of time of the signal processing chain from the onboard frequency oscillator to the antenna. Since the group delays among the various signal paths within the satellite are not the same, signals do not exactly emerge from the transmitting antenna at the same time. This error is corrected in the navigation message.

**Signal travel** As there is no atmosphere on the Moon the ionospheric and tropospheric delays are not accounted for, which are the highest perturbations on Earth applications. Moreover, multipath errors appear when a signal arrives at the receiver after having been reflected from an object such as the surface of a building. Then it arrives with a slight delay that has to be corrected. The error can be considered very low on the Moon with the absence of infrastructure, with exception of the lunar base.

**GNSS receiver** The hardware used within the receiver may also limit precision by introducing inaccuracies in the clock receiver. Receiver-ranging errors, appearing when measuring carrier phases, will not be considered since these errors seem to be negligible for high-quality receivers. Indeed, as not many people will use the service (astronauts), expensive but more efficient receivers can be used.

**User Equivalent Range Error** To summarize, the following GNSS errors are considered:

- due to the spacecraft:  $\sigma_{ephemeris} = 1.5$  [m],  $\sigma_{clock\_error} = 1.5$  [m],  $\sigma_{group\_delay} = 0$  [m].
- due to signal travel:  $\sigma_{atmosphere} = 0$  [m],  $\sigma_{multipath} = 0.03$  [m].
- due to GNSS receiver:  $\sigma_{clock\_error} = 0.03$  [m],  $\sigma_{range\_error} = 0$  [m].

The global error can be seen as a measure of the precision for point positioning:

$$UERE = \sqrt{\sigma_{ephemeris}^2 + \sigma_{clock\_error}^2 + \sigma_{multipath}^2 + \sigma_{clock\_error}^2} = 2.12m \quad (3.2)$$

At last, position error is calculate using the UERE and PDoP:

$$\begin{cases} @1\sigma, pos_{error} = PDoP \cdot UERE \\ @2\sigma, pos_{error} = 2 \cdot PDoP \cdot UERE \\ @3\sigma, pos_{error} = 3 \cdot PDoP \cdot UERE \end{cases} \quad (3.3)$$

**Time error** Since the localization and time services are inseparable, it is known that the several error sources identified for the position also degrade the quality of the time service. More precisely, the time error  $time_{error}$  can be computed as in equation 3.4, with the same UERE as for the position and with  $c$  the speed of light.

$$\begin{cases} @1\sigma, time_{error} = TDoP \cdot UERE/c \\ @2\sigma, time_{error} = 2 \cdot TDoP \cdot UERE/c \\ @3\sigma, time_{error} = 3 \cdot TDoP \cdot UERE/c \end{cases} \quad (3.4)$$

## Operational Performance Cases

**Moon Relief** The result of the constellation selected in section *Mission Analysis* 3.1.2 is presented in figure 3.2 on the lunar surface. As reminder, the minimum elevation parameter was used to simulate a scenario taking into account the Moon relief. For a simulation duration of 24h, the service level is the following: availability is  $\approx 0.966$ , the global GDoP 2.73, the position error @3 $\sigma$  = 11.74[m], and the time error @3 $\sigma$  = 43 [ns]. Thus, all requirements previously set are validated.

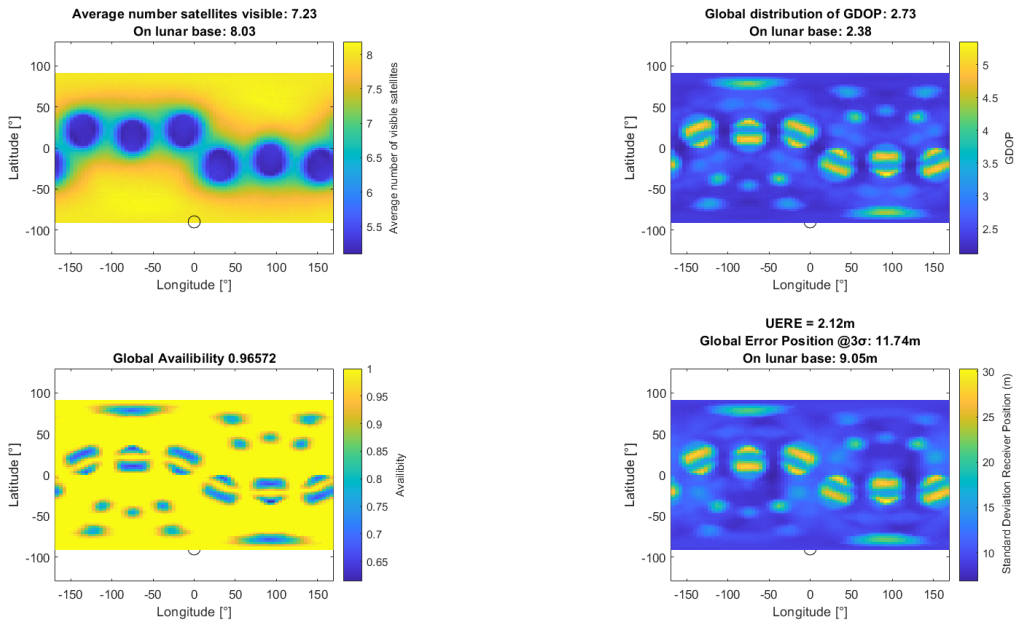


Figure 3.2: Pegasus GNSS performance on lunar surface at 10° minimum elevation.

**Nominal** For this second study, the parameter is replaced by the antenna aperture angle  $\theta=22[^\circ]$ . The result obtained in this case is better as every device within the beam is supposed to receive the GNSS signal.

**Low Lunar Orbit** Taking 125 [km] as the maximum altitude of the LLO, the selected beam has to cover a virtual Moon radius of  $1737 + 125 = 1862[km]$ . The performance on LLO is depicted on figure 3.3. During nominal operations, the availability is equal to 1, the global GDoP 1.85, the position error @3σ = 6.90[m], and the time error @3σ = 32 [ns].

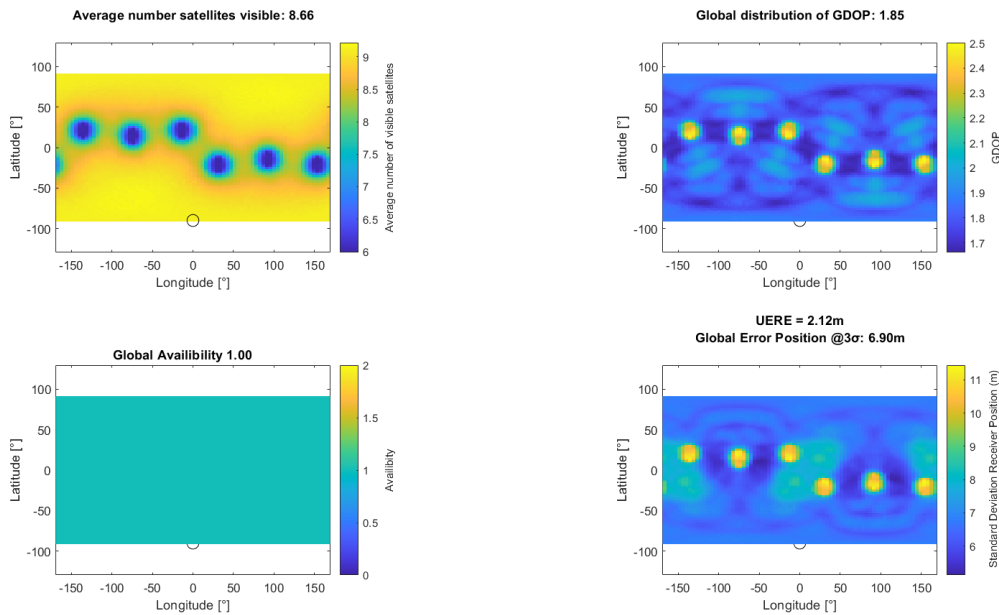


Figure 3.3: Pegasus GNSS performance on LLO (22° aperture beam)

**Lunar surface** During nominal operations, the availability is 1, the GDoP  $1.84 \leq 4$ , the position error  $@3\sigma = 6.78[m]$  globally, and  $6.74[m]$  around the lunar base, the time error  $@3\sigma = 32[ns]$ . The performance on LLO and lunar can be consider as equal cases.

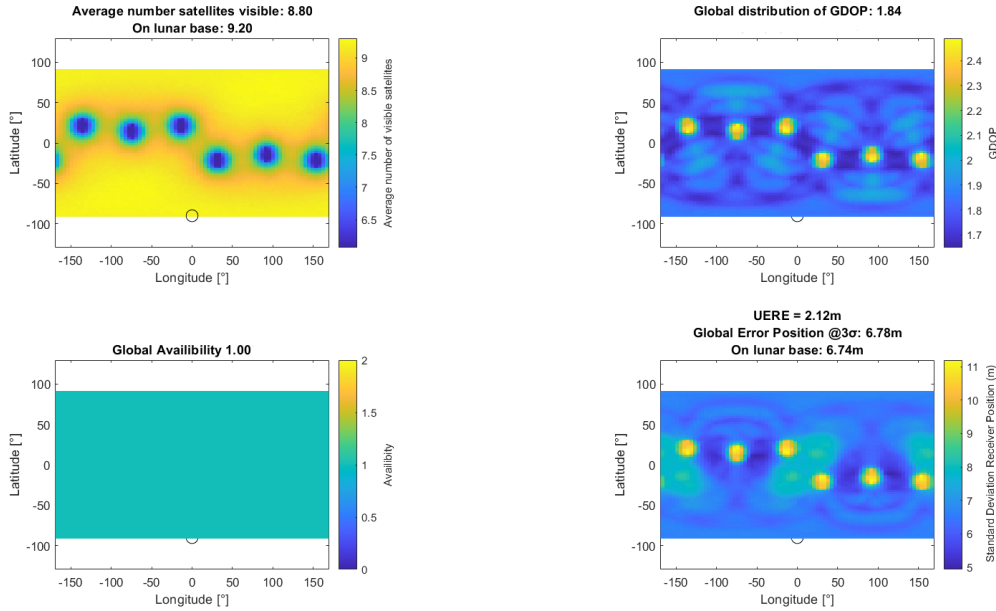


Figure 3.4: Pegasus GNSS performance on lunar surface 22° aperture beam.

**Spacecraft Loss** A loss of payload for a small period of time, or even complete loss of one spacecraft for the rest of the mission, can degrade the service level. This 20 S/C performance results are shown in figure 3.5, where the error position is  $0.81[m]$ , the availability is still  $\geq 0.95$ , the GDOP  $1.95 \leq 4$ , the position error  $@3\sigma = 7.59[m]$ , and the time error  $@3\sigma = 33[ns]$ . Validating that even with the loss of one S/C, the system validates the performance requirements.

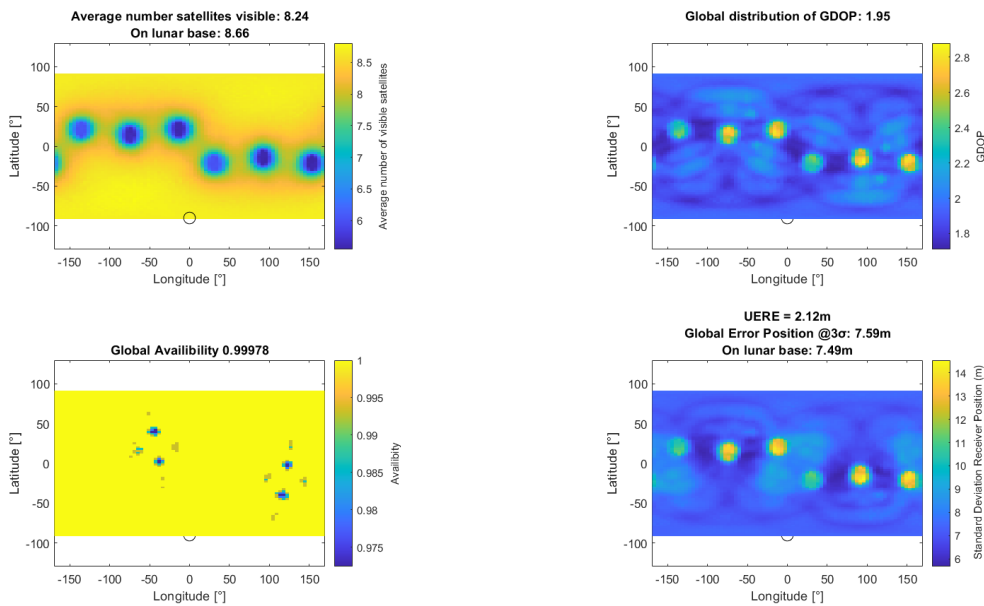


Figure 3.5: Constellation performance with 20 satellites.

### 3.1.3 On-Board Atomic Clocks

Ultra-stable onboard atomic clocks, called Space Atomic Frequency Standards (SAFSs), are the most critical equipment for an accurate GNSS service. All satellites and receivers are as synchronized as possible to a time reference and controlled by very precise atomic clocks. To prevent errors in this reference, since a few nanoseconds could incur some meters in measurements.

#### Technologies State of the Art

Four types of different technologies have been used in GNSS S/Cs, including a new Hg Ion clock, some of their characteristics are presented figure 3.6.

**Rubidium Atomic Frequency Standard** Rb Atomic Frequency Standard (RAFS) is the most used technology in space (see figure 3.7 and table 3.2) as it has a low volume, low cost, and low power consumption compared to other standards, for excellent stability. Furthermore, Rb atoms do not consume themselves rapidly, which is advantageous for the instrument’s lifetime.

**Hydrogen Maser** The active H-maser is one of the most stable technology. However, due to constraints resulting in a voluminous, heavy, and high power device, its usage is mainly restricted to the ground. The passive and miniaturized form is however more suitable on-board S/Cs, with a compromise on the frequency’s stability. It involves a small hydrogen consumption and is stable with a drift of one second in three million years.

**Cesium Beam Frequency Standard** Interest in Cs Beam Frequency Standard (CBFS) comes from the wide availability of Cs on earth as well as its low melting point. Compared to RAFS and H-maser, CBFS show small long-term frequency drifts and reach excellent long-term stability. These advantages come however with a complex vacuum chamber to be maintained for the atomic beam.

**199Hg+ Trapped-ion** Mercury trapped-ion AFS is a recent technology developed by the Jet Propulsion Laboratory (JPL) and sent into space for the first time in 2019.

	H-Maser	Cesium Clock	Rubidium Clock	Hg Ion Clock
<b>Lifetime limits</b>	H <sub>2</sub> dissociation, flow through. Life limited by H <sub>2</sub> supply. Life limited by pump life.	Cesium oven, Cs beam. Life limited by Cs supply	Glass cell with Rb vapor; Rb not consumed	No Consumables; Hg vapor sealed in vacuum tube. Ions held by rf/dc force fields. No wall collisions.
<b>Microwave; state-selection</b>	Microwave cavity 1.4 GHz.	Microwave cavity 9.2 GHz; laser or magnetic deflection state selection	Microwave cavity 6.8 GHz; RF excited Rb lamp	No microwave cavities, RF excited Hg lamp. No lasers.
<b>Radiation</b>	Rad-tolerant; Used in GALILEO.	Rad-tolerant with magnetic state selectors; less tolerant with laser.	Rad-tolerant; Used in GPS; ~100 krad/yr for >10 yrs	Radiation tolerant (Similar to GPS Rb)
<b>Magnetic Sensitivity</b>	Several shield layers; Reference field ~ 1 mG. Highest inherent sensitivity.	Several shield layers	Several shield layers	3 layer shields; Lowest magnetic sensitivity
<b>Temperature Sensitivity</b>	Cavity stabilized to ~ 0.001 C	~ 10 <sup>-13</sup> /C Laser cooled clocks require 0.002 C stabilization	~ 10 <sup>-13</sup> /C	~ 10 <sup>-15</sup> /C Lowest temp sensitivity

Figure 3.6: A comparison of standard space atomic clock technologies and the Hg Ion Clock.

## State of the Art Navigation Systems

The table 3.2 displays the clock technologies used onboard the main GNSS constellations around the Earth: BeiDou (Chinese), Galileo (European), Glonass (Russian), GPS (American), IRNSS (Indian), and QZSS (Japanese). The adoption of a *dual-technology* onboard clocks is dictated by the need to ensure a sufficient degree of reliability by flying two different technologies, as well as better service accuracy.

GNSS System	SAFS	Quantity
BeiDou-2	RAFS	4
BeiDou-3	RAFS	4
	H-maser	2
Galileo	RAFS	2
	H-maser	2
Glonass-M	CBFS	3
Glonass-K1	CBFS	2
	RAFS	2
GPS-II	CBFS	2
	RAFS	2
GPS-IIF	CBFS	1
	RAFS	2
GPS-III	RAFS	2
IRNSS-1A	RAFS	3
QZSS	RAFS	2

Table 3.2: State of the art of GNSS atomic clocks.

As presented in the figure 3.7, up to now, 1034 RAFSs have been sent into space, mainly for GNSS applications. RAFS have been the first to be developed and offer the longer flight heritage. On the opposite, H-maser technology is more recent and complex, but offers better stability and has been more used past years.

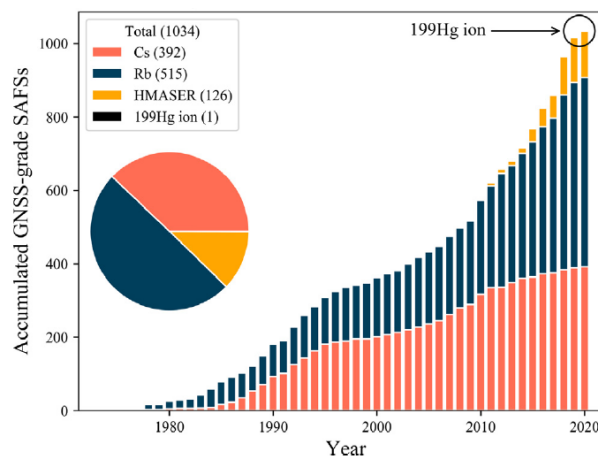


Figure 3.7: Space atomic clock standards sent into orbit. [4]

## Pegasus Space Atomic Frequency Standards

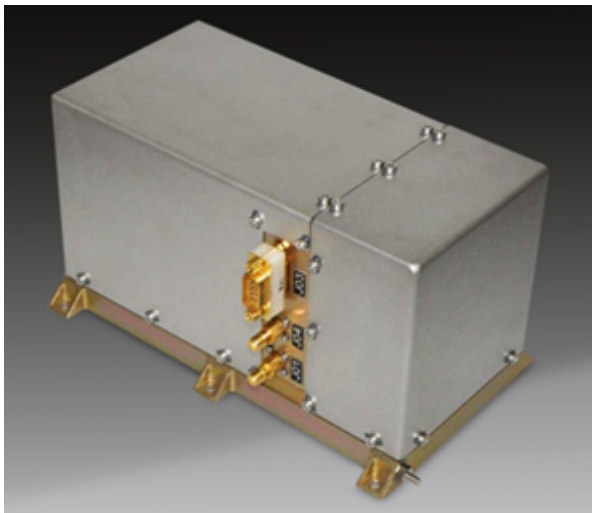
### Selection

The selection of the type of SAFS is a trade-off between reliability, mass, performance and cost. The main challenge is to have clocks compact enough and robust to work in space environment. Cs beam technology, is better for long-term stability and mainly used for ground-based reference clocks, and  $^{199}\text{Hg}$  ion, considered as too recent and not tested enough, have not been selected. The strategy is to chose a compromise between the SAFSs mid-term stability and the recalibration frequency from the Ground Station.

The mini PHM (Fig. 3.8b), made by Leonardo Company, with the contribution of Orolia Switzerland, is planned to be on-board of Galileo Next-Generation Phase, and will be the master clock of Pegasus S/Cs. The Orolia Rubidium SAFS, is selected as backup for reliability. It has demonstrated the capability to operate for 12 years under vacuum without significant degradation.

Atomic clocks are very sensitive to the external environment and great care is required to keep environmental disturbances small. The measures taken for Pegasus can be found in section *AOCS* 4.3.3 and *Thermal Control* 4.6.2.

**Redundancy** Clocks being the most critical equipment for the navigation P/L part, it is important to provide redundancy. In 2017, six PHM and three of the RAFS of Galileo have reported failures, resulting in four satellites having lost at least one clock. Thus, each satellite will have one active rubidium clock and mini-PHM and second one in hot redundancy. With four clocks, the probability that at least one will still be operating at the end of the 10-year mission is higher than 99[%].



(a) Rubidium clocks [5]



(b) Mini Passive Hydrogen Masers [6].

Figure 3.8: Clock equipment



### 3.1.4 Ephemeris and Clock Corrections

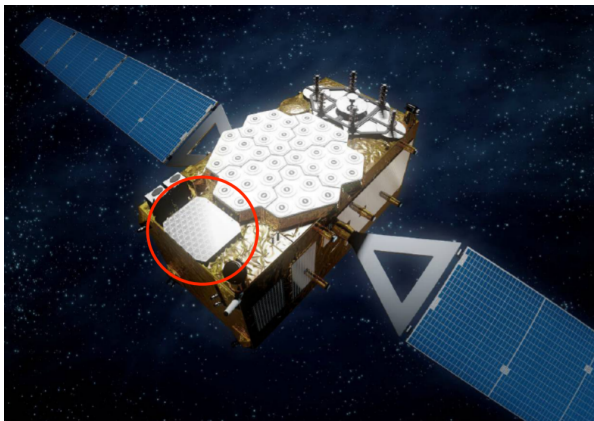
The orbit, clocks, ephemeris, and receivers of the satellite are fundamental to calculate the right positioning and clock deviation of the receiver. Any error in the satellite coordinates or satellite clock, due to clock drift phenomena, will affect the positioning accuracy. Corrections have to be done regularly to limit the error position and clock. On Earth, usually, an ephemeris is valid for only four hours; an almanac is valid with a little dilution of precision for up to two weeks.

#### Ephemeris Correction

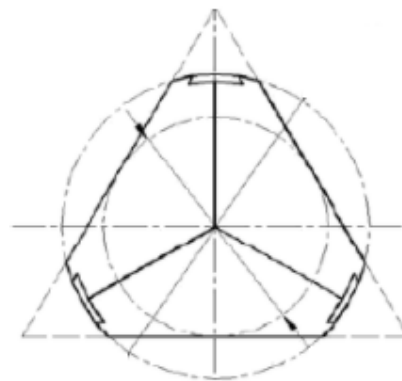
Satellite Laser Ranging (SLR) is a track system allowing a precise positioning of the satellite orbit to measure their trajectory. This system is currently used on more than 100 satellites, including GPS, BeiDou and Galileo (figure 3.9a) [7]. The activity of the earth stations housing laser emitters, including 40 SLR stations, is coordinated within the International Laser Ranging Service (ILRS).

It works very well on long distances such as the Moon, it has been used first for the Lunar Laser Ranging experiment. Also, the APOLLO laser project, operational since 2005, routinely achieves millimeter-level range accuracy between the Earth and the Moon [8]. It is based on the very precise measurement of the time taken for a light pulse (error less than  $1[cm]$ ) to make the round trip between a laser transmitter on Earth and a satellite using Corner Cube Reflectors (CCRs).

The same Laser Retro Reflector (LRR) as in BeiDou will be used as it offers a good reflective area, that will be needed being far from Earth, and having the challenge to point exactly at the CCRs. All Pegasus satellites have two LRR positioned on the Sun and anti-Sun sides, each composed of 90 CRRs (figure 3.9b).



(a) Galileo's LRR array localization. [9]



(b) Beidou Corner Cube Reflectors.

Figure 3.9: Satellite Laser Ranging equipment.

## Clock Offset Correction

**Earth GNSS Method** Space atomic clocks offer very good short-term frequency stability, around 12 hours. Left to run indefinitely, though, the clock would drift significantly. Indeed an error of  $10^{-7}$  [s] on the time synchronization results in an error of 30 [m] in position estimation. On Earth, monitor stations distributed around the world are equipped with atomic clocks standards and GNSS receivers to continuously collect navigation signals. Knowing the position of the stations, it is possible to estimate satellite orbits and clock errors. Then the ephemeris and clock correction is sent from Earth to the S/C.

## Lunar Method Proposal

It is not possible to estimate the clock offset in the same way as it is done on Earth since there are no monitor stations throughout the Moon's surface at this moment. However, since all satellites of the constellation can be visible by a single GS on Earth at a point in time, it is possible to change the paradigm of clock offset correction. The choice is made to not distribute clock offset corrections to each satellite one by one, but rather to synchronize all of them with the same Earth-based time reference every 12 hours. This is possible only with a good estimation of the traveling time of the synchronization signal.

For that, not only the ranging between the GS and each satellite is needed, but also the time delay coming from the propagation through the Earth's atmosphere (propagation in space is fairly simple). It is possible to know with a precision of  $10^{-8}$  [10] the index of refraction (modifying angle and speed of EM waves) in the atmosphere, for a given wavelength and given observable conditions. This is enough to compute the traveling time over the RF path. Finally, the calculated estimation error on the time delay induced by the atmosphere is around  $10^{-14}$ , which is low enough to not perturb Pegasus system.

### 3.1.5 Navigation Signals

Pegasus satellites transmit navigation signals in one frequency band. The signal, including the data modulated by the Pseudo-Random Noise code, is modulated by the carrier at 1559[MHz] (figure 3.10).

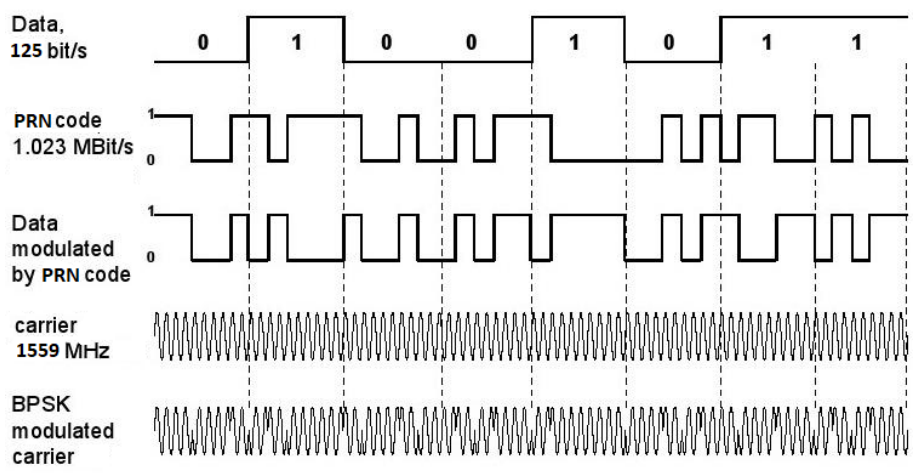


Figure 3.10: Navigation data modulated by the PRN code and carrier.

## Pseudo-Random Noise Code

The Pseudo-Random Noise Code (PRN) is a sequence of 0 and 1, unique to each satellite and known by receivers to allow identification. It is used to measure the travel time of the signal from the satellite to the receiver. The Pegasus ranging codes consists of Gold code binary sequences. Each code is generated using a tapped linear feedback shift register (LFSR). The Pegasus code uses  $LFSR = n = 10$  elements, so it generates a maximal-length sequence of length of  $2^n - 1 = 1023$ . The auto-correlation of the codes has to be narrow but high in amplitude to identify the satellite. But they have bounded small cross-correlation, which is useful when multiple signals are broadcast in the same frequency range.

## Navigation Message

In addition to the PRN ranging codes, a receiver needs to know the time and position of each active satellite. The navigation data is a binary-coded message, at 125 [bit/s]. Pegasus satellites encode this information into the navigation message, providing mainly:

- The ephemeris, own highly accurate orbital data for the transmitting satellite.
- The date, time, and the satellite's status, including ID.
- The almanac: status and low-resolution orbital data for the full constellation. The receiver uses the almanac to acquire a set of satellites based on stored time and location. As each satellite is acquired, its ephemeris is decoded so the satellite can be used for navigation.

**Message Structure** Pegasus navigation message is similar to Galileo's one [11]. Some data is removed since it is unused in this case, such as the ionospheric correction. The data put into the message is presented in table 3.3. The almanac consists of coarse orbit and status information for each satellite in the constellation. Each frame contains a part of the almanac and the complete almanac is transmitted by each satellite in 25 frames total (Fig. 3.10).

Data	Size (bits)	Type
Ephemeris	356	Orbital parameter
System time	32	System time
Clock correction	72	
Broadcast group delay	32	
GST-UTC conversion	99	
Satellite ID	6	Service parameters
Issue of data	N/A	
Signal health status	N/A	
CRC	24	
Satellite almanac	131	Almanac
Almanac references	16	
Signal in space accuracy	24	Integrity

Table 3.3: Data size of the navigation message.

**Super-frame Structure** Every page begins with a Synchronization Word (SW): it is not encoded, its purpose is to allow the receiver to achieve synchronization to the page boundary. Furthermore, it allows the receiver to achieve synchronization to the page boundary.

The second to last section on the page is dedicated to the Cyclic Redundancy Check (CRC). Globally the received page has three levels of error coding:

- A CRC with error detection capabilities after recovery of the received data.
- A one-half rate Forward Error Correction (FEC).
- Tail bits (sequence of zeros) to allow Viterbi decoding.

The last section of the page is for the tail bits for the Viterbi decoding. It has a length of 6 bits and consists of 6 zero-values that are used to enable the completion of the FEC decoding of each page. Each page goes through Viterbi decoding of the data which was created and encoded by convolution.

The navigation message is transmitted on the channel at a rate of 125 [bps]. We use a synchronization pattern of 12 bits with always the same sequence "101101110000". The purpose of this synchronization sequence is to allow the receiver to achieve synchronization to the page boundary to decode the data in the proper fields upon extraction.

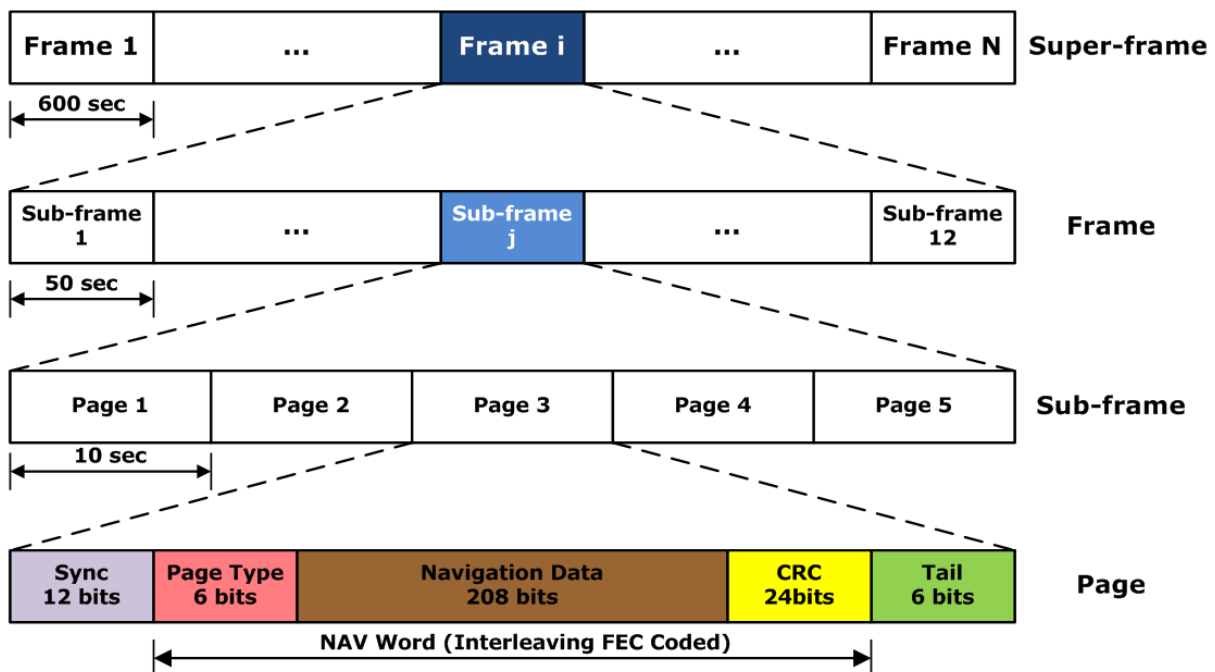


Figure 3.11: Super-frame structure. [11]

### 3.1.6 NS Antenna

This section discusses the process of selecting an antenna for the transmission of GNSS observables to the receivers on the Moon surface. This system is fairly simple to model, the satellites of this constellation are going to shower the Moon surface with the GNSS signal. The receiver model will only be defined by a constant minimum power at the reception that will encompass all noise, configuration, and obstruction uncertainties. The receiver antenna model will also be taken isotropic and neutral in order to give the clients flexibility in their antenna choices.

#### Navigation Link Budget

The analysis starts with the sizing of the antenna by using a Parabolic Model for the Emitter Antenna. The objective is to get a first model on which base the future antenna choice.

The Parabolic Model is taken with an efficiency of 0.6 and a pointing error of  $5^\circ$  which represents the misalignment between the Z-axis and the Moon-Satellite Axis. However, it is preferable to have the sizing of the parabola's beam-width as a calculated parameter to minimize it. Therefore, it will be computed hereafter as the minimum cone to cover the moon given the 10 000 [km] SMA.

For limited level of powers, in the order of magnitude of several hundred Watts the preference goes for an Solid State Power Amplifier(SSPA) over a more traditional Travelling Wave Tube Amplifier. SSPAs have the advantage of being more compact and lighter than TWTAs, but at the cost of a much lower electrical efficiency. This technology is increasingly used in space systems even though TWTAs are still the default choice because it is proven space technology.

The RF navigation link will be operating, like the Galileo Constellation, at 1 559 [MHz] and 125 [bps]. Also using a Direct Sequence Spread Spectrum modulation (DSSS), because of its resilience to jamming and noise reduction. The data stream is divided into small pieces and affected with a frequency channel across the spectrum. The navigation signal is then combined with the PNR at a higher data rate, which divides data based on a spreading ratio. The pattern being redundant makes it more resilient to interference and errors in transmission can be quickly corrected. The allowed chosen Bit Error Rate is  $10^{-6}$  which gives a Signal over Noise Ratio of 4.16 [dB] (figure 3.15b).

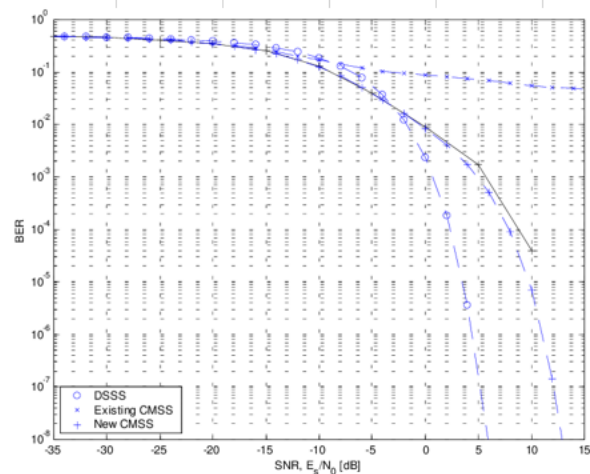


Figure 3.12: BER in function of SNR for DSSS. [11]

Finally, the following table shows the specifications for the signal receiver. To make the system the most accessible possible, the best approach is to create a minimum acquisition threshold requirement for the reception side. Therefore, the link will be sized to be able to provide the navigation signals to a receiver defined only by a minimum acquisition threshold of -160 [dBW] at reception. Considering an isotropic gain of 0 [dB] (neutral) for the receiver antenna. A summary of this baseline data for the link budget computation is in table 3.4.

Type	Data	Value	Unit
S/C	Minimum elevation	5	°
	Lunar orbit SMA	10000	km
	Antenna efficiency	0.6	
	Amplifier efficiency	0.2	
	Internal losses	1	dB
	Depointing error	5	°
Link	Frequency	1559	MHz
	Wavelength	0.192298	m
	Modulation	DSSS	
	SNR Eb/N0 (for BER at 10 <sup>-6</sup> )	4.16	dB
	Bit rate	125	bps
	Demodulator degradation	1.5	dB
	Margin	5	db
Navigation receiver	Antenna Gain	1	
	Minimum received power required	-160	dbW

Table 3.4: Navigation signal baseline data.

The model is further refined by calculating the required beam-width of the parabolic antenna and the impact of the pointing in the minimum gain on the resulting off-centered direction. A summary of all the computations is given below.

$$\theta_{beam-width} = 2 \tan^{-1} \left( \frac{R_{Moon}}{D_{SMA}} \right) \quad (3.5)$$

$$\theta = \sin^{-1} \left( \frac{R_{Moon}}{R_{Moon} + D_{SAM}} \cos(i_{elevation}) \right) \quad (3.6)$$

$$\theta_{3dB} = 2\theta + \theta_{beam-width} + 2\theta_{pointing} \quad (3.7)$$

$$A_{parabolic} = \frac{70\theta_{3dB}}{\lambda} \quad (3.8)$$

$$G_{antenna} = 20 \log \left( \eta_{ant} \frac{70\pi}{\theta_{3dB}} \right) \quad (3.9)$$

$$D_{max} = \sin \left( \pi - \theta - \left( \frac{\pi}{2} + i_{elevation} \right) \right) \frac{R_{Moon}}{\sin(\theta)} \quad (3.10)$$

Type	Data	Value	Unit
Satellite	Beamwidth	21.71	°
	$\theta$	8.48	°
	$\theta_{3dB}$	46.67	°
	Max distance to ground station	11457.74	km
	Maximal Gain	11.24	dB
	Gain at $\theta_{3dB}$	8.24	dB
	Antenna diameter	0.29	m
Link	C/N0	25.13	dB
	C/N0	325.77	Hz

Table 3.5: Navigation signal calculated data.

Based on these parameters it is possible to compute the Link Budget to retrieve the required transmitting power and its associated electrical consumption, with the following link budget problem statement.

$$P_t = 10\log(P_{r,des}) + LM + L_{FSPL} + L_{atmo} + L_{t,int} + L_{pointing} + 10\log\left(\frac{C}{N_0}\right) - G_t - G_r \quad (3.11)$$

$$FSPL = 20\log\left(\frac{4\pi D_{range}}{\lambda}\right) \quad (3.12)$$

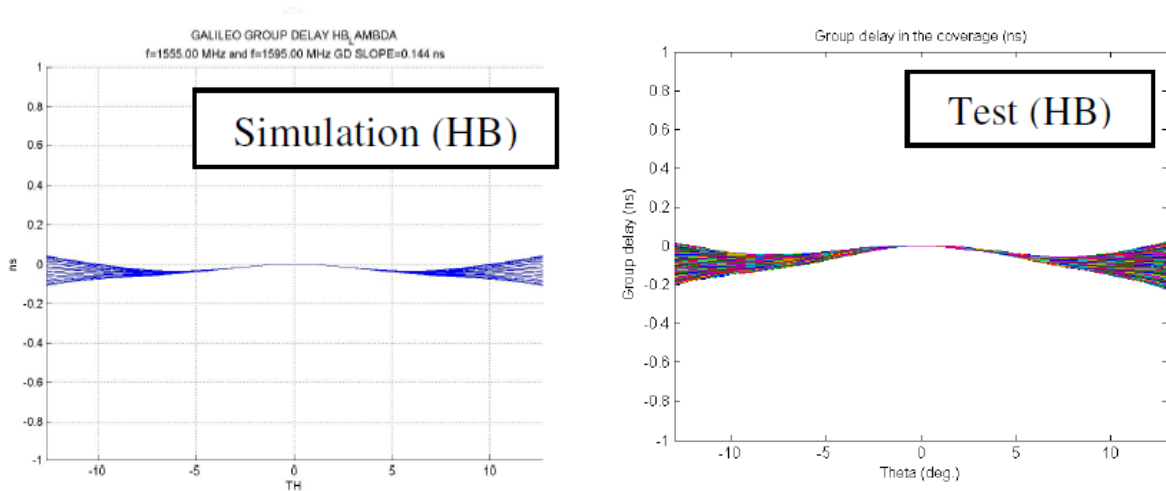
$$L_{atmo} = 0 \quad (3.13)$$

Data	Value	Unit
Free space losses	177.49	dB
Amplifier power	16.74	dBW
Amplifier power	47.22	W
Electrical consumption	236.12	W

Table 3.6: Power budget with depointing using a patch model

### Antenna Model

Even though the previous model is acceptable in terms of complexity and electrical consumption, it should be refined further. In order to provide good quality GNSS observables and a homogeneous signal throughout the Moon, the antenna pattern of emission should be very precise. One of the concerns is the group delays which could lead to incorrect ranging computation at the receiver's side.



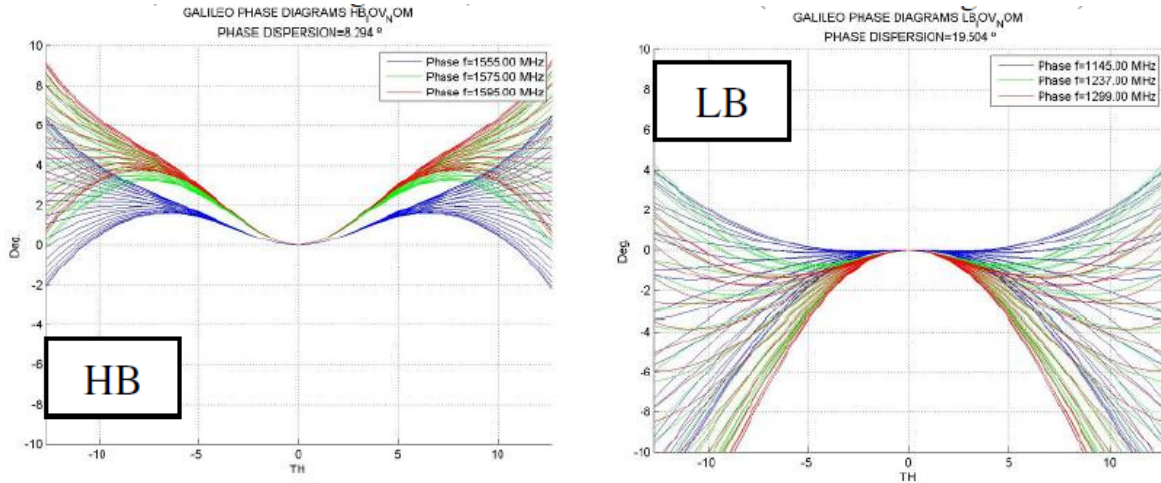
(a) Simulated Galileo group delay variation.

(b) Tested Galileo Group delay variation.

Figure 3.13: Galileo group delay variation over the coverage in high band. [12].

The figure 3.13 shows that it is required to have a homogeneous group delay throughout the useful antenna direction.

A concern is the phase dispersion on the antenna pattern, the goal is to have the most homogeneous phase pattern in our useful beam-width, again so that the ranging computation shall not be biased.

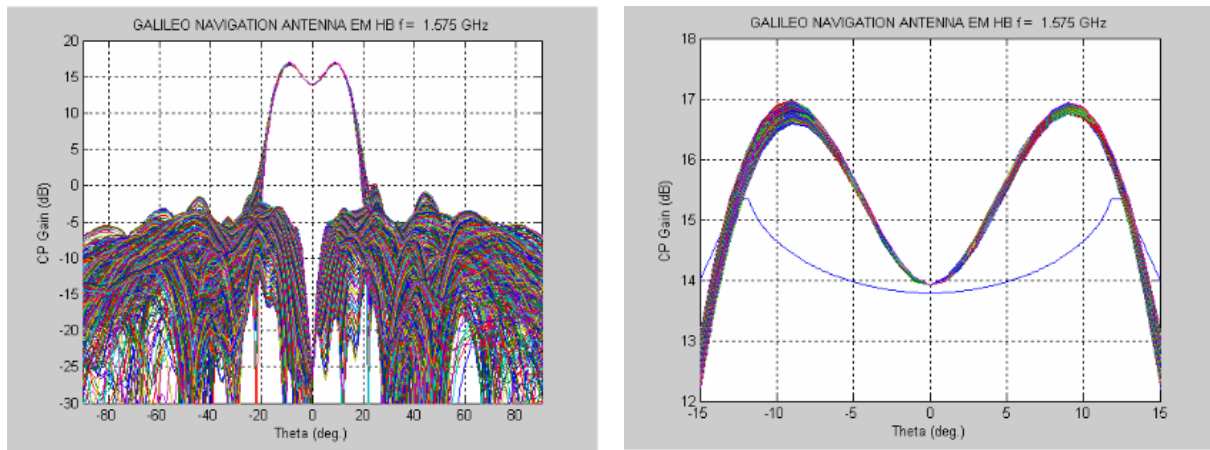


(a) Phase dispersion in High Band.

(b) Phase dispersion in Low Band.

Figure 3.14: Galileo phase dispersion optimizing BFN amplitude excitation. [12].

The other one is to demonstrate an equitable signal to all users on the moon, in other words, design an isoflux antenna to be consistent with this specification.



(a) Full 90° CPC-XPC pattern.

(b) Zoom of CPC in coverage area.

Figure 3.15: Gain radiation patterns in high band: for a carrier frequency of 1575 MHz. [12]

This leads to follow the design of the 42-element Galileo Antenna (Fig. 3.16), and change the space-segment antenna of the previous RF Link model. This results in the following new Satellite Data and antenna shape. Given that the required Beam-width for a GNSS signal is smaller for the Moon than for the Earth, we can get a higher gain for our GNSS antenna than Galileo's. We end-up with an isoflux antenna gain of 15 [dB], of a weight of 15 [kg] (Table 3.7).



Data	Value	Unit
Minimum elevation	5	°
Satellite lunar orbit SMA	10000	km
Antenna Gain at Boresight	15	dBi
Antenna Gain at Moon Limits	15	dB
Internal losses	1	dB

Table 3.7: Galileo model antenna satellite data

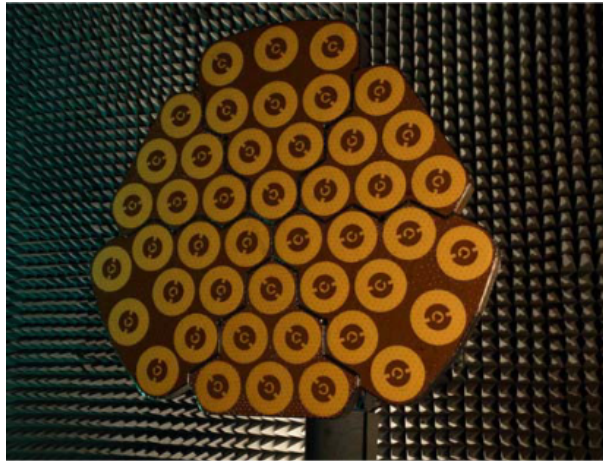


Figure 3.16: Galileo navigation antenna NAVANT [13]

Then the final electrical consumption required to emit the navigation signal towards the Moon surface is computed. The power budget summary is in table 3.8.

Data	Value	Unit
Free space losses	177.49	dB
Amplifier power	9.99	dBW
Amplifier power	9.97	W
Electrical consumption	49.87	W

Table 3.8: Power Budget computed with Galileo Antenna Model Navigation Signal

### Equipment choice and specifications

In order to be able to transmit the Navigation observables, the first step is to transform them into a signal and process it in the signal chain. To do so there is a need to implement the different electronic functions necessary for signal processing (which complement the data processing and namely navigation message assembly) in the Navigation Signal Frequency Generator and Up-conversion Units (NSFGUU).

These units take the input from the clock monitoring unit and complete it with the navigation and integrity data from the up-link. Then do the Pseudo-Random Noise encoding in DSSS and include the modulation process. It is then filtered and converted into an analog signal that is shifted into an L-band signal transmitted to the navigation antenna.



(a) NSG Unit in Galileo.



(b) FGU Unit in Galileo.

Figure 3.17: NSFGUU module photos. [14]

The last part of the signal processing before feeding the signal to the antenna is amplification. As stated earlier, the choice goes for the off-the-shelf SSPA given the relatively low amplified power and the electric consumption to mass trade-off.



(a) Teledyne Paradise Datacom 100W SSPA. [15].

Parameter	Specification
Operating Temperature	-40°C to +60°C
Output Power	Up to 100 Watts
Redundancy	Built-in Control
Maintenance	On/Off Controller
Reference Input Power	From -10 to 5 dBm
Dimensions	495 mm x 203 mm x 203 mm
Weight	20 Kg
Internal Power Consumption	2.5 W

(b) SSPA Teledyne Specifications. [15]

Figure 3.18: EBS Down-link Solid State Power Amplifier.

## 3.2 Emergency Broadcast System

### 3.2.1 Introduction

The SMS services are integrated into the Emergency Broadcast System (EBS), a redundant system to the Telecom constellation project, to maintain communication in case of failure. The purpose is to be able to receive a message from anywhere from the lunar surface and transmit it on the whole lunar surface. The first part is achieved with the orbit choice and satellite density of the constellation, but being able to transmit the message to the rest of the constellation for broadcasting is more difficult. The option of implementing an inter-satellite network was ruled out because of the complexity that it would add to the architecture. Thus, the last solution is through the GS network on Earth.

A synthesis of the units used for the EBS is presented in the following table ??.

Unit	Quantity	Mass [kg]	Power [W]	Operating T [°C]
EBS down-link antenna	1	0.13	67	-120/120
EBS up-link antenna	2	0.18	2.5	-90/90
Transponder	1	5.9	20	-20/60
Amplifier	1	20	2.5	-55/60
Total	5	26.39	92	N/A

Table 3.9: Synthesis of the emergency broadcast units.

### 3.2.2 EBS Signals

#### Operational Principle

**Service Message Types** The system is composed of four different types of messages:

- **SMS:** It is the standard SMS format. The short message includes the unique message identifier, the time of emission, the data with up to 2 [kBytes], the emitter, and the recipient ID. Upon request, other services like health telemetry data from astronauts could be added to the message.
- **E-SMS:** It is the Emergency service through the SMS system. The distress signal is a short message including a unique message identifier, the time of emission, the longitude, latitude, speed, direction, and the number of satellites in view by the user. It will also include the reference number of the beacon that can be tracked to a specific user. This message does not feature a configurable P/L, the data sent is predefined with the previously listed parameters.
- **ACK1:** Acknowledgment message 1 is sent back to the user upon reception of the message to be transmitted to the constellation. The goal is to inform the user that a message has been received at a specific time UTC. In case of emergency, it enables the user to know that a satellite is in range and is trying to forward the message back to Earth.
- **ACK2:** Acknowledgment message 2 is sent back to the user upon reception of the message to be sent by the GS network. This message informs that an SMS of  $X$  bytes of data has been received. The user that activated the EBS knows its message reached by the control center on Earth through the GS network and will be handled appropriately.

**Proposed Solution Timeline** The general proposed solution is depicted in figure 3.19 and described below:

1. Any person with an L-band transmitter should be able to send data from the lunar surface to the closest satellite of the constellation.
2. The S/C sends a message AK1 back to the lunar surface.
3. The S/C then transmits the original message to Earth GSs, adding the satellite ID.
  - (a) If the message received is a message from an emergency beacon (E-SMS), the control center is automatically notified of a critical situation. The message is broadcasted automatically to the whole surface (activating the whole constellation), and ground control will monitor the gravity level of the situation.
  - (b) If the message is SMS, there are two possibilities:
    - The message is targeted to a static site by activating the closest accessible satellite to the receiver.
    - The message is addressed to a mobile receiver by activating all Pegasus S/C and broadcasting on the whole lunar surface. The activation methods lead to a broadcast on the surface on a different scale.
4. The GSs on Earth transmit the message back to Pegasus S/Cs, where the satellite sends a second acknowledgment message (AK2) back to the lunar surface.
5. The activated satellites broadcast the message to the area available under the +Z side of the satellite using an S-band antenna. Up to five different messages can be broadcasted by the same satellite at once thanks to an oversized bandwidth in the downlink.

**Alternative Method** If the scale of the broadcast is not chosen by the GS or a failure of the Telecom constellation is detected, all messages received will be automatically forwarded to the whole lunar surface.

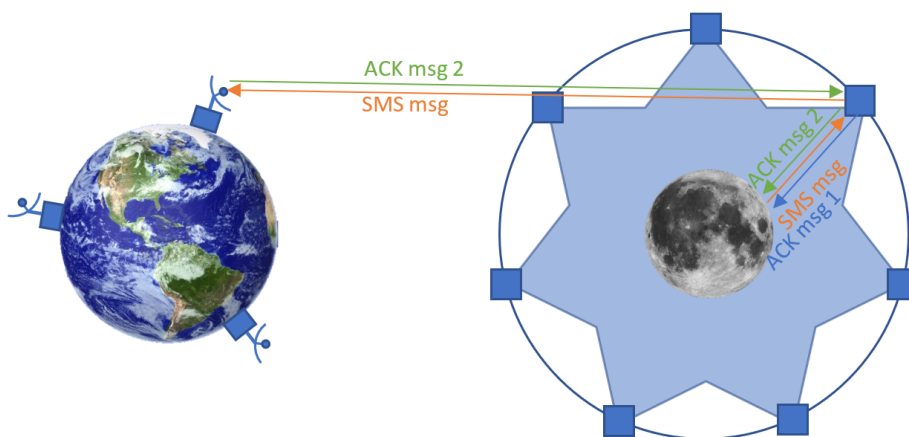


Figure 3.19: Chronological operation for the Emergency Broadcast System.

## Service Level

**Signal Time of Flight** The broad computation for the time it will take for the messages to reach Earth ground stations and Moon surface is presented. The distance between Earth and Moon is 356,500 [km] at minimum and 406,700 [km] at maximum. Taking into account that Pegasus has a SMA of 10 000 [km], and the speed of light  $c = 299\,792\,458$  [m/s]. The time to transmit a message can be calculated as follows:

$$T_{min} = \frac{d_{min}}{c} = \frac{366500}{299792,458} = 1.22[s] \quad (3.14)$$

$$T_{max} = \frac{d_{max}}{c} = \frac{416700}{299792,458} = 1.39[s] \quad (3.15)$$

The time to broadcast a message will oscillate between 2.44 and 2.78 seconds, for the satellites in view from Earth, to achieve total coverage with every satellite the time will increase.

**Global Response Time** After estimating the time of flight for the signal, other delays have to be taken into account for the response time between a sent message and the transmission.

Short messages can be sent to either the whole Moon surface or to the coverage area where the lunar base is located. When only one satellite is used to broadcast to a specific zone, the time to contact the satellite can be approximated to 5 seconds (to prepare the pipe and target the area).

For the E-SMS format, there is no human interaction needed for transmission, the data is broadcasted automatically, so this same delay can be assumed for the transmission to the satellites on view. However, since it is broadcast globally the message will have a delay induced by the time it takes ground stations on the Earth to contact enough satellites to cover the entire lunar surface (around six satellites). This transmission delay is estimated to be approximately ten seconds because all ACK signals have to be received from the ground.

To sum up the different delays from Earth reception to Moon broadcast:

- Time for single satellite broadcast: 5 [s]
- Time for global satellite broadcast: 10 [s]

In a potential future where many people will be on the Moon, it is thought that human interaction will be needed on Earth to interpret the situation, address the problem, and coordinate the aid. A permanent mission center will thus be able to respond to the emergency messages in real-time.

**Availability** The service availability depends on two parameters: communication between space/users segment and between ground/space segments. Lunar coverage and impact of the eclipses on the telecommunication with Earth have been studied to compute the EBS availability at 100 [%].

**Lunar Coverage** As said in section *Navigation 3.1.2*, to provide an accurate navigation service four satellites must be visible at all times from any point on the lunar surface. Indeed, as seen in figure 3.4, the constellation has been sized for navigation purposes and there is a minimum of six satellites visible at all times to have good navigation service accuracy. Since the user needs to be visible by only one satellite to ensure SMS uplink coverage, the constellation is oversized for the EBS.

**Eclipse Impact** Pegasus three polar planes have a RAAN difference of  $120 [^\circ]$  between each other, only one plane can be hidden by the Moon and prevent S/C to communicate with Earth. In this case, the angle is such that only one satellite is completely hidden (Fig. 3.20). Thus during the whole mission, at least 20 satellites are in contact with Earth, which justifies the 100[%] availability.

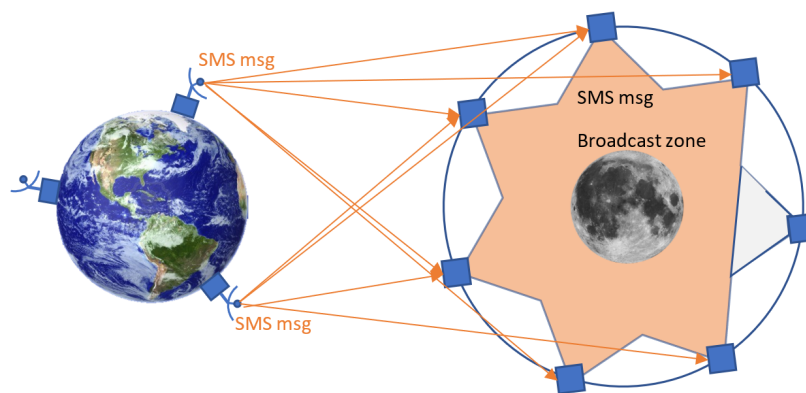


Figure 3.20: EBS eclipse availability.

### 3.2.3 EBS Antennas

The sizing of the antenna and signal processing for the EBS system was made starting from the previous study in section 3.1.6. The system, which roughly works as a bent-pipe and allows Earth Ground Control to broadcast SMS data over the Moon, would seem quite straightforward, at face value, but in actuality deserved to be studied a little further to be reasonably achievable.

A first sizing was done at 406 [MHz] for the Moon up-link, however, the resulting system would have required to use of a more expensive and complex antenna. Given that Pegasus doesn't have to comply with existing system on the Moon as Galileo SAR system had to do with Earth systems, the decision was made to customize requirements on the Moon. The same antenna used for TMTC will be used for EBS down-link to Earth, therefore the sizing of the Earth down-link will be covered in the TMTC section 4.1.

### EBS Down-link Budget

Similarly, as for the Navigation Link Budget the Link analysis is started by using a Parabolic Model for the Emitter Antenna. This, to have a first model on which to base the future antenna choice. The same baseline parameters as in section 3.1.6 where taken for the parabola, Efficiency: 0.6, Pointing Error: 5 [deg].

The selected type of amplifier is again a Solid State Power Amplifier (SSPA) instead of a Travelling Wave Tube Amplifier. This is because the satellite is still in the power domain of SSPAs and the priority was given to the mass budget over the electrical power budget.

The system will operate in down-link at 2,150 [MHz] and a bit rate of 16,000 bps which is the bit rate required for Galileo's SAR (2 kbytes), in order to be able to reserve one channel. The Link Margin is 5 [dB] which is usual.

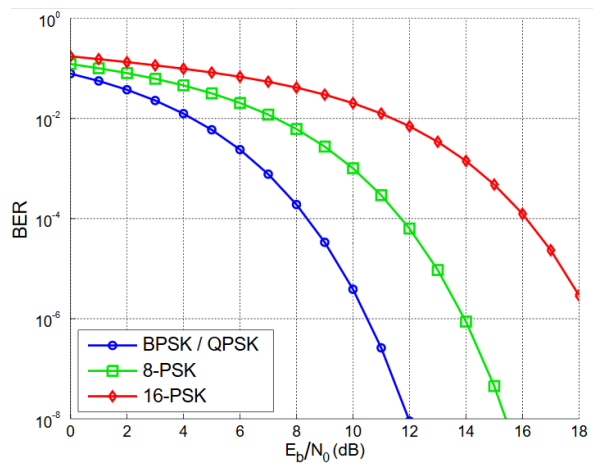


Figure 3.21: BPSK BER abacus [16]

The selected modulation is BPSK because of its good signal over noise property. For this modulation the goal is a  $10^{-6}$  Bit Error Rate, this gives a Signal over Noise Ratio of 10.5 [dB].

Regarding the receiver antenna model a parabolic antenna was initially taken, however, the calculations of its dimensions are done a posteriori to aim at a 15 [dB] of Effective Isotropic Radiated Power (EIRP), which is one of Galileo's SAR requirements that allows to size the space-segment antenna to transmit a reasonably powered signal. A summary of the base data can be found below.

Type	Data	Value	Unit
S/C	Minimum elevation	5	°
	Lunar orbit SMA	10000	km
	Antenna efficiency	0.6	
	Amplifier efficiency	0.2	
	Internal losses	1	dB
	Depointing error	5	°
Link	Frequency	2150	MHz
	Wavelength	0.139	m
	Modulation	BPSK	
	SNR $E_b/N_0$ (for BER at $10^{-6}$ )	10.5	dB
	Bit rate	16000	bps
	Demodulator degradation	1.5	dB
	Atmospheric losses	0	dB
Margin	5	db	
GS	Antenna diameter	0.416	m
	Antenna efficiency	0.5	
	Noise temperature	200	K

Table 3.10: Emergency Broadcast Signal Down-link Baseline Data

Based on this data to size the parabolic antenna to the required beam-width that makes it possible to shower the Moon with the SMS signal. Using the previous formulas 3.5, 3.6, 3.7 and 3.10 in section 3.1 to compute the dimensions of the antenna gain parameters from the pointing error and the elevation angle. The required diameter found is 0.21 [m]. The details of this computation, including receiver antenna, can be found below.

Type	Data	Value	Unit
S/C	Beamwidth	19.71	°
	$\theta$	8.48	°
	$\theta_{3dB}$	46.67	°
	Max distance to ground station	11457.74	km
	Maximal gain	11.24	dB
	Gain at $\theta_{3dB}$	8.25	dB
	Antenna diameter	0.21	m
Link	C/N0	52.54	dB
	C/N0	179523	Hz
GS	Antenna gain	52.70	dB
	Antenna gain	17.21	dB
	G/T	-5.79	dB

Table 3.11: Emergency Broadcast Signal Down-link Calculated Data

Keeping in mind the 15 [dB] of EIRP requirement, and an iterative method was used and an antenna of 0.36 [m] diameter was chosen for the reception of the Emergency Signal. The bore-sight gain of a parabolic antenna can be calculated with the following formula:

$$G_{parabola} = 10\log(\eta_{efficiency}(\frac{\pi D_{parabola}}{\lambda})^2) \quad (3.16)$$

Given this data and the problem perspective the following Link Budget problem statement can be used as the solution:

$$P_t = LM + L_{FSPL} + L_{atmo} + L_{t,int} + L_{pointing} + 10\log(\frac{C}{N_0}) - 10\log(\frac{1}{KT_r}) - G_t - G_r \quad (3.17)$$

Based on the 15 [dB] of EIRP, the following expression can verify the requirement of the parabolic antenna choice:

$$EIRP = 10\log(P_t) - L_{t,internal} - L_{t,pointing} + G_t \quad (3.18)$$

Data	Value	Unit
Free space losses	180.28	dB
Amplifier power	9.26	dBW
Amplifier power	8.45	W
Electrical consumption	42.23	W
EIRP	15.0	dB

Table 3.12: Emergency Broadcast Down-link Power Budget with Depointing



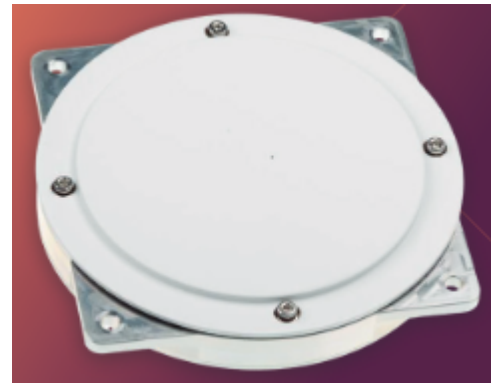
## Down-link Equipment

The Electrical Consumption of 42.15 [W] gives freedom to chose a cheaper off-the-shelf antenna; like the *Anywaves* S-Band Antenna, which will need some adaptation for input power but otherwise meets the minimum requirements. It would require also to have a slightly higher directivity going from  $90^\circ$  of half-power beam-width to  $70^\circ$  to have a 6 [dBi] antenna gain at the edge of the Moon (8 [dBi] at bore-sight). These antennas have been used and qualified by CNES for space flight and the materials already have Advance Label.

The Gain of this antenna is less than the satellite's best configuration, however, a modification can be made on both sides of the transmission to meet the 15 [dB] EIRP requirement. The new antenna data for our link budget can be found below (see data-sheet A.2).

Data	Value	Unit
Minimum elevation	5	$^\circ$
Satellite lunar orbit SMA	10000	km
Beam-width at 3dB	70	$^\circ$
Antenna Gain at boresight	7.5	dBi
Antenna Gain at Moon edge	6	
Antenna efficiency	0.92	dBi
Amplifier efficiency	0.2	
Internal losses	1	dB
Depointing error	5	$^\circ$

(a) Down-link satellite data.



(b) Anywaves S-Band model [17]

Figure 3.22: EBS Anywaves antenna

As stated earlier, there is a need to partially compensate the loss in the Transmitter Antenna with this equipment choice. To match the 15 [dB] EIRP an iterative method was used to chose a parabolic Receiver Antenna with a diameter of 0.47 [m]. The computation is done With the parameters of the transmission link, and using the same link budget formulation and EIRP formula as in earlier equations 3.17 and 3.18. The results are listed in the table 3.23.

Data	Value	Unit
Antenna diameter	0.47	
Antenna efficiency	0.5	
Noise temperature	200	K
Antenna Gain	55.59	
Antenna Gain	17.45	dB
G/T	-5.56	dB

(a) Receiver data

Data	Value	Unit
Free space losses	180.28	dB
Amplifier power	11.24	dBW
Amplifier power	13.30	W
Electrical consumption	65.52	W
EIRP	15.04	dB

(b) Power budget with depointing

Figure 3.23: Emergency Broadcast Anywaves Down-link

The electric consumption increased 24 [W] which is still reasonable. And all requirements are met for the transmission. Given the required power, the same amplifier choice and sizing are made, taking the SSPA from Teledyne Paradise but for a 2,150 [MHz] frequency (Fig. 3.18a). Furthermore, given Pegasus coverage mentioned in section 3.2.2, the loss of the EBS down-link system on one satellite is largely compensated for the other satellites of the constellation. Therefore, there is no need to implement redundancy for this system.

### EBS Up-link Budget

A Galileo like operating frequency of 406 [MHz] is possible for Pegasus GNSS System only at the high cost of a complex six-element antenna. The decision is then to operate at 950 [MHz] since there is no need to accommodate to any existing system of emergency signal emission from the Moon. It is known from Galileo's specification that it's possible to process signals at -159 [dB] of power and that there is also a minimum noise level to gain ratio to the respect of -17 [dB]. That is achieved with a Gaussian White Noise model with a Noise Temperature of 269 [°K], which is the black body temperature equivalent of the Moon's radiation level.

Following a similar link specification as in the previous section, with a BPSK modulation and a 2 [KBps] of bit rate coming from the Ground Emitter.

In addition, multiple access could be handle using Time Division Multiple Access with a cost on the data rate if necessary.

For the modeling of the Ground Emitter the best choice is to take a neutral antenna so that the clients of the system can use a wide set of antennas that just need to meet the minimum requirements that we are going to compute in this section and that will provide the necessary minimum acquisition threshold on the space-segment. The summary of baseline data can be found in figure 3.13.

Type	Data	Value	Unit
S/C	Minimum elevation	5	°
	Lunar orbit SMA	10000	km
	Antenna efficiency	0.6	
	Minimum input power	-159	dBW
	Internal losses	1	dB
	Depointing error	5	°
	Noise temperature	200	K
	G/T requirement	-17	dB
Link	Frequency	950	MHz
	Wavelength	0.30	m
	Modulation	BPSK	
	SNR Eb/N0 (for BER at 10 <sup>-6</sup> )	10.5	dB
	Bit rate	16000	bps
	Demodulator degradation	1.5	dB
	Atmospheric losses	0	dB
	Margin	5	db
GS	Antenna Gain	0	dB
	Antenna efficiency	0.6	

Table 3.13: Emergency Broadcast signal up-link baseline data

To select specific antennas that would minimize the power required on the emitter's side comparison between two types of antennas will be done. But first, the set of baseline data shall be completed with the following information on the satellite data and link data using the the previous equations 3.6, 3.7 and 3.10.

Type	Data	Value	Unit
S/C	Beamwidth to cover the Moon	19.71	°
	$\theta$	8.48	°
	$\theta_{3dB}$	46.67	°
	Max distance to ground station	11457.74	km
	Required antenna gain at Moon edge	6.01	dB
Link	C/N0	52.54	dB
	C/N0	179523	Hz

Table 3.14: Emergency Broadcast signal up-link calculated data

Now it is possible to compare two directive types of antennas: parabolic and helical. To get the gain of the parabolic antenna the equation 3.16 is used. To model the helical antenna a few parameters need to be fixed to fix our operation mode:

- Because the objective is to maximize the directivity it is necessary to be in axial mode, hence the circumference of the helical antenna needs to be in the order of magnitude of the traveling wavelength  $\lambda$ .
- To have a maximum efficiency of the antenna, the number of turns needs to be 6.
- To have best performance, choice of spacing between the turns is 0.23 of the circumference.

Now, the helical antenna bore-sight gain in axial mode can be computed with this formula:

$$G_{axial} = 10 \log \left( 15 \frac{C^2 SN}{\lambda^3} \right) \quad (3.19)$$

Antenna type	Data	Value	Unit
Parabolic	Max antenna gain	11.25	dB
	Gain at $\theta_{3dB}$	8.25	dB
	Diameter	0.45	m
Helical	Circumference	0.30	m
	Diameter	0.095	m
	Spacing	0.07	m
	Number of turns	6	
	Efficiency	0.8	
	Gain at boresight	13.16	dB
	Gain at Moon edge	10.75	dB
	Gain at $\theta_{3dB}$	10.16	dB
	$\theta_{3dB}$	44.27	°
Total length	0.41	m	

Table 3.15: Emergency Broadcast signal up-link parabolic and helical antennas calculated data

The parabolic antenna has a gain quite close to the minimum required gain. In order to have a better tolerance to unknown conditions for the emitter signal and lower their electrical consumption (keeping in mind the system must catch emergency signal emitted in emergency conditions) Pegasus will use the more directional helical antenna.

However helical antennas can be lengthy, which could make the placement for the launcher configuration complicated. This is also a reason for the increase in the frequency of the carrier so that the dimensions required to work in axial mode would be smaller. To improve the system, a multi helical antenna configuration is taken into consideration.

After a few iterations, the configuration of two antennas gave a good trade-off between the cost of the space segment and the simplification of emitter systems for ground emitters.

Data	Value	Unit
Circumference	0.30	m
Diameter	0.095	m
Spacing	0.069	m
Number of turns	6	
Efficiency	0.8	
Number of antennas	2	
Gain at boresight	13.17	dB
Gain at Moon edge	13.76	dB
Gain at $\theta_{3dB}$	13.17	dB
$\theta_{3dB}$	44.27	°
Total length	0.41	m

Table 3.16: Emergency Broadcast signal up-link multi helical antenna calculated data

A comparison of the performance of the link budget in terms of required antenna power and electrical consumption from the Emitter's point of view can be found hereafter.

Type	Data	Value	Unit
Single antenna	Free space losses	173.63	dB
	Amplifier power	11.38	dBW
	Amplifier power	13.77	W
	Electrical consumption	22.90	W
Multiple antennas	Free space losses	173.63	dB
	Amplifier power	8.37	dBW
	Amplifier power	6.87	W
	Electrical consumption	11.45	W

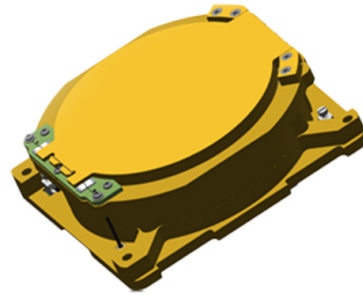
Table 3.17: Emergency Broadcast signal up-link emitter power budget comparison

Given that a smartphone uses 5 [W] of emission power, the value of 6.8 [W] is low enough to be compatible with numerous emergency conditions. Furthermore, the estimated electrical consumption for the Emitter is also compatible for long enough signal broadcasting.

The helical antenna selected is Helios antenna from Helical Communication Tech. This antenna has the very interesting advantage of being able to unfold itself at deployment making the space required smaller during the previous phases of the satellite’s life-cycle. This can be observed in the following photos.



(a) EBS Up-link Helix antenna model.



(b) EBS up-link Helix antenna folded.

Figure 3.24: EBS up-link Helix antenna photos of deployment. [18]

In the same way as for the down-link, given Pegasus coverage (at least 4 satellites always in sight), the loss of the EBS downlink system on one satellite is largely compensated by the other satellites of the constellation. Therefore, there is no need to implement redundancy for this system

### Transponder choice

For the signal processing functions, the same transponder model from Galileo is taken, which is the Search And Rescue Transponder from Kongsberg. The only difference is that it should be adapted to work with the frequency specifications of 1 [GHz] input with LNA to 2.15 [GHz] of the output signal.

The relevant specifications are listed below. An exhaustive list of the electronic functions and specifications can be found in the appendix of this report.



(a) SART model.

Parameter	Specification
Input frequency	1000 MHz
Output frequency	2150 MHz
Mass	5.9 Kg
Power consumption	20 W
Dimensions	397 mm × 207 mm × 118 mm

(b) SART main specifications.

Figure 3.25: Kongsberg Search And Rescue Transponder used for the EBS. [14]

### 3.2.4 Portable EBS User Specifications

**User Needs** The EBS can be used by multiple users on the lunar surface. The coverage of the entire surface means that having a mobile transponder easy to carry is mandatory to enable astronauts and robots to use the network. Thus, for astronauts, the device needs to be handheld, similar to the Galileo SAR transponders (Fig. 3.26). For easier usability, the device shall be able to record the voice of the astronauts when pressing a button: raw voice data or transcript as an SMS can be sent to the lunar base.



Figure 3.26: Example of a Galileo SAR beacon

#### Antenna User Specifications

**Down-link Signal** The downlink signal processing system shall have a minimum acquisition threshold of  $-170$  [dBW] (before antenna gain) at a frequency of  $2.150$  [GHz]. The type of antenna is not important but it should be noted that either a patch antenna or any wide beam angle antenna can be used for this purpose. It is noted that current technologies make it possible to use directional antennas with RF trackers to detect roughly our satellites.

**Up-link Signal** The uplink antenna should be able to send signals with a strength of  $8.3$  [dBi] at a frequency of  $950$  [MHz]. The uplink antenna should aim to have the widest beam angle for the best coverage because the exact position of the satellites of the Pegasus constellation is unknown to the ground emitter.

### 3.3 Payload Synthesis

As a summary of the extensive study about the P/L of Pegasus satellites, its mass and power consumption are recalled in table 3.18, whereas its performance is given in table 3.19. In addition, in figure 3.27 is provided a figure that regroups our different services and support equipment, to have a clear mapping of the interactions between space/ground (Earth links) and user/space (Moon links) segments. As a reminder, the Earth link is not only used for telemetry/telecommand but also ephemeris/clock corrections and Emergency Broadcast Signal transmission.

System	Mass [kg]	Power [W]
Navigation	93.1	364.5
Emergency Broadcast	26.39	92
Total	119.49	456.5

Table 3.18: Synthesis of the payload units.

System	Situation	Service level			
		GDoP	Position error [m]	Time error [ns]	Availability [%]
Navigation	Nominal	1.84	6.78	32	100
	Loss of 1 S/C	1.95	7.59	33	100
	Moon relief	2.73	11.74	43	96.6
EBS	Worst case	N/A	N/A	N/A	100

Table 3.19: Synthesis of the payload performance (lunar surface, errors @ $3\sigma$ ).

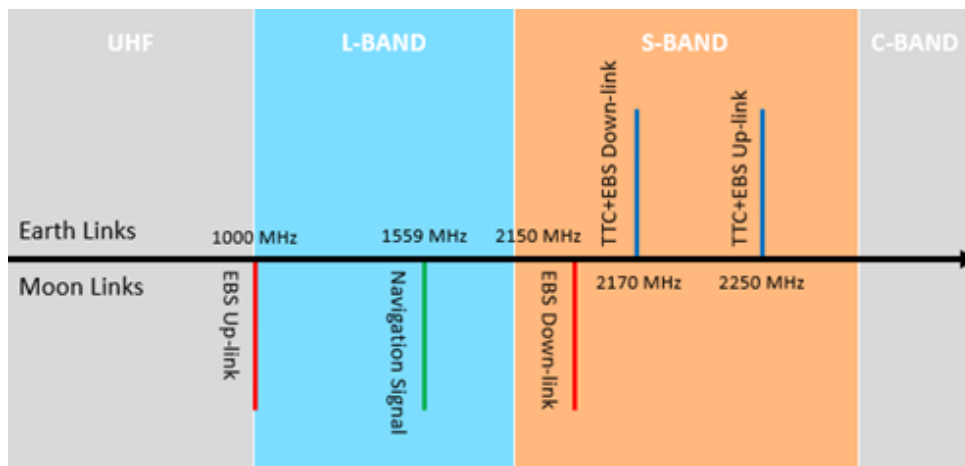


Figure 3.27: Synthesis of the carrier frequencies used by Pegasus antennas.

## Chapter 4

# Platform

Now that the payload of Pegasus satellites has been defined in detail in the previous chapter, this one this focus on the second and last system of a S/C: the platform. Hence, several subsystems necessary for the functioning and survival of the S/Cs are described in the following sections. A close look will be kept at the mass and power consumption of these additional items since they are necessary for guaranteeing the success of the mission, but do not directly contribute to it.

More precisely,

- Section 4.1 presents the *Telemetry, Tracking and Command* subsystem,
- Section 4.2 presents the *Propulsion* subsystem,
- Section 4.3 presents the *Attitude and Orbit Control System*,
- Section 4.4 presents the *Electrical Power* subsystem,
- Section 4.5 presents the *On-Board Data Handling & Software* subsystem,
- Section 4.6 presents the *Thermal Control* subsystem,
- Section 4.7 presents the *Structure* of the Pegasus satellites,



## 4.1 Telemetry, Tracking and Command

This chapter details the process of selecting an antenna for the transmission of TTC and EBS signals to the Earth. It's reminded that the choice was made in chapter 3.2 to merge the TTC and EBS data into the same telecommunication link. The discussion regarding data processing from TTC will be discussed in the section *On-Board Data Handling* 4.5.

### 4.1.1 Link Budget

An energy-efficient approach is taken, meaning that the link budget problem statement is done looking at minimizing the electrical consumption on the space segment. The type of antenna considered for the link budget is a parabolic one.

The issue of pointing the antenna towards a specific ground station on Earth is simplified by pointing the antenna towards the geometric center of the Earth and covering with our signal the full visible surface of the Earth. This can be done quite easily since only  $1[^\circ]$  of beam-width is required to cover the Earth from our Moon Orbit.

**TTC Down-link** Taking a very commonplace model, the minimum visibility elevation will be  $5 [^\circ]$  with a pointing error of  $5 [^\circ]$  as well and the link margin is  $5 [dB]$ . The type of amplifier is taken as a Solid State Power Amplifier with an efficiency of 0.2, this choice will be justified a posteriori.

Regarding the beam-width of the parabolic antenna, as stated earlier only  $1[^\circ]$  is necessary to cover the earth. A first iteration of the Link Budget gave us a very low electric consumption for such an optimized antenna: in the order of magnitude of  $10^{-1} [W]$ . Therefore, in order to save space, a wider beam-width of  $10[^\circ]$  was taken to the price of a higher electric consumption but decreasing the size of the antenna by two.

Noise temperature at the ground station is taken at  $269 [K]$ , the black body model of the Moon, since it's easier to point towards the full Moon, this strategy seems easier to model in order to get worse conditions to link budget problem statement. The size of the parabolic antennas on Earth is taken as  $7 [m]$  of diameter as it's a much commonplace and easy to access equipment by contrast with NASA's Deep Space Network and their  $13 [m]$  antennas that come with a very high cost.

Taken as before in chapter 3.2 a SNR of  $10.5 [dB]$  is necessary to reach a BER of  $10^{-6}$  of a BPSK modulation. BPSK is taken for its good resilience to noise.

The details of our baseline data can be found in table 4.1.



Type	Data	Value	Unit
S/C	Minimum elevation	5	°
	Lunar orbit SMA	10000	km
	Max depointing error	5	°
	Beamwidth	10	deg
	Antenna efficiency	0.6	
	Amplifier efficiency	0.2	
	Internal losses	1	dB
	Noise temperature	311	K
Link	Frequency	2170	MHz
	SNR Eb/N0 (for BER at 10 <sup>-6</sup> )	10.5	dB
	Bit rate	10500	bps
	Demodulator degradation	1.5	dB
	Atmospheric losses	0.2	dB
	Margin	5	dB
GS	Antenna diameter	7	m
	Antenna efficiency	0.5	
	Noise temperature	269	K

Table 4.1: TTC down-link baseline data.

These data are developed using some previously mentioned formulas. The parabola diameter equation 3.8, the link angles used to calculate the distance between the two bodies and the half power beam angle on equation 3.6 and 3.7. The formulas used to retrieve the parabolic antenna bore-sight gain in equation 3.16.

A custom approximation is taken for the worst-case scenario for the distance between a ground station on Earth and a satellite of the constellation taking into consideration minimum visibility elevation. The formula used is as follows:

$$D_{max} = \sqrt{(R_M + SMA)^2 - R_M^2} + \frac{\sin(\frac{\pi}{2} - \sin^{-1}(\sin(\frac{\pi}{2} + i_{elev})\frac{R_E}{R_M}) + i_{elev})}{\sin(\frac{\pi}{2} + i_{elev})} D_{T,M} \quad (4.1)$$

With  $R_E$  and  $R_M$  representing Earth's and Moon's mean radius at the equator,  $i_{elev}$  the minimum elevation, the semi-major axis of the satellite's circular orbit (Section 2.2.5) and  $D_{E,M}$  the Earth-Moon distance at apogee. The values are computed from our baseline data, and grouped in the following table 4.2.

Navigation Signal Calculated Data			
Type	Data	Value	Unit
S/C	$\theta_{3dB}$	20	$^{\circ}$
	Max distance to GS	417702.67	km
	Maximal Gain	18.66	dB
	Gain at $\theta_{3dB}$	15.61	dB
	Antenna diameter	0.48	m
Link	C/N0	50.71	dB
	C/N0	117811.94	Hz
	Wavelength	0.14	m
GS	Antenna Gain	12669.06	
	Antenna Gain	41.03	dB
	G/T	16.73	dB

Table 4.2: Navigation Signal calculated data.

Finally, the required transmitting power is computed using the same Link Budget Problem statement as earlier (Section 3.17). The results can be found in the table 4.3 below.

Data	Value	Unit
Free space losses	211.59	dB
Amplifier power	9.07	dBW
Amplifier power	8.07	W
Electrical consumption	40.37	W

Table 4.3: TTC down-link power budget with pointing error.

### TTC Up-link

To verify the sizing of the up-link part of the telecommunication channel, using the same antenna, the same logic and baseline data as in the down-link part is used again here. The only modifications are made for the link carrier frequency which is now 2250 [Hz] and the Noise Temperature in the Gaussian White Noise Model from the satellite's perspective which is 311[°K], Earth's black body model temperature. The following up-link required transmitting power (Table 4.4) is valid for each satellite of our constellation.

Data	Value	Unit
Free space losses	211.91	dB
Amplifier power	9.7	dBW
Amplifier power	9.34	W
Electrical consumption	46.68	W

Table 4.4: TTC Up-link power budget with pointing error.

### 4.1.2 Required Transmitting Power Simulation

In order to refine the previous TTC Link Budgets, the Pegasus constellation has been implemented in the Astrodynamics Software *FreeFlyer* from a.i. solutions. A capture of this simulation can be found in figure 4.1 below.

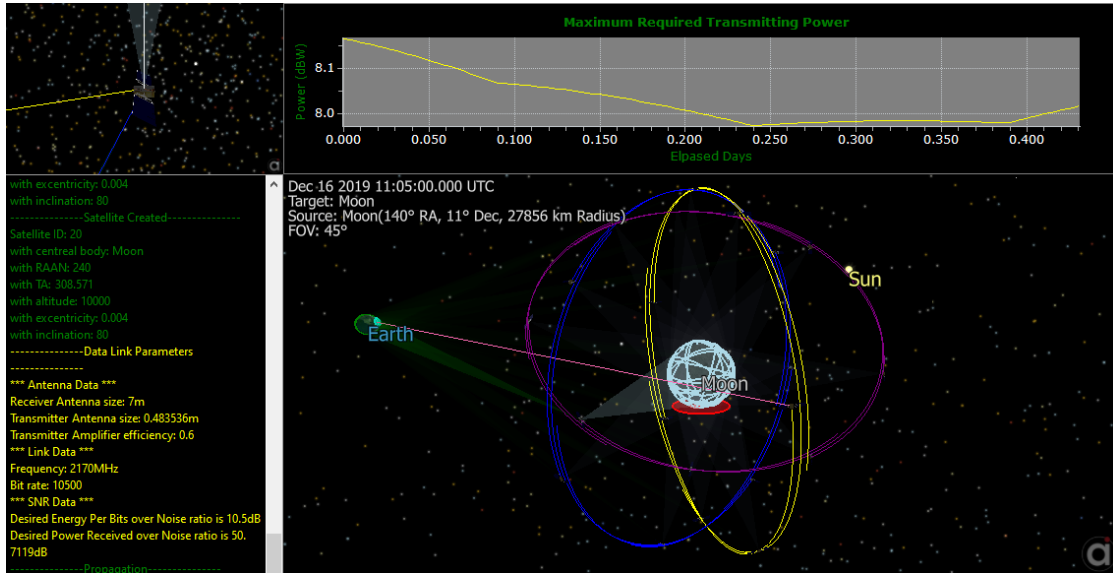


Figure 4.1: Screenshot of Pegasus constellation simulated.

The implemented link budget problem statement is computed at every step of the propagation for each satellite of the Constellation. The epoch of simulation runs for 27 days, which covers one apogee of the Moon that occurs during the night at day 16. Then, the maximum of required transmitting power is plotted over time in the figure 4.2.

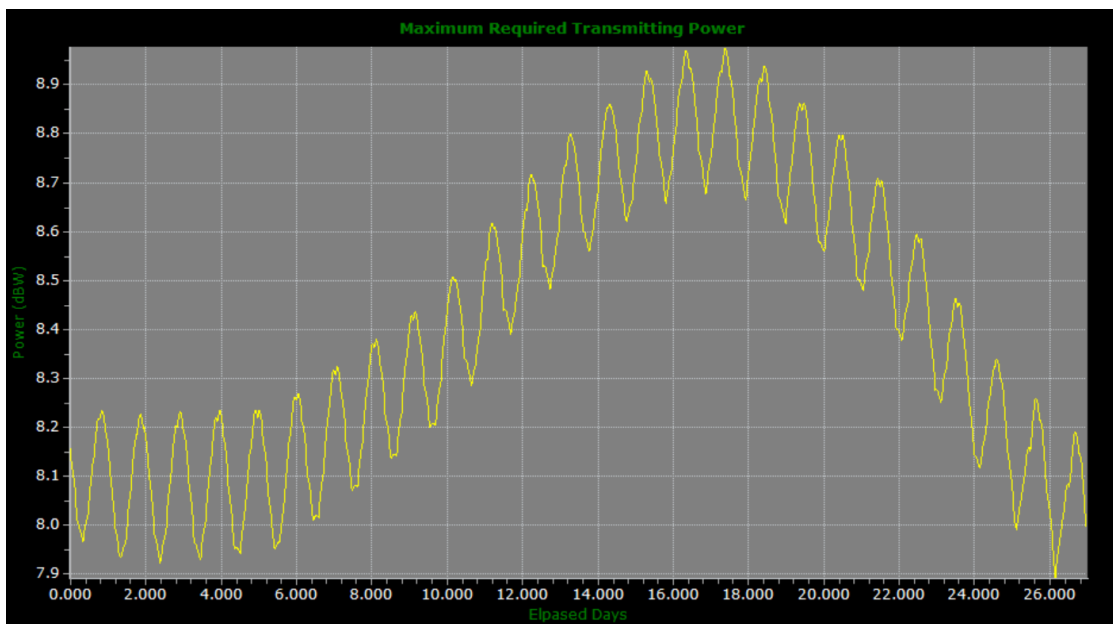


Figure 4.2: Required transmitting power simulated.

The maximum required transmitting power over time reaches a peak of 8.98 [dB] when the Moon is at its apogee. This value is slightly more accurate than the one from our previous analysis which was looking for the worst ever possible scenario. This comes from the difference between the exact distance between the ground station and farther satellite of the constellation and the worst-case distance estimated in the previous section. Therefore, our results are enhanced with this simulation.

### 4.1.3 TTC Equipment

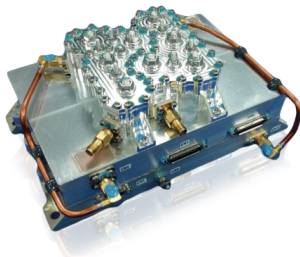
A synthesis of the units presented in this section can be seen table 4.5. Some of the equipment has been mentioned before, the Solid State Power Amplifier of Teledyne Paradise, referenced section *Navigation* 3.18, is used as an amplifier for several systems.

Part	Unit	Quantity	Mass [kg]	Power [W]	T [°C]
TTC	TTC antenna	2	10	40.3	-70/120
	Transceiver	2	1.25	18	-20/60
	Amplifier	2	20	2.5	-55/60
	Total	5	62.5	121.6	N/A

Table 4.5: Synthesis of the TTC units.

Regarding the Transponder model choice, the STC-MS03 S-Band TTC Transceiver from Honeywell was taken. This transponder is compatible with the link parameters. But needs a small adjustment on its frequency range to include our 2170 [MHz] frequency on its transmitting frequency range. It also has the advantage of being ESA Class-S qualified.

The main specifications of this equipment are listed below and the complete datasheet and diagram of implemented electronic functions can be found in Appendix A.3.



Parameter	Specification
Temperature Range	-20°C to +60°C
Minimum acquisition threshold	-120 dBm
Mass	1.25 Kg
Power consumption	18 W
Dimensions	160 mm × 110 mm × 44 mm

(a) STC-MS03 S-Band TTC (b) SART main specifications. Source: adapted from Kongsberg SART. from Honeywell

Figure 4.3: Transceiver Honeywell chosen for TTC Link.

## 4.2 Propulsion

### 4.2.1 Introduction

The objective of the propulsion part is to select the propulsion system used by the thrusters and to estimate the propellant needed for the whole mission to be able to size the tank. Once on the lunar transfer orbit, after the maneuver performed by the launcher from LEO, Pegasus satellites have to perform all nominal propulsion tasks:

- interplanetary maneuvers and lunar orbit insertion.
- station-keeping around the Moon.
- unloading of the wheels.
- control maneuvers to avoid collisions.
- orbit decay for the end of service.

For this part, the simulations have been done using *FreeFlyer*, as for section TTC 4.1. First, the choice of the propulsion system is studied in section 4.2.2, and the propellant mass necessary for the 10 years mission estimated 4.2.3, taking into account the dry mass calculated in section *Structure* 4.7. At last, the equipment identified for the Propulsion subsystem are described 4.2.4.

### 4.2.2 Propulsion system choice

Nuclear propulsion is not considered for safety reasons related to the launch; the lunar base, and environmental protection. Chemical and electrical propulsion systems can both be selected. Each one offers different specifications for which the main differences are the maneuver time  $\tau$  and mass of propellant  $m_p$  needed for correction. To avoid using as much propellant as possible, and to reduce the satellites' total mass, we consider a propulsion system using only electrical propulsion.

The first simulations of station-keeping have shown that chemical propulsion is possible but very demanding in propellant mass:  $\Delta V = 0.7$  [km/s] of impulsive maneuver required per year. The most important advantages of electric propulsion, with respect to conventional propulsion systems, are a low propellant consumption, allowing longer operations and a reduced spacecraft mass while allowing a highly controllable thrust for precise pointing. It is usually best in an application for attitude control or station keeping. It is also interesting for interplanetary purposes when the time is not an issue. That is why the deployment and end-of-life phases have been more deeply studied later in this section, exception of the lunar orbit insertion.

Hall-effect thrusters have been investigated as they offer a good balance between specific impulse  $I_{sp}$  and thrust  $Th$ . They take advantage of both electromagnetic (higher thrust) and electrostatic (higher  $I_{sp}$ ) technologies. Hall thrusters create a stream of electrically charged xenon ions accelerated by an electric field and confined by a magnetic field. As justified later in this section, the PPS 1350-G thruster ( $I_{sp} = 1660$  [s] and  $Th = 90$  [mN]) is considered for the mission. For every maneuver, one thruster has been simulated, to estimate the mass of propellant for the whole mission.

### 4.2.3 Xenon mass estimation

For all nominal propulsion tasks, speed change  $\Delta V$  and propellant mass  $m_p$  required have been estimated, the synthesis is presented in table 4.6. The main tasks requiring high speed change are the lunar orbit insertion, inclination correction and end-of-life maneuvers (around 30% for three of them).

Propulsion task	Affected parameter	$\Delta V[m/s]$	$m_p[kg]$	% needed
Interplanetary travel	N/A	N/A	6	4.3
Lunar orbit insertion	N/A	N/A	38	27.8
North/South correction	Inclination	889	42	30.8
East/West correction	Eccentricity & SMA	61	5	3.6
Wheels unloading and collision maneuvers	N/A	N/A	2	1.4
Orbit decay	SMA	969	44	32.3
Total	N/A	N/A	136	100
Total with 10% margin	N/A	N/A	149.6	100

Table 4.6: Xenon mass estimation for nominal tasks.

The way the propellant has been estimated for each mission phase is explained below. One can notice that the different phases are not presented in chronological order because estimating the propellant requires knowing the total mass of the satellite, which varies over time due to the propellant consumption. It is, therefore, easier to use the dry mass of the satellite as a starting point and to add successively the propellant used during each mission phase, in reverse chronological order.

#### End-of-life phase

The purpose of the end-of-life maneuvers is to reach a perigee altitude smaller than the Moon radius (see section *Mission Analysis* 2.3.2). This would indeed mean that the satellite crashes on the Moon. In the figure 4.4 can be seen the maneuver simulation using Freeflyer. For a satellite dry mass of  $\approx 710$  [kg],  $m_p \approx 44$  [kg] are required to reach the perigee and approximately 82 days of burst. One can notice that it takes longer to modify the altitude when getting closer to the Moon's surface. The simulation has been done in one maneuver, but in reality, this would require several to avoid possible collisions and precise location of impact, preferably on the North pole to avoid issues with the lunar base.

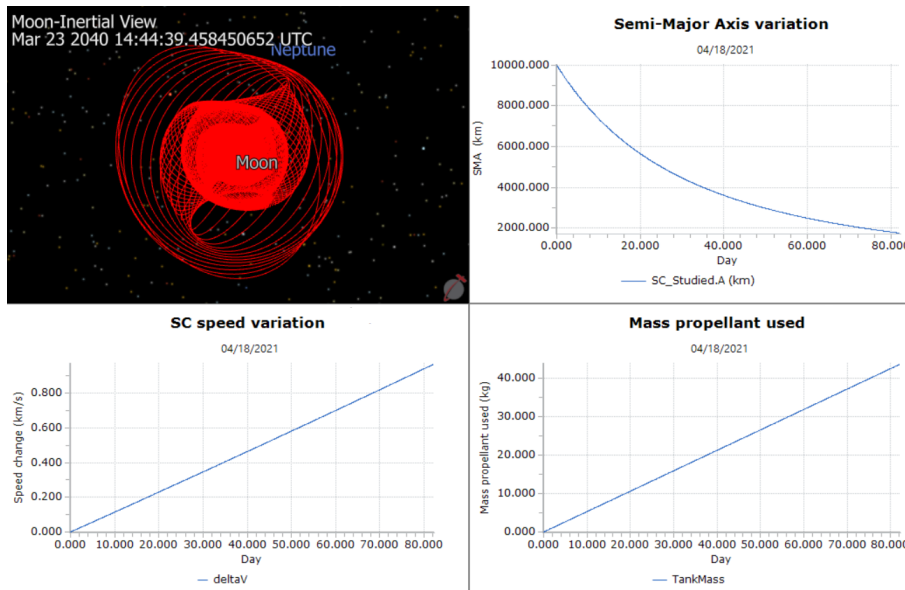


Figure 4.4: End of life simulation to estimate  $m_p$ .

### Station-keeping

Without station-keeping, for each Keplerian parameters, periodic variations around a mean value are observed (figure 4.5). The inclination is perturbed due to Earth and Sun gravity pull. The eccentricity is mainly perturbed by the solar radiation, not so much of the Moon oblateness as the altitude is high. The SMA seems stable but a correction of the eccentricity induces a variation of the SMA.

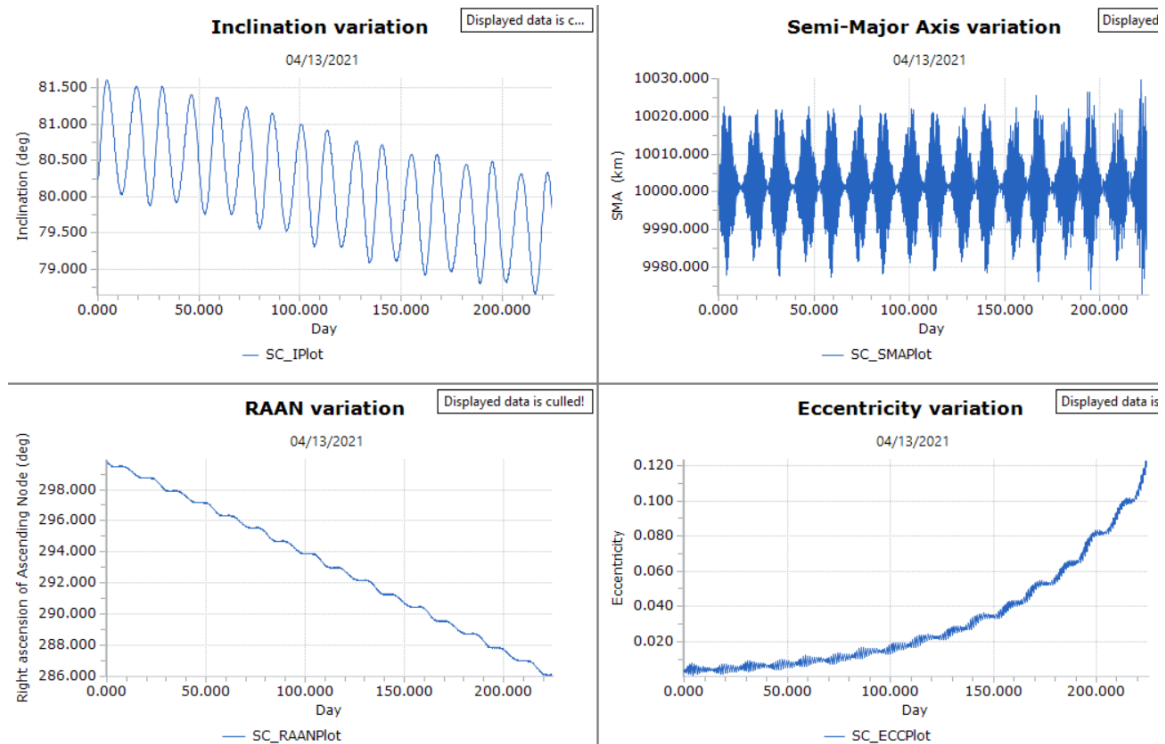


Figure 4.5: Keplerian parameters drift over 200 days.



The purpose is to correct the mean values when drifting too much:

- Eccentricity correction to get back to 0.003 when reaching 0.015. The average maneuvering time at the periapsis is about 180 minutes.
- SMA correction to keep the distance between +/- 30 [km]. Most of the maneuvering times at the periapsis are between 30 to 130 minutes.
- Inclination correction to keep the angle between +/- 1 [°]. The average maneuvering time at the node is about 190 minutes.
- No AoP correction as the orbit is almost circular.
- No RAAN correction as the orbits drift similarly, it is possible keep an angle of 120[°] between each. The RAAN precession is about 15 [°/year].

As shown figure 4.6, for 10 years, orbital parameters are correctly fixed. For a spacecraft wet mass of 754[kg] at the end of the deployment phase, the station-keeping requires approximately  $m_p \approx 47$  [kg] of xenon.

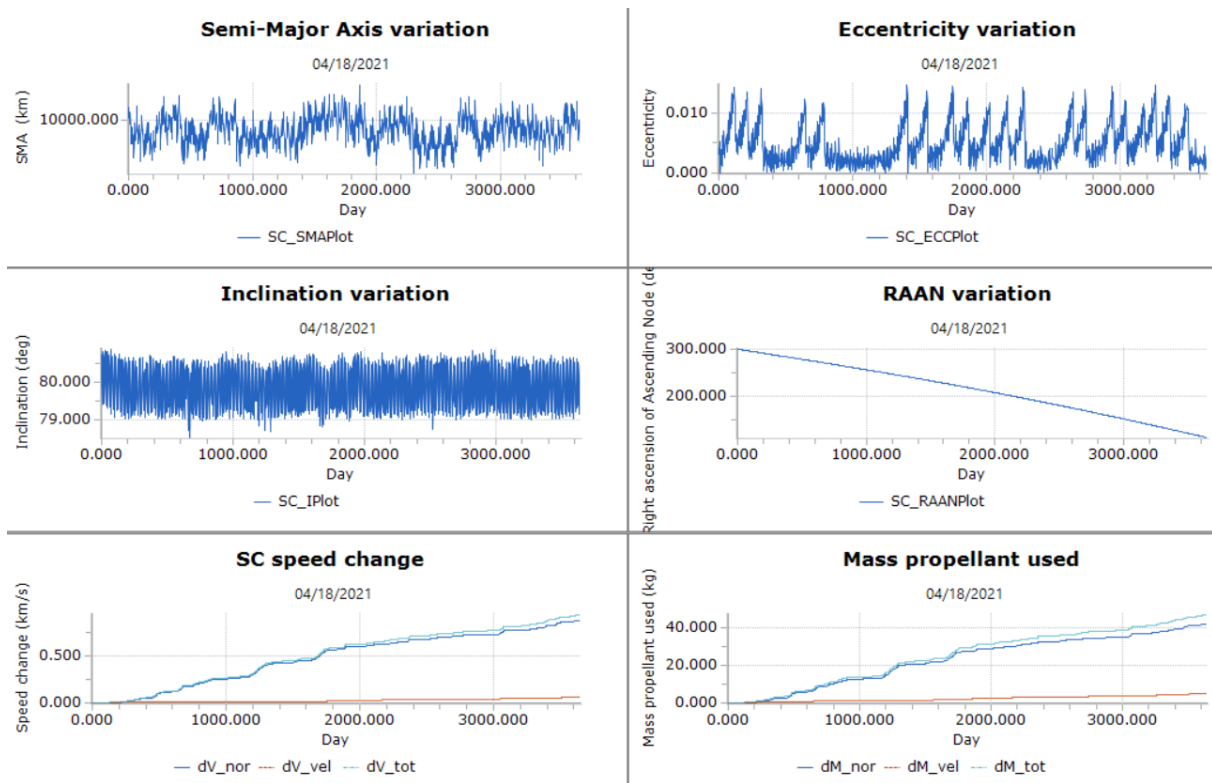


Figure 4.6: Station-keeping simulation over 10 years.

## Wheels unloading and collision maneuvers

As explained in section *AOCS* 4.3, solar sailing can only unload the wheels on two axes, thence thrusters are necessary for the last one. Moreover, some maneuvers might be needed to correct trajectories to avoid collisions. Both have been estimated at 2 [kg] of xenon together.

## Deployment phase

As presented section *Mission Analysis* 2.3.1, a LELET transfer is considered for the deployment phase. First, a very low-thrust arc  $Th = 0.08$  [N] is performed consuming 7[kg] of propellant. Then, there is a second longer manoeuvre requiring  $Th = 0.5$  [N], when approaching the Moon, to proceed to the lunar capture and eccentricity/perigee altitude diminution. For an initial wet mass  $m_0 = 1000$  [kg],  $m_p = 61$  [kg] of propellant are required for the phase.

The differences between the article [2] and the current proposal are:

- $I_{sp} = 1660$  [s] instead of  $I_{sp} = 3000$  [s], resulting in higher propellant necessary for the phase. As  $I_{sp} = \frac{T}{\dot{m}g_0}$ , for the same thrust, a diminution of 1.8 of the  $I_{sp}$  involves 1.8 times higher propellant mass flow  $\dot{m}$ . This difference implicates a consumption of  $7 * 1.8 = 12.6$ [kg] for the first manoeuvre and 97.2[kg] for the second.
- $h_p = 10000$  [km] instead of  $h_p = 100$  [km], resulting in less propellant necessary to perform the second manoeuvre, as the S/C does not need to get close to the lunar surface. It is assumed  $m_p = 40$  [kg] are needed for the lunar orbit insertion.

Thus, we would need  $m_p = 12.6 + 40 = 52.6$ [kg] for the deployment phase, with a wet mass of  $m_0 = 1000$ [kg], ie  $\frac{m_p}{m_p+m_1} = 1 - \exp(-\frac{\Delta v}{v_e}) = 0.0526$ . Knowing the mass necessary at the beginning of the station-keeping  $m_1 = 786$ [kg], a value of 136[kg] of xenon is computed for the mission.

#### 4.2.4 Electrical Propulsion System

The Electrical Propulsion System (EPS) is designed with the following modules:

- Thruster (low pressure system).
- Xenon flow regulation (low/high pressure system).
- Xenon storage tank (high pressure system).
- Power.
- Digital interface and communication system (discussed in section *OBDH*. 4.5)

A synthesis of the units used in this section is presented on table 4.7 and the flow regulation of these functions on figure 4.7. The datasheets for the equipment can be found in Appendix A.4.

Unit	Quantity	Mass [kg]	Power [W]	Operating T [°C]
Thruster	4	5.3	1500	-60/160
Robotic arm	2	15	40	N/A
Pressure regulator system	1	5.9	0	27/45
Storage tank	2	7	0	5/55
Xenon propellant	N/A	149.6	N/A	N/A
Power processing unit	1	10.9	126	-35/70
Filter unit	4	1	0	N/A
Total	13	235.97	6206	N/A

Table 4.7: Synthesis of propulsion units.

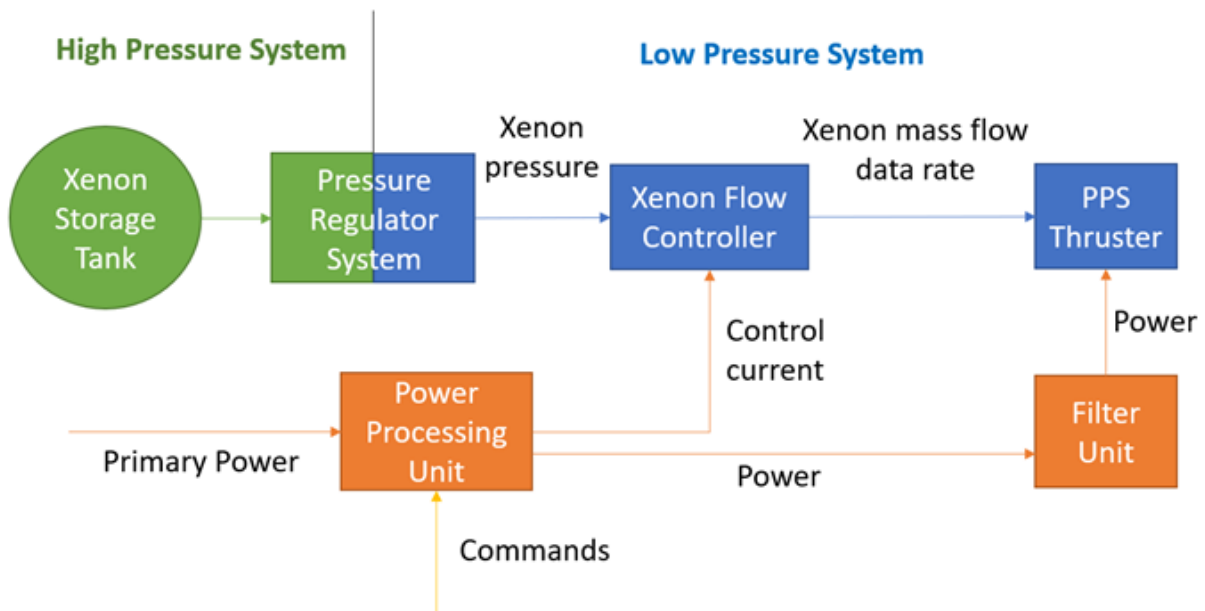


Figure 4.7: Flow regulation loop of the electrical propulsion system.

## Thruster module

### Thrusters

The PPS 1350-G thruster is considered for the mission. It is an electrostatic Hall-effect thruster manufactured by SAFRAN. It was successfully used for SMART-1 (1st ESA mission to the moon using only electrical propulsion in 2001) and more recently on two geostationary satellites: Inmarsat-4A F4 (2013) and Hispasat AG1 (2016). Its great advantage lies in its very high specific impulse  $I_{sp} = 1660$  [s] and very good thrust to electric power ratio  $Th/P = \frac{0.09[N]}{1500[W]} = 60[mN/kW]$ , which limits the activation time or the number of thrusters required. For more precision, read the datasheet of the thruster in Appendix A.4.

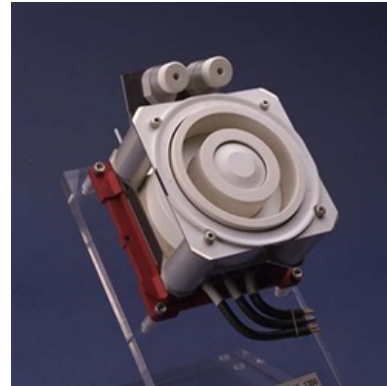


Figure 4.8: PPS 1350-G thruster [19].

Today, new solutions exist with better characteristics, such as the PPS 5000 ( $I_{sp} = 3000$  [s],  $Th = 200$  [mN]), but they require much more power. The PPS 1350-G has been chosen because preliminary studies have shown it is possible to perform propulsion tasks only using it. Thus, the total power required has been limited and the solar array sizing reduced (see section *Electrical Power* 4.4.6).

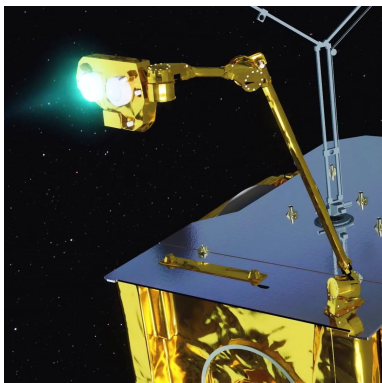


Figure 4.9: Eutelsat-172B robotic arm [20].

### Robotic arms

Pegasus satellites are equipped with two 2meter-long articulated thruster arms: one 1[m] beam, the second one of 0.75[m], and one 210 x 300 [mm] plate to put the thrusters. On the figure 4.9 is presented a similar system used on Eutelsat-172B (2017). Instead of thrusters embedded at the corners of the satellite, the twin deployable robotic arms can be moved freely about its body using three joints. It is used for the orientation of the thrusters and to control thrust direction and attitude. One pair of PPS 1350-G are placed on each of the arms, including one nominal thruster and one redundant.

This system has been selected instead of a platform thruster orientation mechanism or numerous non-movable thrusters for several reasons:

- Continuity of service: as station-keeping maneuvers must be performed without loss of service, the chosen propulsion system needs to be able to push in the +X, -X, +Y, and -Y directions while keeping the Moon side correctly pointed.
- Yaw law: as the S/C might be subject to a rotation around its Z-axis during station-keeping maneuvers, robotic arms provide the required flexibility in thrust direction modification.
- Contamination of antennas and solar arrays: the off-center position of the thrusters enables to limit of their contamination on sensitive surfaces of the satellites.
- Deployment phase: as 2 nominal thrusters have to be ignited in the same direction for lunar insertion, robotic arms allow this configuration with only four thrusters aboard.

## Xenon flow regulation module

A Xenon Pressure Regulator and Feed System (XPRFS), illustrated figure 4.10, based on bang-bang type regulation, regulates the high pressure xenon (max 12 [MPa]) down to a constant low pressure at 0.2 [MPa]. It incorporates a system of valves, a plenum volume, pressure transducers, and flow restrictors. The XPRFS provides a high degree of redundancy and failure tolerance, to ensure reliability  $> 0.998$ . The unit is supplied by ArianeGroup and has been used on nine satellites since 2005 **propulsion:PRS** (its datasheet is given in Appendix A.4).

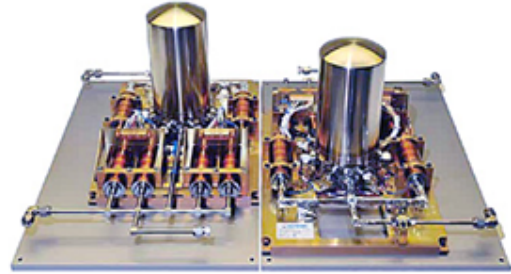


Figure 4.10: XPRF System. [21]

The low-pressure xenon is then fed into the Xenon Flow Controller (XFC). The XFC includes a thermo throttle which allows to provides fine control of xenon mass flow rate to the thruster anode and cathode. Two XFCs are already included in each PPS 1350-G, for a total of 8 XFCs.

## Xenon storage tank module

**Xenon characteristics** In section *Xenon mass estimation* 4.2.3, a total of 150 [kg] of xenon, with 10[%] margin, have been estimated for the mission. An advantage of using xenon is that it has a low critical pressure of 5.84 [MPa] (dot line on the figure 4.11a) to reach a supercritical fluid state. Between 6 [MPa] to 8 [MPa], a sharp increase of the density from 1.2 to 1.6 [kg/L] can be noticed. It allows the storage of more propellant mass in the same tank volume with a small increase in pressure. For a density of 1.6 [kg/L], if we consider 150 [kg] of xenon, the tank volume needs to be at least 94 [L] in total.

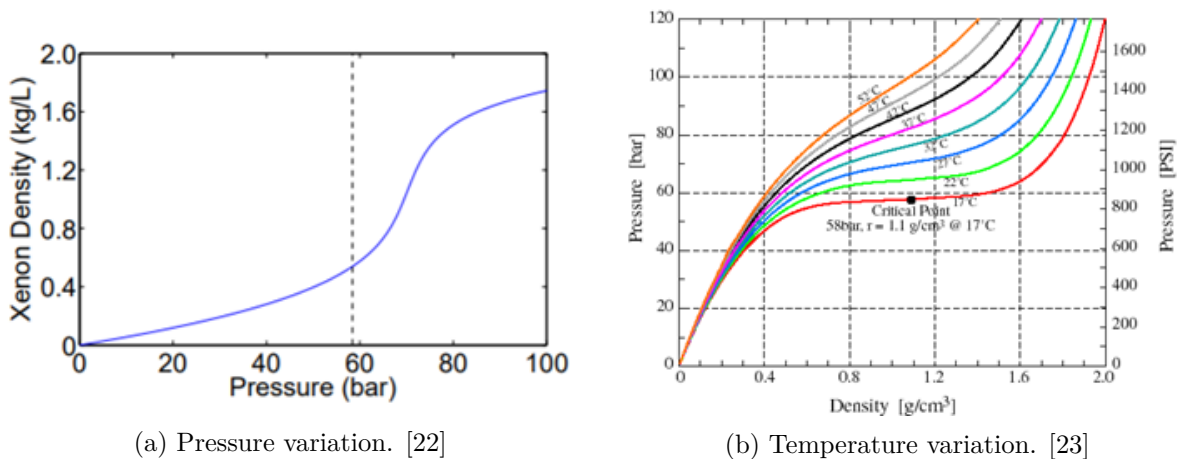


Figure 4.11: Xenon density variation depending on  $P$  and  $T^\circ$

As presented in figure 4.11b, xenon critical temperature is 17 [°C]. Thus, the density also depends on the temperature of storage: for the same pressure, the higher is the temperature, the lower is the density. The maximum expected operating pressure is 12 [MPa] as it is the maximum inlet pressure allowed by the XPRFS.

## Tank

The ETS VIII xenon tank [24] (figure 4.12) is selected as it is high performance, lightweight, and easy to manufacture. Two of them are needed as one tank can stock up to  $89[kg]$  of propellant. For ground processing at the launch facility, the xenon must be maintained in a supercritical state and its temperature cannot exceed  $55 [^{\circ}C]$  during loading, to avoid exceeding the tank maximum design temperature. To get a density of  $1.6 [kg/L]$ , the selected initial load pressure at  $12 [MPa]$  is  $42 [^{\circ}C]$ .

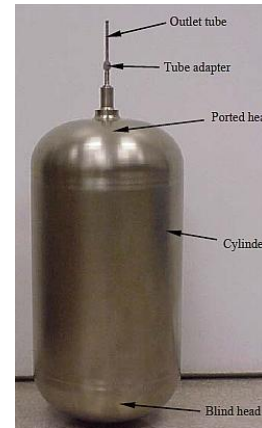
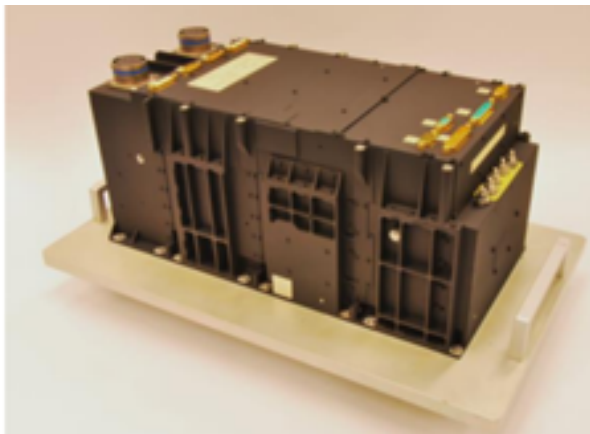


Figure 4.12: ETS VIII xenon tank.

## Power module

**Power Processing Unit** The Power Processing Unit (PPU) is responsible for the ignition and regular operation of the PPS. PPU MK1 (figure 4.13a), made by Thales Aliena Space [25] and already used on SMART-1, is selected. It controls the xenon flow and generates the required power to the thruster. It conditions the electrical power, represented by "Primary power" on the figure 4.7, from the  $50 [V]$  of the Power Distribution Unit to meet the  $300/350 [V]$  thruster requirements. For more details, its datasheet is given in Appendix A.4.

**Filter unit** With the thrusters behaving as noise generators at high frequencies, a Filter Unit (FU) is needed to provide filtering. One FU is located upstream of each plasma thruster to limit electromagnetic conduction from the thruster towards the PPU, for a total of 4 FU. The FU selected (figure 4.13b) has been validated with PPU Mk1 and was used for coupling tests PPS1350-G [25].



(a) Power Processing Unit Mk1 made by TAS.



(b) Filter Unit validated for the PPU Mk1.

Figure 4.13: Equipment of the power system.

## 4.3 Attitude and Orbit Control System

### 4.3.1 Introduction

In this section, the AOCS (Attitude and Orbit Control System) of the Pegasus satellites are detailed. This subsystem is responsible for controlling the attitude and position of the satellites throughout their lifetime, as well as sun acquisition by orienting the solar arrays. This section intends to bring more details about the several AOCS modes implemented aboard the Pegasus satellites for different mission phases (section 4.3.2), the way the system aids thermal constraints (section 4.3.3), the method used to desaturate the reaction wheels (section 4.3.4) taking into account the disturbing torques mentioned on section 2.4.4, and the chosen AOCS equipment (section 4.3.5). The following general functions must be performed.

- Initially, Pegasus is launched and inserted into an ellipsoid lunar transfer orbit by Ariane 6. After separation, it should be able to conduct sun acquisition, and solar array deployment autonomously and establish a three-axis attitude control commanded by ground operations.
- Pegasus then requires a reliable attitude and orbit control system, to successfully make insertion into lunar orbit at 10,000 [km] with an inclination of 80 [°]. Therefore, the AOCS must control a sequence of orbital maneuvers and perform accurate velocity increments through accurate three-axis attitude control and variable thruster cut-off timing.
- After having reached the correct lunar orbit, the satellite should maintain an accurate lunar pointing for high precision navigation service. Besides, implementing a *yaw steering law* (section 4.3.3) in order to meet payload equipment thermal constraints. Moreover, this specific attitude must be maintained during orbit corrections for ensuring continuity of service.

Regarding the AOCS requirements in terms of pointing accuracy and pointing stability, it should be noted that they are not stringent at all for navigation satellites since they broadcast their navigation signal in a very wide beam below them (see chapter 3). A pointing error of 1 [°] in pitch, yaw, and roll is typically acceptable. This low level of accuracy explains why the AOCS architecture of the Pegasus satellites is quite simple and doesn't require a lot of high-end equipment.

The orientation of the satellites is constrained by the need to have one panel facing the moon at all times, and one panel having no sun incidence for payload equipment thermal constraints as stated before. Thus, the following axis convention is defined (Fig. 4.14); where the moon side will be the +Z side, the +X side will be the anti-sun side created by the Yaw steering Law, and +Y and -Y are imposed by said constraints.

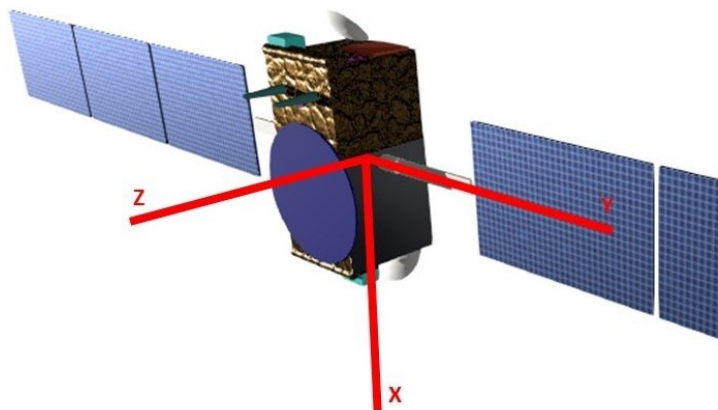


Figure 4.14: Satellite Axis convention.

### 4.3.2 AOCS Modes

The designed AOCS subsystem was developed considering the system requirements for different phases. In total, Pegasus has thirteen different modes that have been presented in deliverable *System Engineering Report*. The main ones for AOCS are summarized in table 4.8.

Mode	Description
Initialization	AOCS maintains the stand-by condition until a satellite separation signal is detected or a reconfiguration signal is received. After receiving these signals, AOCS sets the component configuration automatically.
Sun Acquisition Mode	AOCS searches for sun direction and acquires a sun-pointing attitude, in which the sun sensor is aligned to the sun direction. After the sun-pointing attitude is established, the solar arrays are deployed. Because the visibility from the ground is not guaranteed, the sun acquisition mode is done automatically.
Earth/Moon Acquisition Mode	AOCS maintains Pegasus yaw axis, the +z axis, pointing to the center of the moon in the lunar Attitude Control circular orbit.
Transfer Orbit Mode (Thrusting)	AOCS maintains Pegasus oriented toward the direction of the burn to insert the spacecraft into lunar orbit. This model takes into account the ignition of two PPS thrusters simultaneously.
Transfer Orbit Mode (Coasting)	AOCS maintains Pegasus oriented to keep the atomic clocks on the cold side of the spacecraft. This mode is used during most of the transfer and assumes all thrusters are off.
Normal Operation Mode	This mode is used for moon navigation from a circular lunar orbit. AOCS keeps the Pegasus three-axis attitude fixed in an inertial frame using the reaction wheels, which will then be desaturated by solar sailing.
Eclipse Mode	This mode is used for moon navigation from a circular lunar orbit. The thrusters will not be used during this mode to correct or desaturate.
Orbit Correction Mode	AOCS conducts orbital manoeuvres firing the thrusters.
Safe Mode	In this mode, AOCS continues outputting attitude control commands, to maintain ground communication using minimum on-board resources.

Table 4.8: AOCS modes description



### 4.3.3 Yaw Steering Law

**Introduction** As it has been seen in chapter *Payload 3*, the atomic clocks on board the payload of the satellite are very sensitive pieces of equipment, with a small thermal range of  $-5$  to  $10$   $^{\circ}\text{C}$  and a maximum temperature variation of  $\pm 1$   $^{\circ}\text{C}$  over 24 [h]. These thermal constraints can only be respected by maintaining one of the panels of the satellite with no sun incidence and by placing the clocks on this panel (that will be called the *anti-sun side*). The attitude steering law that enables to maintain one panel without sun incidence while keeping another panel pointed to the Moon is called a *yaw steering law*. Its name comes from the fact that both constraints can be met by rotating the satellite around its single Z-axis. For this to be possible, as it is shown in figure 4.15, the spacecraft must rotate  $90$   $^{\circ}$  in a quarter of orbit (approximately 6 [h] for the Pegasus satellites).

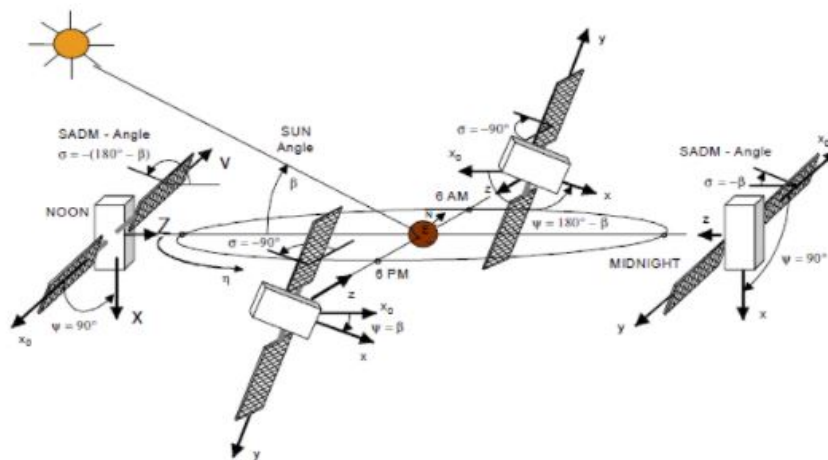


Figure 4.15: Representation of the yaw steering law [26].

**Conclusions** Undoubtedly, the introduction of a yaw steering law aboard the satellites, imposed by the sensitivity of atomic clocks, is a major design driver for several subsystems. That's why the main consequences of it on the other subsystems are summarized here:

- Thermal subsystem: due to the yaw steering law, the incident thermal fluxes will be very different from one side to another. On figure 4.15, it can be noticed that the *anti-sun* side (+X side) won't receive any solar flux during normal operations, but it can also be observed that the incident fluxes on the +Y and -Y sides will be very limited. This will be confirmed in the thermal analysis of section 4.6.
- Power subsystem: as figure 4.15 shows, the Y-axis of the satellite (where the solar panels are located) is always perpendicular to the Sun direction. This implies that rotating the solar panels around their axis would be enough to keep a  $90$   $^{\circ}$  incidence angle of the solar rays on them. This is advantageous since it is the configuration in which the solar cells can extract the maximum electrical power. This conclusion will be used in the design of the solar panels (see section 4.4).
- Structure: since the +X, +Y, and -Y sides will face the Sun for shorter periods than the other sides, the radiation level that they will encounter will be less. Hence, the design of the shielding around the satellite won't be the same everywhere (see section 4.7).

**Momentum requirement** As the yaw steering law requires to rotate the spacecraft around its Z-axis, it might be a sizing element for the actuators used for rotation: the reaction wheels. The purpose of this paragraph is to determine the minimum torque and kinetic momentum capacities of the reaction wheels so that the yaw steering law can be realized. Therefore, simple reasoning is performed. Assuming that the satellite needs to rotate of  $180 [^\circ]$  during 10 hours (with 1 hour of acceleration and 1 hour of deceleration), the rotation speed  $\omega_{S/C}$  that it must reach is given by equation 4.2.

$$\omega_{S/C} \approx \frac{180 [^\circ]}{8 [h]} \approx 1.091 \cdot 10^{-4} [\text{rad/s}] \quad (4.2)$$

Since this rotation must be reached in one hour, the angular acceleration of the satellite during the acceleration and deceleration phases is given by equation 4.3. This acceleration is generated by a torque  $T_{wheel}$  originating from a reaction wheel, as it is shown in equation 4.4.

$$\alpha_{S/C} = \frac{\omega_{SC}}{1 [h]} \approx 3.03 \cdot 10^{-8} [\text{rad/s}^2] \quad (4.3)$$

$$\begin{aligned} T_{wheel} &= -T_{S/C} = I_{S/C,z} \cdot \alpha_{S/C} \\ \text{with } I_{S/C,z} &= \frac{1}{12} \cdot m \cdot (l_x^2 + l_y^2) \approx 300 [\text{kg.m}^2] \\ \iff T_{wheel} &\approx 9.09 \cdot 10^{-6} [\text{N.m}] \text{ over one hour} \\ \iff \Delta H_{wheel} &\approx 0.033 [\text{N.m.s}] \end{aligned} \quad (4.4)$$

Hence, the torque that must be provided by the reaction wheel and the variation of kinetic momentum that it must withstand are respectively equal to  $T_{wheel} \approx 9.09 \cdot 10^{-6} [\text{N.m}]$  and  $\Delta H_{wheel} \approx 0.033 [\text{N.m.s}]$ . These values were kept in mind for the choice of the reaction wheels to place aboard the Pegasus satellites.

#### 4.3.4 Reaction wheel desaturation: solar sailing

It has been decided to rely on *solar sailing* for desaturation of the reaction wheels around two axes: the Z and X axes. This means that the satellites will take advantage of the small solar radiation pressure available in lunar orbit for desaturation purposes [27]. It should be noted that the solar pressure  $P_{SP}$  in lunar orbit has an order of magnitude of  $4.5 \cdot 10^{-6} [\text{N/m}^2]$ . The third axis will be desaturated using the electrical thrusters defined in section 4.2.

To desaturate around the Z-axis (figure 4.14), one solar array is rotated  $90 [^\circ]$  by its Solar Array Drive Mechanism (see section *AOCS Equipment* 4.3.5) so that it is parallel to the solar rays, while the other stays perpendicular to them (Fig. 4.16). In this situation, a torque around the Z-axis is created and can be estimated as follows. Assuming that (a) each solar array has a size of  $7.5 [\text{m}^2]$  ( $1.25 [\text{m}] \times 6 [\text{m}]$ ) and a center of pressure located at  $\frac{1.25}{6} = 4.8 [\text{m}]$  of the center of gravity of the spacecraft, (b) the torque generated by the perpendicular solar array is negligible, the torque generated around the Z-axis can be computed:

$$T_z = F \cdot l = P_{SP} \cdot S \cdot l \approx 6.4 \cdot 10^{-5} [\text{N.m}] \quad (4.5)$$

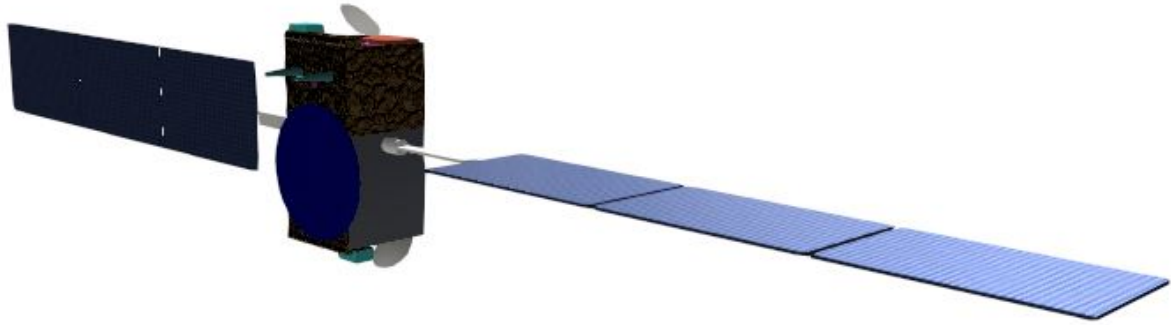


Figure 4.16: Desaturation around the Z axis

To desaturate around the X-axis, both solar arrays are rotated of  $45^\circ$ , but in opposite direction. The geometry is then similar to a wind turbine (figure 4.17). In this case, the specularly reflected solar particles generate a force normal to the surface [27], which tends to rotate the satellite around the X-axis (Fig. 4.14). If we assume that the proportion of specularly reflected particles  $\sigma = 0.25$ , the torque generated around the X-axis can be computed as:

$$T_x = 2 \cdot F \cdot l = 2 \cdot \frac{\sqrt{2}}{2} \cdot \sigma \cdot P_{S1} \cdot \frac{\sqrt{2}}{2} \cdot S \cdot l \approx 1.6 \cdot 10^{-5} \text{ [N.m]} \quad (4.6)$$

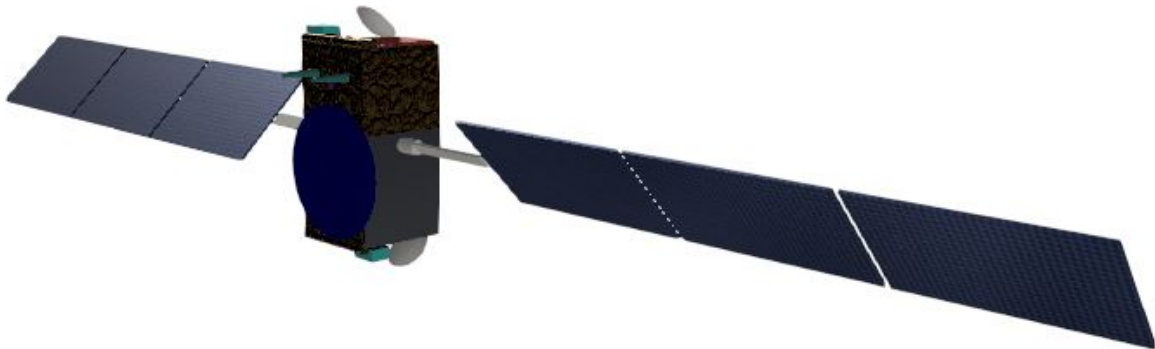


Figure 4.17: Desaturation around the X axis

Since the computed torques  $T_x$  and  $T_z$  are (at least) one order of magnitude higher than the other disturbing torques present in lunar orbit, it has been proven that the reaction wheel desaturation along the  $X$  and  $Z$  is possible with solar sailing. As it has been mentioned before, the electrical thrusters of section 4.2 will be responsible for the desaturation around the third axis.

#### 4.3.5 AOCS Equipment

The Pegasus AOCS subsystem relies on sensors and actuators. While the sensors provide information about the spacecraft's attitude and/or position, the actuators are used to control them. In the following paragraphs, the several sensors and actuators of the AOCS subsystem of the Pegasus satellites will be described.

A summary of the equipment is presented in the table 4.9, recalling the different units of it, their mass, power, and operating temperatures. The data sheets for all sensors and actuators can be found in Appendix A.5.

Unit	Quantity	Mass [kg]	Power [W]	Operating T [°C]
Sun Sensor	2	0.035	0.13	-25/70
Star Tracker	2	2.6	12.6	-30/70
Reaction Wheel	4	4.85	90	-20/70
SADM	2	4.25	4.6	-25/70
Total	10	33.17	304.66	N/A

Table 4.9: Synthesis of the AOCS units

## Sensors

**Sun Sensor** The Sun Sensors are responsible for sun acquisition. They help the spacecraft determine its orientation with respect to the Sun by measuring angles between their mounting base and incident sunlight. Aboard the Pegasus satellites, their main purposes will be (i) to provide the necessary information to the Solar Array Drive Mechanism (SADM) so that the solar panels can be pointed towards the Sun and guarantee energy production; (ii) provide the necessary information to the reaction wheels so that they can execute the yaw steering law (see section 4.3.3). After a short study, the NewSpace Systems (NSS) NFSS-411 sensor (figure 4.18) has been selected because of their acceptable performance levels and their small masses and power consumption.



Figure 4.18: NFSS-411 Sun Sensor [28].



Figure 4.19: AA-STR Star tracker [29].

**Star tracker** The star trackers are highly reliable and represent the latest technology in the field of autonomous attitude determination. It is used for inertial attitude determination by tracking stars' positions in deep space and comparing them to an onboard database. This inertial attitude can then be translated into an attitude with respect to the Moon if the spacecraft knows its position (which is the case thanks to the ephemeris described in section 3.1.4). In the Pegasus satellites, the AA-STR (figure 4.19) used for ESA's Herschel telescope will provide robust and accurate three-axis attitude determination with very low mass and power consumption.

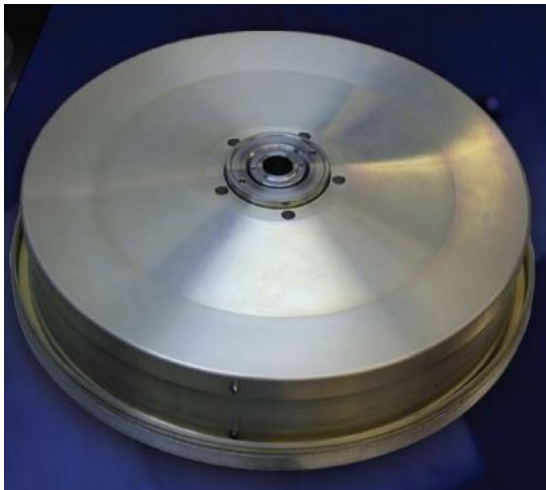
The design of the AOCS system was chosen, taking into account additional equipment to be fault-tolerant. As a consequence, Pegasus will have two sun sensors and two-star trackers in hot redundancy.

## Actuators

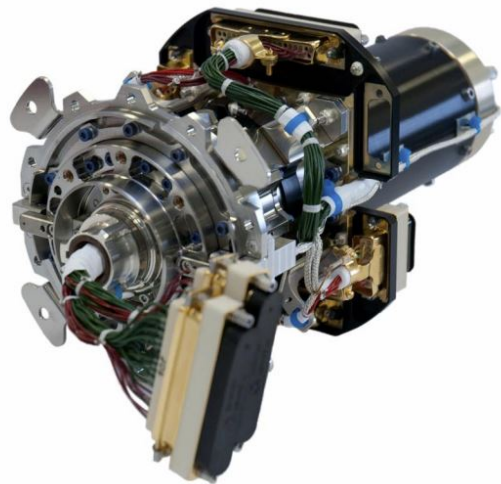
**Reaction Wheels** The reaction wheels aboard the Pegasus satellites are responsible for controlling the rotation of the spacecraft in three axes. This three-axis rotation is indeed necessary for (among others) guaranteeing lunar pointing of the +Z face and sun pointing of the -X face, and for compensating the disturbance torques existing in lunar orbit. A configuration of four redundant RSI 4-75/60 wheels (figure 4.20a) with an angular momentum storage capacity spanning a range between 0.04 [Nms] and 68 [Nms] is implemented. These wheels have indeed torque and momentum capacities that are high enough for the Moon environment and the yaw steering law (see section 4.3.3).

**Solar Array Drive Mechanism** The Solar Array Drive Mechanism (SADM) constitutes the interface between the solar array and the satellite. Moreover, it enables the solar array to rotate around its axis to face the Sun in the best possible way (and hence to generate the most electric power). As it will be seen in section 4.3.3, the introduction of the yaw steering law combined with the rotation of the SADM makes it possible to keep an incidence angle of  $90^\circ$  between the solar rays and the solar panels in every situation. Based on the size and mass of the Pegasus solar panels (computed in section 4.4), the Septa 33 SADM (figure 4.20b) has been chosen and its datasheet is given in Appendix A.5. This actuator is designed with a focus on robustness and for a lifetime of more than 12 years, is fully space-qualified and is used in GALILEO.

**Electrical thrusters** As it has been seen in section 4.3.4, the electrical thrusters that have been presented in section 4.2 have an important role in the AOCS subsystem since they are responsible for reaction wheel desaturation around one axis. That's why they are reminded here, even if they should not be considered as new equipment.



(a) RSI 12-75/60 Reaction Wheel [30].



(b) SEPTA-33 SADM [31].

Figure 4.20: Actuators.

## 4.4 Electrical Power

### 4.4.1 Introduction

The purpose of this section is to design the power subsystem of the Pegasus satellites. This is only possible after a thorough analysis of the several spacecraft modes defined in section 4.3 and the determination of the worst-case power consumption during the day and during the night. Standards primary and secondary sources are chosen to supply the satellites with energy: solar arrays deliver the necessary electrical power when they are illuminated by the Sun and a battery is used during eclipses. Knowing the power that has to be delivered, the solar arrays and the battery can be sized.

### 4.4.2 Power Budget

Before designing the solar array and sizing the battery, the satellite's power consumption must be estimated. This consumption relies on the several spacecraft modes defined in section 4.3. Each mode corresponds indeed to a given configuration of ON/OFF subsystem, as it is depicted in table 4.10, expected or attached S/C status are also shown. A more precise version of this table is available in Appendix, where the power consumption of each mode is computed by summing the individual consumption of every component (this individual consumption can be found at the equipment summary tables on every section describing a Pegasus' subsystem).

S/C Mode	Status		SubSystem status					
	Exp	Att	T/C	E/P	Prop	TTC	P/L	Avionics
Off/Standby		X	Off	Off	Off	Off	Off	Off
Test mode		X	On	Off	Off	Off	Off	On
Launch		X	On	Off	Off	On	Off	Off
Initialization	X		On	Off	Off	On	Off	On
Sun acquisition	X		On	On	Off	On	Off	On
Earth/Moon acquisition	X		On	On	Off	On	Off	On
Transfer orbit (thrusting)	X		On	On	On	On	Off	On
Transfer orbit (coasting)	X		On	On	Off	On	Off	On
Normal operation	X		On	On	Off	On	On	On
Eclipse	X		On	On	Off	On	On	On
Orbit correction	X		On	On	On	On	On	On
Safe	X		On	On	Off	On	Off	On
Intermediate safe	X		On	On	Off	On	On	On

Table 4.10: Spacecraft modes and their subsystem configuration.

From this summary table, the consumption of the satellite can be computed in the different configurations (the complete table can be found in Appendix A.6), and both the solar array and the battery can be sized. Here, it should be noted that the solar arrays will be sized in order to be able to provide enough power for the *Orbit Correction Mode*. The most demanding mode (*Transfer Orbit Mode (thrusting)*) will only be used during the day while combining the power produced by both the solar array and the battery. All in all, the power to be provided by the solar array can be summarized as in table 4.11.



Subsystem	Power [W]
Thermal	≈ 150
Electrical	≈ 10
Propulsion	≈ 1650
TTC	≈ 70
Payload	≈ 500
Avionics	≈ 400
Total	≈ 2800
Total + 10% margin	≈ 3100

 Table 4.11: Power consumption in *Orbit Correction Mode*.

Since this power consumption is subject to uncertainty, an additional 10[%] margin is taken into account. Hence, we size the solar array so that it can provide 3100 [W].

Regarding the battery, it will be sized based on the *Eclipse mode*, a special mode that has been designed to maintain the availability of the service during the long eclipses faced in lunar orbit. In this mode, consuming heaters must be switched on and it is chosen not to fire the electrical thrusters. Hence, the power to be provided during the eclipse by the battery can be summarized as in table 4.12.

Subsystem	Power [W]
Thermal	≈ 600
Electrical	≈ 10
Propulsion	≈ 0
TTC	≈ 70
Payload	≈ 500
Avionics	≈ 400
Total	≈ 1600
Total + 10% margin	≈ 1800

 Table 4.12: Power consumption in *Eclipse Mode*.

Again, since this power consumption is subject to several uncertainties, an additional 10[%] margin is taken into account. Hence, we size the battery so that it can provide 1800 [W] during the longest eclipses.

### 4.4.3 Architecture Definition

#### Topology

Two main architectures can be considered for designing a power subsystem involving a battery: the battery follower topology and the regulated topology. In the first case, the battery is directly connected to the solar arrays (for the battery charging) and to the equipment (battery discharging). As a consequence, the output power of solar arrays and the power needs of the equipment must remain in the operating range of the battery, to prevent damaging prematurely the battery. This implies constraints for the solar array sizing and induces non-negligible variations of the electrical power delivered by the battery (the discharge voltage of the cells depending on the state of charge).

That is the reason why a regulated topology is chosen. In this second configuration, a Battery Discharge Regulator (BDR) regulates the power delivered by the battery, so that the power bus is maintained at a constant voltage. A Battery Charge Regulator (BCR) controls the power delivered by the solar arrays to ensure that the charging power respects the charging requirements of the battery. This regulated architecture offers also the advantage of being more efficient and capable of delivering higher power peaks.

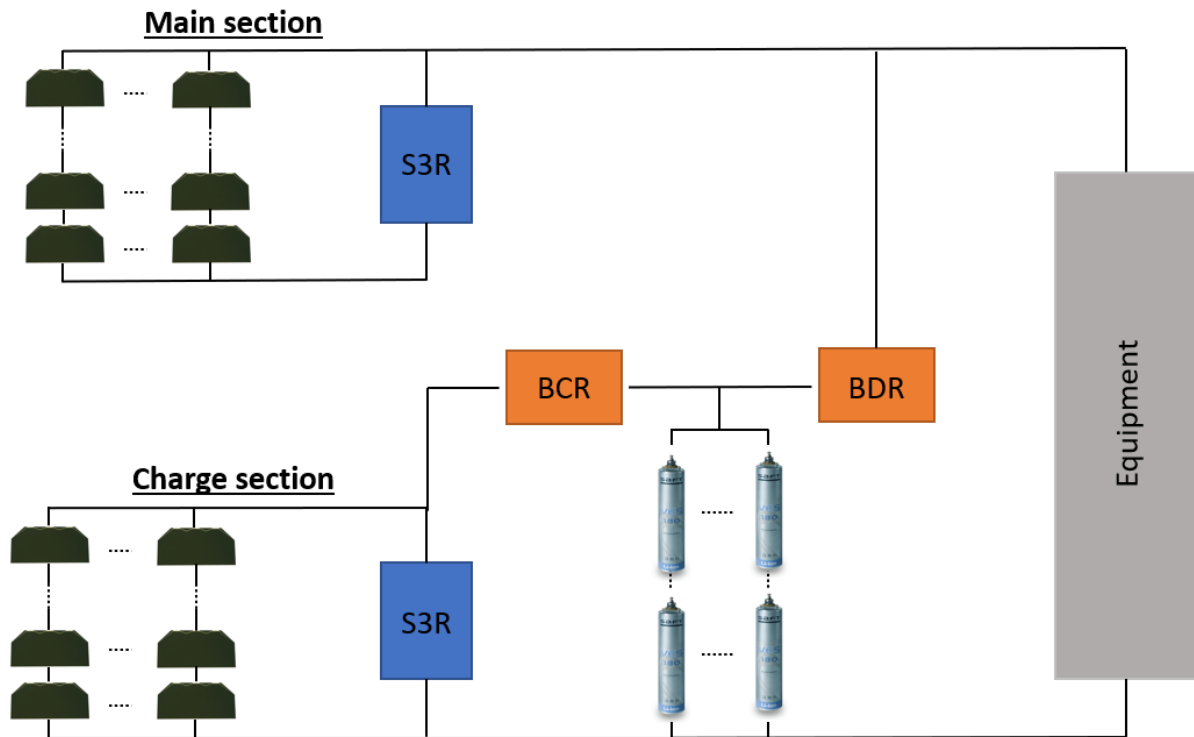


Figure 4.21: Schematic of the power subsystem.



## Solar Arrays Regulator

When solar arrays are illuminated by the Sun, they supply directly the equipment with energy (with or without the battery, in addition, section 4.4.5). As the power delivered by the solar arrays depends on various parameters (sun incidence, temperature, radiations dose), it is necessary to add an additional regulator aimed at controlling the power delivered to the bus. Two main controllers are usually used: the Maximum Power Point Tracker (MPPT) and the Direct Energy Transfer (DET).

The MPPT adapts the solar array voltage to deliver the exact required power to the equipment and is able to track the maximal power point voltage  $V_{mp}$  and current  $I_{mp}$  (which are the voltage and current for which the solar array delivers the maximum power). It is, therefore, able to maximize the delivered power whatever the sun incidence and the temperature of the solar cells.

On the other hand, the DET delivers a constant output voltage to the power bus. The corresponding cell operating voltage is close to the maximal powerpoint only if the solar array is sized in a proper way and if the conditions of temperatures, sun incidence, and radiations dose do not vary a lot during the lifetime of the mission. If both conditions are not respected, there is a risk that the delivered power is not sufficient for the correct functioning of the equipment.

An architecture based on a DET is chosen as it has the advantage to have a lower cost, it is less complex and less dissipative than the MPPT (that has an efficiency of approximately 95%). In addition, the yaw steering law and the rotation of the solar panels allow keeping a constant sun incidence. As a consequence, the sun's illumination only varies depending on the seasons and the eclipses. Due to this quasi constant illumination, the temperature of the cells is expected to remain stable and the efficiency of the solar arrays can be well predicted over time. Therefore, the sizing can be precisely done, and despite the fact that the DET does not track the maximum power point, the required power can be effectively delivered to the bus.

Even with good sizing, some variations of the generated power are expected due to seasonal effects, variations of the temperatures of the solar cells, or the performance reduction of the cells. To limit these variations, a Sequential Series switching Regulator (S3R) is used. This component increases the flexibility of the system by connecting or de-connecting sections of the solar arrays in order to deliver sufficient power in all situations.

The resulting architecture for the power generation and conditioning is depicted in figure 4.21. As it can be noticed, a part of the solar cells is dedicated to the charging of the battery (charge sections), while the other part (main sections) is used to supply directly energy to the equipment when the solar arrays are illuminated.

#### 4.4.4 Electrical Power Equipment

##### Power Conditioning Unit

Physically, the power conditioning is ensured by single equipment called Power Conditioning Unit (PCU) that contains the S3R, BCR, and BDR. The chosen PCU is produced by *Airbus Defense and Space*, provides a regulated 50[V] bus and is one failure tolerant [32]. The BDR has a modular architecture, each module being able to deliver 1 [kW], for a maximum of 6 [kW]. According to the power budget made in the section 4.4.2, a 2 [kW] BDR is sufficient for the Pegasus satellites. The PCU datasheet can be found in Appendix A.6.

##### Power Distribution Unit

As it has been said in the previous section, the PCU provides a regulated 50 [V] bus at its output. Despite the fact that most of the Pegasus equipment is designed for this voltage, some of them aren't. That's why a PDU (Power Distribution Unit) is needed aboard the satellite. However, thanks to the relatively small size of such a unit, its volume is neglected. Regarding its mass, it will be taken into account thanks to a simple empirical formula (Section 4.4.7).

##### Battery Cells

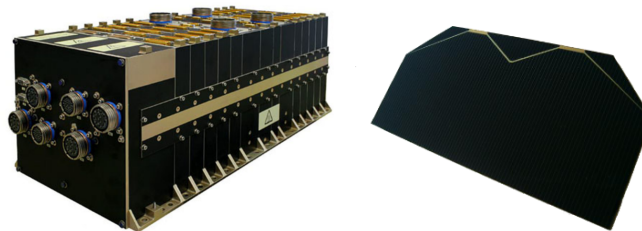
Li-Ion batteries are chosen for their high specific energy and high energy density that allow saving mass and volume. In addition, their thermal dissipation is lower than other cells like the NiCd or NiH2 cells and they can operate in a wider range of temperatures. Even if they require protection to avoid overcharge and over-discharge, this technology is nowadays well mastered and Li-ions cells have become a standard for space applications. After a short market analysis, the Li-ion *SAFT VES180* battery cells are selected since they offer excellent energy density, they are qualified since 2007 and have been used with success in many applications, as for example the Galileo In-Orbit Validation satellites. The corresponding datasheet is given in Appendix A.6.



Figure 4.22: SAFT VES180 battery cell [33].

##### Solar Cells

In the framework of this project, the triple junctions 3G30C Advanced solar cells of the company *AZUR SPACE* have been chosen. The corresponding datasheet can be found in Appendix A.6. This choice is explained by their high efficiency, especially at the End-Of-Life and by the fact that this type of cell have been widely used in the past decades [34].



(a) Airbus PCU 50V [32]. (b) Azur Space solar cell [35].

Figure 4.23: Chosen PCU and solar cells.

#### 4.4.5 Battery Sizing

##### Eclipse Duration

As it has been explained and proven in section 2.4.2, Earth eclipses are drivers for the sizing for the power subsystem since they cause the solar panels not to generate power for approximately 2 [h] 35 [min].

##### Battery Design

As the chosen PCU can only handle voltages between 27.5 [V] and 48 [V] and the battery cells' voltage varies between 3 [V] and 4.1 [V], it can be concluded that the number of cells to be placed in series  $S_{bat}$  must be 10 or 11. For failure tolerance purposes, the highest possible number is selected and the maximum/minimum/average battery voltages are obtained in table 4.13.

Property	Voltage [V]
$S_{bat}$	11
Minimum battery voltage	33
Maximum battery voltage	45.1
Mean discharge battery voltage	39.1

Table 4.13: Voltage properties of the battery.

Besides, the mean discharge current of the battery at night can be computed as:  $I_{dis} = \frac{P_{night}}{\eta_{BDR} \cdot V_{dis}}$ , with  $P_{night}$  the power to be provided during eclipse,  $\eta_{BDR}$  the efficiency of the Battery Discharge Regulator and  $V_{dis}$  the mean discharge battery voltage. The result is depicted in equation 4.7.

$$I_{dis} = \frac{P_{night}}{\eta_{BDR} \cdot V_{dis}} = \frac{1800 \text{ [W]}}{0.96 \cdot 39.1 \text{ [V]}} \approx 47.35 \text{ [A]} \quad (4.7)$$

To continue the sizing of the battery, the duration of the longest eclipse that can be encountered along the orbit of the satellite is needed. This duration is approximately  $T_{eclipse} = 2 \text{ [h]} 35 \text{ [min]}$  as it has been shown in section 2.4.2. By multiplying  $I_{dis}$  by  $T_{eclipse}$ , the maximum charge amount that can be discharged during an eclipse ( $Q_{d,max}$ ) is obtained. Moreover, in order for the battery to sustain the number of cycles, it will face during its lifetime, its maximum allowable *depth of discharge* (DOD) is limited to 70%. This means that an additional margin should be taken into account before finding the minimum capacity of the battery. Finally, based on this minimum capacity, the number of battery cells  $P_{bat}$  to place in parallel is obtained, together with the maximum DOD effectively reached and the effective battery capacity (equation 4.8).

$$\begin{aligned} P_{bat} &= 4 \\ DOD_{max} &= 0.64 \\ Q_{bat} &= 192 \text{ [A]} \end{aligned} \quad (4.8)$$

Now that the battery is sized (number of cells in series and in parallel), its failure modes can be investigated: the open-circuit and short-circuit failures. As it is known that every open-circuit failure will transform into a short-circuit failure after some time, only this last type must be analyzed. Because of the choice made regarding the number of battery cells in series ( $S_{bat} = 11$  instead of 10), it can be proven that the designed battery is failure operational.

As a summary of this reasoning, the main properties of the Pegasus battery are recalled in table 4.14, and a graphical representation of it is depicted in figure 4.24.

Property	Data	Unit
Number of cells	44	
Battery capacity	192	[A.h]
Mean discharge voltage	39.6	[V]
Power output	1800	[W]
Battery weight	48.84	[kg]
Battery volume	3.21e+07	[mm <sup>3</sup> ]

Table 4.14: Main properties of the designed battery.

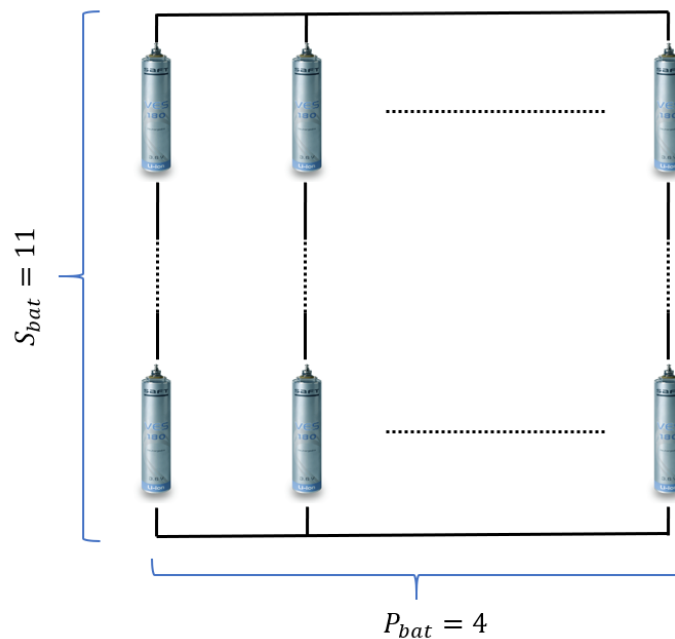


Figure 4.24: Design of the battery.

#### 4.4.6 Solar Arrays Sizing

##### Solar Cells Degradation

Solar radiations are responsible for the early degradation of solar cells. It is important to characterize their effect as it will have a direct impact on the solar array sizing. A simulation is performed with the software *SPENVIS*, which uses a model developed by the Jet Propulsion Laboratory. The simulation duration is set to 10 years, and the spacecraft is placed at a distance from the Sun equivalent to 1 AU, in “near-Earth interplanetary” conditions. In this configuration, it is considered that the spacecraft is outside the Earth Magnetosphere (no influence of the trapped particles), but that it is at a sufficient distance from the Sun (best model possible for a satellite orbiting the Moon). As the penetration of the particles depends on the characteristics of the solar cells, the simulation is performed specifically for the Azur 3G30 cells. Results obtained are depicted in the figure 4.25.

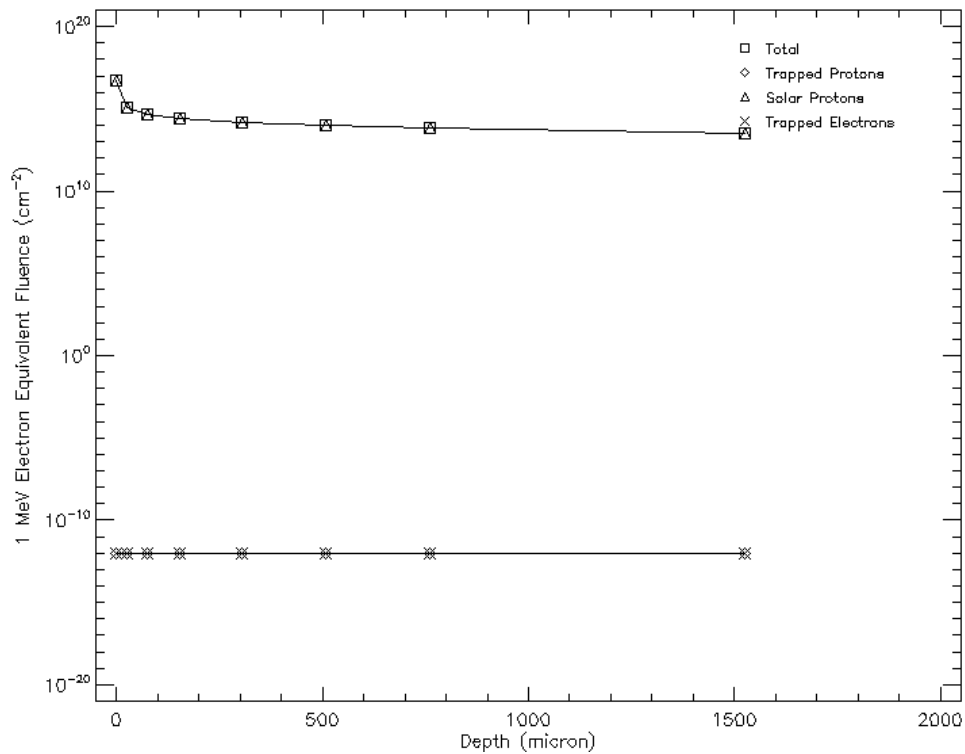


Figure 4.25: Equivalent Fluxes versus depth in the Azur 3G30 solar cell simulation.

The figure 4.25 shows the cumulative 1 [MeV] Electron Equivalent fluence versus the depth. The cumulative 1 [MeV] Electron Equivalent fluence is a way to quantify the total fluence of particles of various energy by considering only electrons of 1 [MeV] (the energy of the real incoming particles is equal to the equivalent fluence times 1 [MeV] ). As depicted on the figure 4.25, after 10 years of mission, the average equivalent fluence over the depth is  $1e15$  [ $particles.cm^{-2}$ ]. This value is then used for estimating the performance decrease of the solar cells. One can make a second comment about the results: as expected, trapped electrons and protons have no contribution (the satellite never crosses the radiation belts) and the total equivalent fluence is only due to solar protons.

## Solar Array Design

The solar arrays have to be sized in a worst-case scenario which corresponds to the *End Of Life* (EOL) and at maximum temperatures. Indeed, in these conditions, their efficiency is the lowest. It is here assumed that the solar panel's temperature is maintained below 60 [°] during the whole mission since this temperature yields a good compromise between loss of performance of the solar cells, and complexity of the thermal control system. This assumption will need to be confirmed in the section describing the thermal subsystem of the satellite (Section 4.6)

The first step that needs to be performed is to determine the electrical characteristics (mainly the operating voltage and current) of the solar cells at EOL and maximum temperature. These values are generally computed by starting from the characteristics at the *Beginning of Life* (BOL) and by successively taking into account the effects of (1) radiation and (2) temperature on them. Even if a DET architecture is not able to follow the maximum power point of the cells, one considers that the operating voltage and current are respectively  $V_{mp}$  and  $I_{mp}$ . The lack of power induced by this approximation will be covered by the margin that will be then taken into consideration.

According to the datasheet of the solar cells:

$$\begin{aligned} I_{mp, BOL, @28^{\circ}C} &= 0.5044 \text{ [A]} \\ V_{mp, BOL, @28^{\circ}C} &= 2.411 \text{ [V]} \end{aligned} \quad (4.9)$$

1) After 10 years of mission (EOL), according to the results obtained in the section 4.4.6, solar cells will receive an equivalent fluence of  $1e15 [e.cm^{-2}]$ . The following electrical properties are thus expected for the cells:

$$\begin{aligned} I_{mp, EOL, @28^{\circ}C} &= 0.4866 \text{ [A]} \\ V_{mp, EOL, @28^{\circ}C} &= 2.246 \text{ [V]} \end{aligned} \quad (4.10)$$

2) Considering a temperature difference of  $\Delta T = 60 [^{\circ}C] - 28 [^{\circ}C]$ , the expected variations of  $V_{mp}$  and  $I_{mp}$  due to temperature effects are:

$$\begin{aligned} I_{mp, EOL, @60^{\circ}C} &= I_{mp, EOL, @28^{\circ}C} + \Delta T \cdot \frac{\Delta I_{mp}}{\Delta T} = 0.4866 + 32 \times 0.28 \times 0.001 = 0.4956 \text{ [A]} \\ V_{mp, EOL, @60^{\circ}C} &= V_{mp, EOL, @28^{\circ}C} + \Delta T \cdot \frac{\Delta V_{mp}}{\Delta T} = 2.246 - 32 \times 7.2 \times 0.001 = 2.016 \text{ [V]} \end{aligned} \quad (4.11)$$

*Note:* Electrical data considered here corresponds to the behavior of the solar cells receiving a solar flux of  $\Phi_{Sun} = 1367 [W.m^{-2}]$ . Thanks to the yaw steering law and the Solar Array Drive Mechanisms that maintain an optimal sun incidence, an effective incoming flux close to this value is expected, no additional margin must be taken into consideration.

The solar arrays are then split into two parts: a first part responsible for providing power to the satellite (main section), and a second part aiming at recharging the battery (charge section). For both of them, the same sizing strategy is applied.

1. First, the minimum number of solar cells  $N_{Serie}$  to be put in series into a string is computed, it is directly linked to the voltage that must be delivered to the bus. As a Switch series regulator is used, the operating point (which is the intersection between the solar array characteristic curve and the imposed voltage) will always stay on the right side of the maximum powerpoint. In other words, the total solar array string voltage at the maximum power point (at EOL and 60 [°C]) must be lower than the imposed voltage (bus voltage for the main section; battery voltage for the charge section). Moreover, in order to place the operating points as close as possible to the maximum power point,  $N_{Serie}$  is chosen to be the maximum possible while remaining still lower than the regulated voltage.
2. As a second step, the number of strings  $N_{//}$  to be placed in parallel is determined, based on the power that must be provided to the satellite directly (for the main sections), or to the battery (for the charging sections).

First, the sizing of the charge section is made. Therefore, it is assumed that the charge voltage is equal to the mean discharge voltage and that the voltage drop between the solar array and the battery is 1.25 [V]. In that case, it is found that the minimum number of solar cells to be put in series into a string  $N_{Serie,charge} = 19$ . The number of strings to put in parallel is then computed based on the power required to fully recharge the battery in between two eclipses and on the combined efficiency of the Battery Charge Regulator and the S3R. The result is  $N_{//,charge} = 13$ . However, for reliability reasons, it is decided to choose  $N_{//,charge} = 14$  in order to be tolerant to the loss of one string.

Regarding the main sections, knowing that the bus voltage is 50 [V] and assuming that the voltage drop between the solar array and the bus is 1.25 [V], it is found that  $N_{serie,main} = 24$ . Based on the power to provide to the satellite (3100 [W]) and the efficiency of the S3R, the number of strings to be put in parallel is obtained:  $N_{//,main} = 131$ . Again, for reliability reasons, this number is augmented by one unit.

As a summary of the solar array sizing, table 4.15 displays the main properties of the solar array of the Pegasus satellites. It should be noted that, due to the fact that the main and charging sections were sized independently, a small excess power is available when the battery is fully charged. A graphical representation of the array is also depicted in figure 4.26.

Property	Data	Unit
Number of solar cells - Main Section	$24 \times 132 = 3168$	/
Number of solar cells - Charge Section	$19 \times 14 = 266$	/
Total number of solar cells	3434	/
Total power output	3325	[W]
Total surface of the solar panel	14.65	[m <sup>2</sup> ]
Solar panel weight	78.5	[kg]

Table 4.15: Main properties of the designed solar panel.

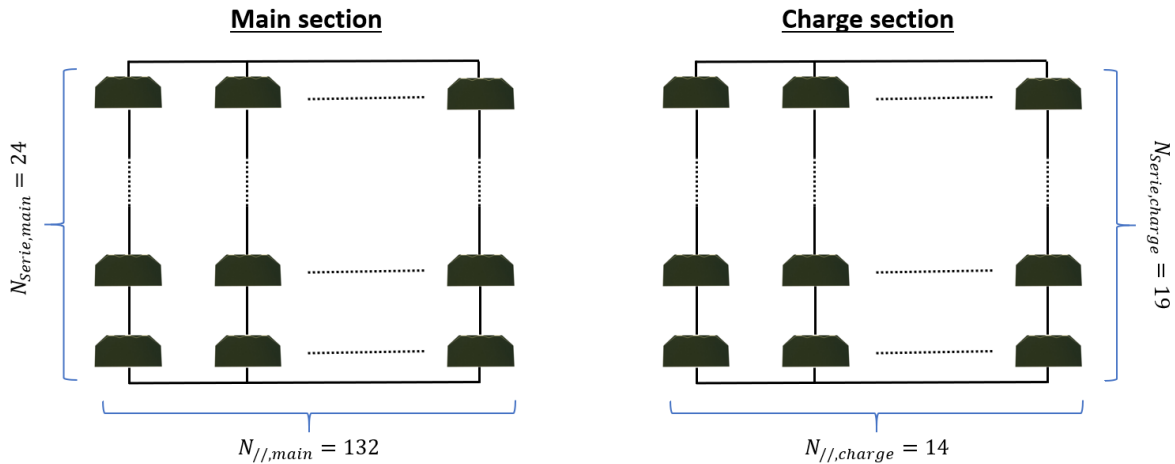


Figure 4.26: Design of the solar array.

#### 4.4.7 Synthesis

Table 4.16 displays the equipment (and its properties) that has been selected for the Power subsystem of the Pegasus satellites. Since the efficiency of the solar panels and battery has already been taken into account in the design, it is assumed here that they do not consume any extra power. As a reminder, the solar panels are tolerant to the loss of two strings (one in the charge section, one in the main section). Moreover, it is well-known in the space industry that the solar panels and the battery together account for approximately 80% of the Power subsystem mass and cost. An extra unit is thus added in table 4.16 to respect this empirical formula. This unit corresponds to, amongst others, the PDU and the wires.

Unit	Quantity	Mass [kg]	Power [W]	is Operating T [°C]
Solar panel	2	39.5	3325	-150/120
Battery	1	48.84	1800	-10/35
PCU	1	16.3	N/A	-15/70
Extras (PDU, wires, ...)	/	15.9	N/A	N/A
Total	N/A	≈ 160.04	N/A	N/A

Table 4.16: Synthesis of electrical power units.

As a final comment, one can make sure that, by combining the power output of the battery and the solar array, it is possible to provide enough power for the most demanding mode (*Transfer Orbit Mode (thrusting)*) for short period of time. As it can be seen in Appendix A.6, this mode requires ≈ 3800 [W], which is smaller than the 5100 [W] of combined power that can be delivered.



## 4.5 On-Board Data Handling and Software

### 4.5.1 Introduction

The first driving parameter in the conception of an OBDH was the simplicity and a minimalist approach. The architecture of all satellites will be identical throughout the constellation of 21 satellites. Galileo architecture [36] has been used as a basis to establish our own, while only using appropriate sensors and equipment useful for the mission. The diagram presented in figure 4.27 is split into two main sections, the platform, and the payload. The two parts are linked by a data bus handled and a *Payload to Platform Interface*.

**Payload** The payload is dedicated to fulfilling of the mission objectives, in the present case it is to provide services to the users, which are navigation and emergency broadcasting. It handles:

- Precise timing with atomic clocks.
- Gold codes generation.
- Navigation signal processing with up-converting.
- Navigation signal broadcasting on the Moon.
- EBS signal reception from the lunar surface.
- EBS signal emission and reception from Earth GS.
- EBS signal processing and broadcasting on the Moon.

**Platform** The platform is dedicated to the survival of the satellite and the mission, it handles:

- Orbit determination and correction maneuvers to be done.
- Propulsion to provide thrust and orbit insertion/correction.
- Power production and storage to provide energy to the S/C equipment.
- Attitude control to orient the S/C and the solar arrays to provide energy.
- Thermal control to resist to the space environment.
- Telemetry, tracking, and control signal to update S/C status.

### 4.5.2 OBDH Equipment & Tasks

A synthesis of the units presented in this section can be seen in table 4.17. The datasheets for the equipment can be found in Appendix A.8.

Unit	Quantity	Mass [kg]	Power [W]	Operating T [°C]
Spacecraft Management	2	6.5	23	-25/65
Remote Terminal	2	3.25	12	N/A
Real-time Clock	2	N/A	N/A	N/A
Total	4	19.5	70	N/A

Table 4.17: Synthesis of the OBDH units.

**Remote Terminal Unit** All of the signal data processing is handled by a Remote Terminal Unit (RTU). The goal of using this equipment in the architecture is to reduce the required computing power by the PCDU of the platform and to only transmission relevant data through the bus interface.

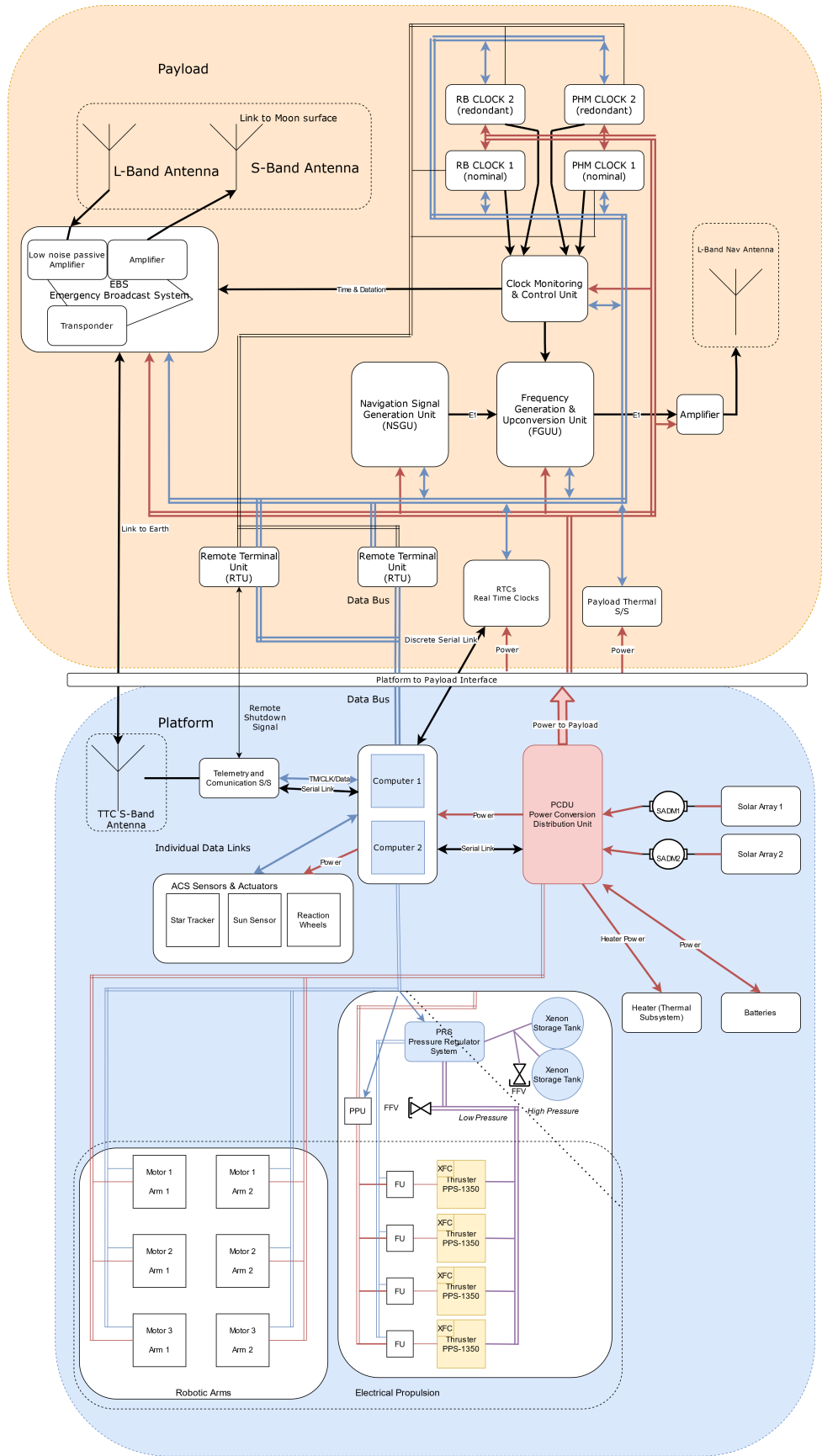


Figure 4.27: OBDD top level diagram.

**Spacecraft Management Unit** The main computational part is handled by the two onboard Spacecraft Management Units. From there, the computers are connected to all the other subsystems of the S/C. It receives orders from TTC subsystem or follows the planned mission with the different levels of automation linked to the S/C modes. It is also responsible for the memory of the satellite. The two computers units will be activated upon separation of the satellite from the launcher, via a pyrotechnic fuse.

We choose an On-Board Computer (OBC) from the brand RUAG, the CREOLE ASIC. (Appendix A.8). It features an onboard redundancy with two different computers working together, with each 374 [Gbit] long term storage capacity and 512 [MB] of system memory. Our satellites only need to store ephemeris files for position estimation, EBS data history, and logs for recent activity. All of those usages do not exceed 32 [Gbit] capacity. An automatic transfer of all log files to the operation center is performed every day. After a month of storage, every file can be deleted. If the EBS system ends up generating more data than expected, the data will be deleted 48 hours after ground backup.

**Real-time Clocks** Real-time clocks are present on the P/L side and are connected to the computers in two different ways. The first one is a direct serial linked with reduce latency to get the most accurate system time possible from the clocks, the second connection is with a data bus to update parameters or reset the clocks.

**Power Delivery** Power lines are handled by the PCDU, receiving commands from the computer to activate/deactivate selected equipment depending on the active S/C modes.

**Platform to Payload Interface** The communications between the platform and the P/L are handled by two data buses linked to the RTU on the payload side. They are in charge of signal and data processing to avoid a calculation overload at the computer level.

## Thrust Control

- A constant thrust of the electrical thrusters is achieved with an algorithmic loop into the Power Processing Unit and gives us the analog control signal for all of the Xenon Flux Controllers.
- The Pressure System Regulator is activated before each burn to adjust then maintain the pressure in the low-pressure part where the thrusters are. It uses a control loop algorithm too and responds to a limited number of commands thanks to the high level of automation in the system. Two different loops are present. The first one is dedicated to the ignition of the thrusters and the second one is used to maintain constant pressure.
- The system controls the discharge voltage and the difference between the ground of the satellite and the voltage in the cathode. This referential is called the cathode reference potential.
- Other housekeeping parameters are issued by the thruster automatically and handled as telemetry data by the computers.

### 4.5.3 Global Redundancy

This section sums up the main redundancies implemented into the S/C subsystems. The redundancy has been implemented to provide Fail Operational (FO) service, nominal tasks completed by the remaining equipment in case of a failure event, or a degraded mode in the worst-case scenario. Detailed information about the design of each subsystem can be found in their respective section. Failures will be taken into account and order by Fault Detection, Isolation, and Recovery (FDIR) standard. The lowest FDIR level being 0 and the highest level being 4 and handled by the ground teams while the spacecraft switches to Safe Mode.

#### OBDH

- Spacecraft Management Unit (4 computing units)  
The spacecraft features two main On-Board Computers (OBC) in hot redundancy to provide FO service with up to two compute unit failures. Every OBC then contains two redundant compute units in hot redundancy. With this setup, two different voting pools take place one after the other. The first one compares inside an OBC the result of the two compute units. Another pool is then performed between the two OBCs. This enables the satellite to automatically diagnose a faulty compute unit inside an OBC. In normal operation, the idle compute unit of every pair can be used to perform updates and testing before applying a new software patch. In that case, the system is only working on two compute units.
- Remote Terminal Unit (x2)  
Another key to the survival of the mission is good communication between the P/L and the platform. RTUs are used to ensure such communications and perform signal conversions without the help of the main computers. The satellites have two redundant RTUs in hot redundancy to ensure a FO service and good communication with the P/L.

#### AOCS

- Star Tracker (x2)  
Without star trackers the S/C cannot calibrate its orientation in space, this constraint imposes a redundancy on the star trackers. In case of failure of one star tracker or in case of different results from the voting system, the spacecraft switches automatically to sun pointing mode / safe mode until the ground operators deactivate the faulty sensor.
- Sun sensor (x2)  
The sun sensors are used to refine the yaw steering law and to provide information to the Solar Array Driving Mechanism. Refining the yaw steering law requires two operational sun sensors. In case the spacecraft loses one, the mission can continue in degraded mode using only the star trackers to tune the yaw law.
- Reaction wheel (x4)  
The satellite needs one reaction wheel per axis to orient itself in all directions. In the design, a fourth wheel was added to provide redundancy in case of a one-wheel failure. In that case, the S/C needs to reconfigure itself to replace the defective wheel with the spare one. With the actual design, losing two wheels seems to have a very low probability but would mean the end of the mission.



## Payload

- Rubidium Atomic Frequency Standard (x2)  
 Two RAFSs have been integrated, following the steps of Galileo. RAFS are more stable in the long run, with a long life cycle and flight heritage, but are less precise. This stability is needed during the entire mission, hence the hot redundancy with a comparison of voting results. The mission is FO with one RAFS disabled and degraded with both of the clocks disabled.
- Passive Hydrogen Maser (x2)  
 PHM clock has the best precision, but with a shorter life cycle than the previous one. They are in hot redundancy to ensure the resulting voting and a FO mechanism with the loss of one clock. As for the RAFS, the system can work in degraded mode with both of the clocks disabled.
- Navigation Signal Generation Unit (x2)  
 NSGU is critical to the mission, it generates the navigation signal from the atomic clocks and golden sequences. The two pieces of equipment don't need to run at the same time, this one has been configured in cold redundancy.
- Frequency Generator and Up-converter Unit (x2)  
 FGUU is responsible for generating the L-band signal from the NSGU. Losing this equipment means the end of the spacecraft mission. The choice was made to implement the second one in cold redundancy with a possible reconfiguration with commands from the ground.

## Propulsion

- Thruster (x4)  
 The propulsion systems is entirely based on hall effect thrusters that are used for, among others, inserting the S/C in lunar orbit, station-keeping, and desaturate the reaction wheels. In order to desaturate the wheels in all directions, two robotic arms were installed on the -X and +X sides of the satellite. Redundancy is needed in case of thruster failure to provide the thrust to inject into orbit and later correct it. To be FO, one pair of thrusters are placed on each of the arms, one pair including one nominal thruster and one cold redundant.
- Filter Unit (x4)  
 The FU is used to filter the electrical current going to the thruster. If two thrusters are connected to a single FU, the loss of the equipment would mean the loss of one arm and thus the loss of the mission. The low cost of this equipment and its small form factor enables us to put one FU per thruster.

## Power

- Solar array charging section  
 An additional string is added so that the design is tolerant to a one-string loss.
- Solar array main section  
 An additional string is added so that the design is tolerant to a one-string loss.

### 4.5.4 Modes Transitions

OBDH subsystem handles the ON/OFF of every unit and other subsystems, which depends on the modes S/C. The description of the mode and be seen on the deliverable *System Engineering Report*. On the figure 4.28, all the S/C modes are present with their possible transitions. The sequence begins with the off state and will end up in a loop between *Normal* mode and *Orbit Correction* mode. In the case of an eclipse, the spacecraft will automatically switch into *Eclipse* mode when the solar power goes to zero, then resume normal operation at the end of the eclipse when the solar panels capture sunlight again.

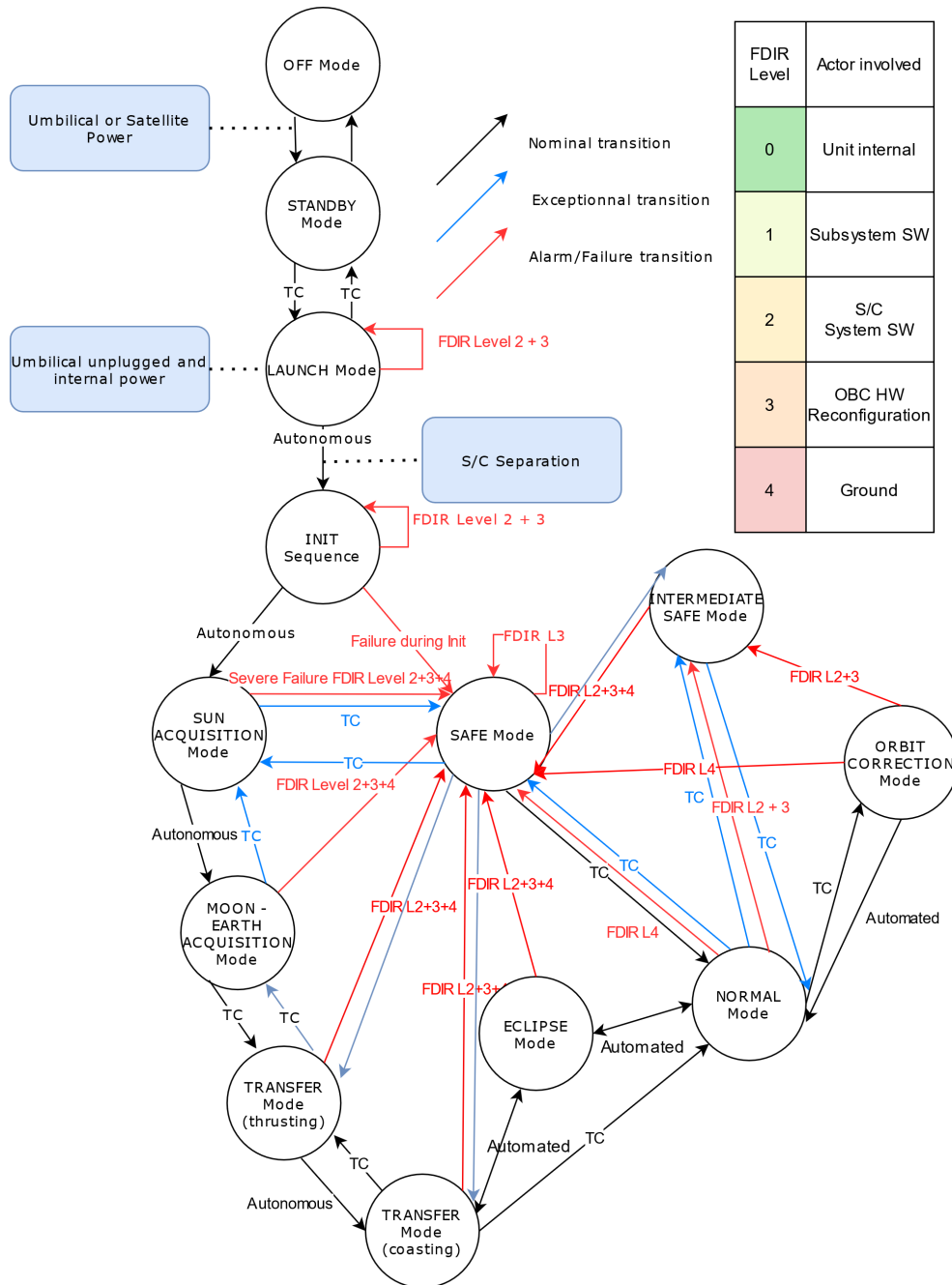


Figure 4.28: Modes switching diagram.

## 4.6 Thermal Control

### 4.6.1 Introduction

The main objective of this study is to determine and size thermal protections and hardware needed to ensure that the temperature of each equipment remains within pre-defined tolerances. For this purpose, different sub-tasks must be performed:

- Define properly inter-dependencies between thermal control equipment and other subsystems.
- Search thermal characteristics of each equipment (operating temperature ranges and estimation of their heat dissipation).
- Perform simulations to estimate the incoming heat fluxes received by the satellites.
- Select thermal control technologies.
- Model the thermal behavior of the S/C and compute the temperature of each equipment.
- Compare results obtained with the temperature tolerances, and iterate if needed.

### 4.6.2 Equipment Temperature Ranges

After the selection of the components needed in the different subsystems of the Pegasus satellites, their Qualification temperature tolerances (in operating conditions) are searched in the data sheets and transformed into Design temperature tolerances that are then listed in table 4.18. It is recalled that the Design tolerances are calculated by taking the Qualification temperature ranges and by removing successively Qualification and Acceptance Margins, as specified by the the ESA ECSS-E-ST-31C standard [37]. The Calculated temperature ranges provided by the thermal models are then compared to the Design temperature tolerance, by taking into account the uncertainties of the models.

Component	Design temperature tolerance [°C]	Need for stability
Structure	-85/80	No
Solar arrays	-170/120	No
Battery	15/30	No
PCDU	-10/55	No
Thrusters	-60/160	No
Xenon Pressure Regulator	27/45	No
Xenon tank	5/55	No
Star trackers	-30/60	No
Sun sensors	-27/70	No
Reaction wheels	-20/70	No
S/C Management Unit	-25/50	No
RB atomic clock	-5/10	+/-1° in 24h
PHM atomic clock	-5/10	+/-1° in 24h
NGSU	-20/70	No
Nav antenna	-120/120	No
SMS antenna (Up and Downlink)	-40/85	No

Table 4.18: Temperature tolerances of the main equipment of the satellite (operating conditions)

It is noticed that atomic clocks have very strict thermal constraints, with a small temperature variation tolerance and a need for stability. For this reason, it is decided to put them on a face that never faces the Sun, to limit the variations of the thermal fluxes. A specific control law called the "Yaw Steering Law" is therefore needed.

#### 4.6.3 Yaw Law and Incoming Heat Fluxes Simulation

Due to the high variation of the solar flux magnitude on all faces (see figure 2.11 in section 2.4.1), some thermal requirements listed in the table 4.18 (especially the requirements for the clocks) cannot be met with a classical attitude evolution over the orbit. For this reason, a *yaw steering law* must be implemented, that makes sure that one face of the satellite (the face where the clocks are placed) never sees the Sun. Practically, the yaw law relies on a rotation of the satellite around its Z-axis and has been described in section 4.3. Since this law modifies the incoming fluxes on the different sides of the satellite, they have been re-computed thanks to the software *Systema* and are depicted in figure 4.29. The initial *RAAN* used for the simulations has been set to  $0^\circ$ , but similar fluxes are expected for the satellites of the other orbital planes. Indeed, since the yaw steering implies that the incoming Sun rays remain in the same satellite semi-infinite plane as explained in 4.3.3, the influence of the *RAAN* will only induce a dephasing between the incoming solar fluxes of the different satellites.

Some comments can be made about the new heat fluxes obtained:

- The Yaw Steering Law works as expected since the face "Anti-Sun Side" never receives direct solar flux. Other direct consequences of the control law are that the face "Sun Side" receives a high flux due to its permanent exposition to the sun, and that the faces "+Y Side" and "-Y Side" are never exposed to the direct solar flux. However, placing atomic clocks on these sides would present a risk as a small modification of the attitude of the satellite (for example in safe mode, when the yaw law is not operating anymore) would increase drastically the received solar heat flux and thus damage the clocks.
- This new fluxes evolution enable to determine the sides where radiators could be placed. The anti-sun, +Y and -Y sides seem to be wise choices since they often face deep space.
- Two times per year, the satellite enters into the shadow of Moon during some minutes for several consecutive orbits. In such a configuration, the direct solar flux received by the Sun side oscillates between 0 and high values, as it can be observed on figure 4.29c.
- Lunar eclipses occur due to the alignment Sun-Earth-Moon, the Moon is in this configuration in the shadow of the Earth. As a consequence, direct solar fluxes received by all faces are zero for a quite long period. This behaviour can be seen three times on figure 4.29c.
- For each face, three different "cold cases" can thus be identified:
  - When the face is less exposed to the Sun (or even not exposed at all) due to the orientation of the satellite with respect to the Sun (high frequency occurrences).
  - When the satellite is in the shadow of the Moon (called lunar eclipse). If a worst case is considered, this eclipse occurs at each orbit (i.e. approximately each 23[h]) and lasts 1 [h] 23 [min].
  - When the satellite is in the shadow of the Earth (Earth eclipse). This phenomenon occurs 2 or 3 times a year and can last up to 2 [h] 35 [min].



From these observations, it is concluded that the Earth eclipse is the sizing factor for the thermal control as well as for the electrical design.

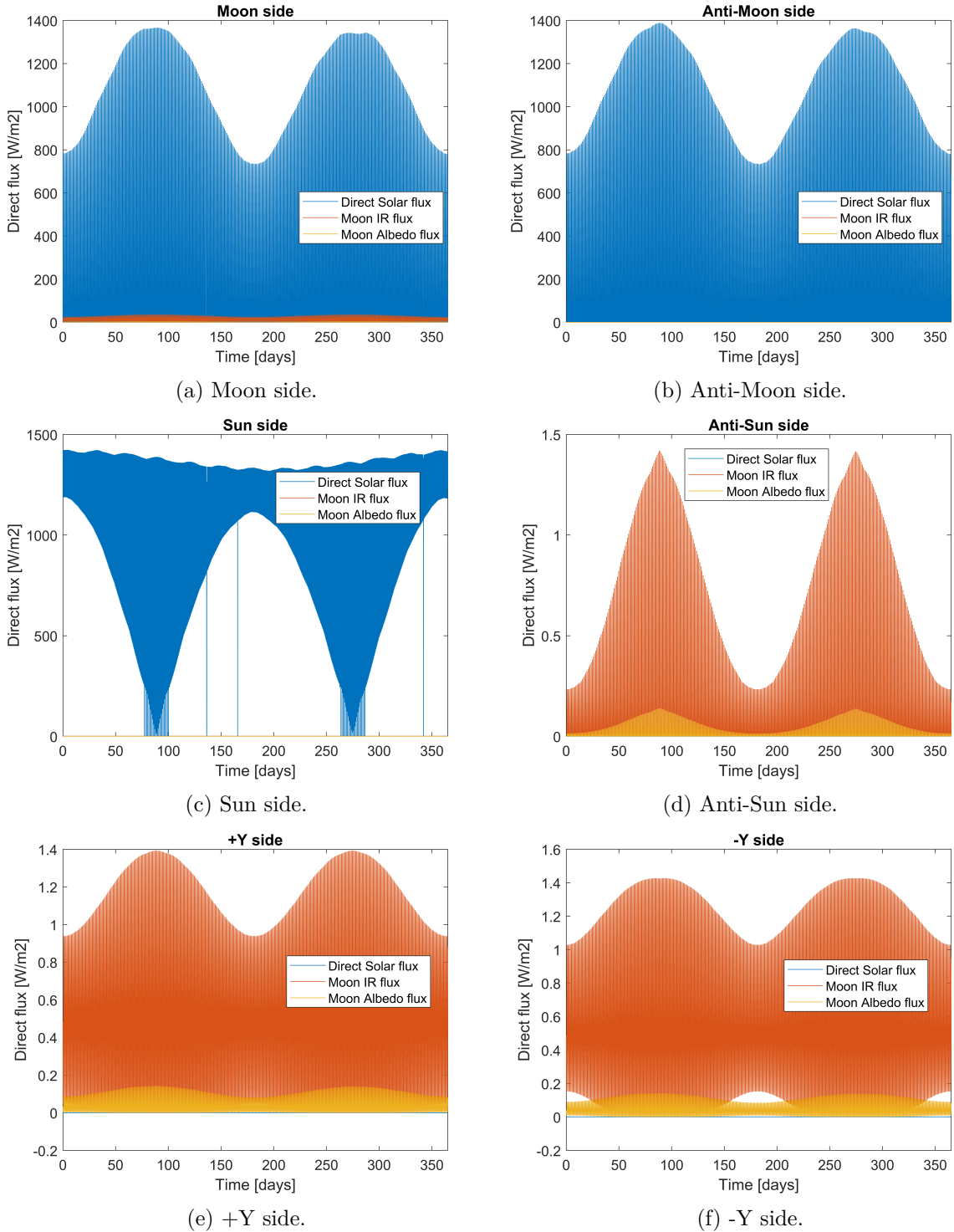


Figure 4.29: Thermal fluxes on the six surfaces (with yaw steering law).

#### 4.6.4 Thermal Budget

In this section, the thermal budget is quickly recalled. It will indeed be used several times to compute the transient temperature evolution of the spacecraft with a first simplified model (section 4.6.5) and to estimate the steady temperature of each face of the satellite (section 4.6.6). It should be noted that equation 4.12 can be applied to whatever system with temperature  $T$  and that the term  $C.(T - T_0)$  represents the conduction between the system at temperature  $T$  and another system at temperature  $T_0$ .

$$Q_{IN} - Q_{OUT} = m \cdot C_p \cdot \frac{dT}{dt} \quad (4.12)$$

with  $Q_{IN} = Q_d + \alpha_s.(A_s.\Phi_{sun} + A_e.\Phi_{albedo}) + A_e.\epsilon.\Phi_{moon}$

with  $Q_{OUT} = F.A_{rad}.\epsilon.\sigma.(T^4 - T_{sp}^4) + C.(T - T_0)$

In equation 4.12, several symbols must be defined.

$Q_{IN}$	Incoming power	[W]
$Q_{OUT}$	Outgoing power	[W]
$Q_d$	Dissipated power	[W]
$\Phi_{sun}$	Solar flux	[W/m <sup>2</sup> ]
$\Phi_{albedo}$	Moon albedo flux	[W/m <sup>2</sup> ]
$\Phi_{moon}$	Moon IR flux	[W/m <sup>2</sup> ]
$A_s$	Surface to Sun	[m <sup>2</sup> ]
$A_e$	Surface to Moon	[m <sup>2</sup> ]
$A_{rad}$	Radiative surface	[m <sup>2</sup> ]
$F$	View factor	∅
$\alpha_s$	Absorbptivity	∅
$\epsilon$	Emissivity	∅
$\sigma$	Stefan-Boltzmann constant	[W/m <sup>2</sup> /K <sup>4</sup> ]
$T$	System temperature	[K]
$T_{sp}$	Space temperature	[K]
$m$	System mass	[kg]
$C_p$	Specific heat capacity	[J/kg/K]
$C$	Thermal conductance	[W/K]

Table 4.19: Components of the thermal budget equation.

#### 4.6.5 First model: global study

In this first model, several assumptions are made:

- the whole satellite and its components have the same temperature  $T_{rad}$ ,
- the satellite is a box of 2 [m] x 1 [m] x 1 [m], recovered with two different materials:
  - radiators of the OSR type (Optical Surface Radiator) with  $\alpha = 0.06$  and  $\epsilon = 0.83$  on parts of the anti-sun, +Y and -Y sides,
  - Multi-Layer Insulation (MLI) with absorptivity  $\alpha = 0.25$ , and emissivity  $\epsilon = 0.05$  on the sun, moon, anti-moon sides, and on the remaining parts of the anti-sun, +Y, and -Y sides.
- the proportion of the anti-sun, +Y and -Y sides covered with OSR are respectively called  $\beta_{AS}$ ,  $\beta_{+Y}$ ,  $\beta_{-Y}$  and are kept as parameters that can be varied.
- the satellite thermal capacity is estimated by an equivalent body consisting of 150 [kg] of aluminium (with a thermal capacity of 892 [J/kg/K]) and 250 [kg] of electronic equipment (with a thermal capacity of 108 [J/kg/K]).
- all satellite components together dissipate approximately 400 [W]. This value was obtained after estimating the power dissipation of the most dissipating units (PCDU, Battery...).
- the view factor  $F$  is 1.

Thanks to the fluxes computed by means of Systema, it is possible to compute the evolution of the satellite temperature by solving the thermal budget of equation 4.12 expressed in an Euler explicit form. In these equations, the interest of assuming that the whole satellite is at the same temperature is noticed. As an example, the temperature evolution over one year is depicted in figure 4.30 (left), for a spacecraft without radiators. In this figure, the influence of lunar and Earth eclipses is clear in reducing the temperature. Moreover, it can be observed that the S/C temperature reached is way too high since it oscillates between 35 [°] and 85 [°C].

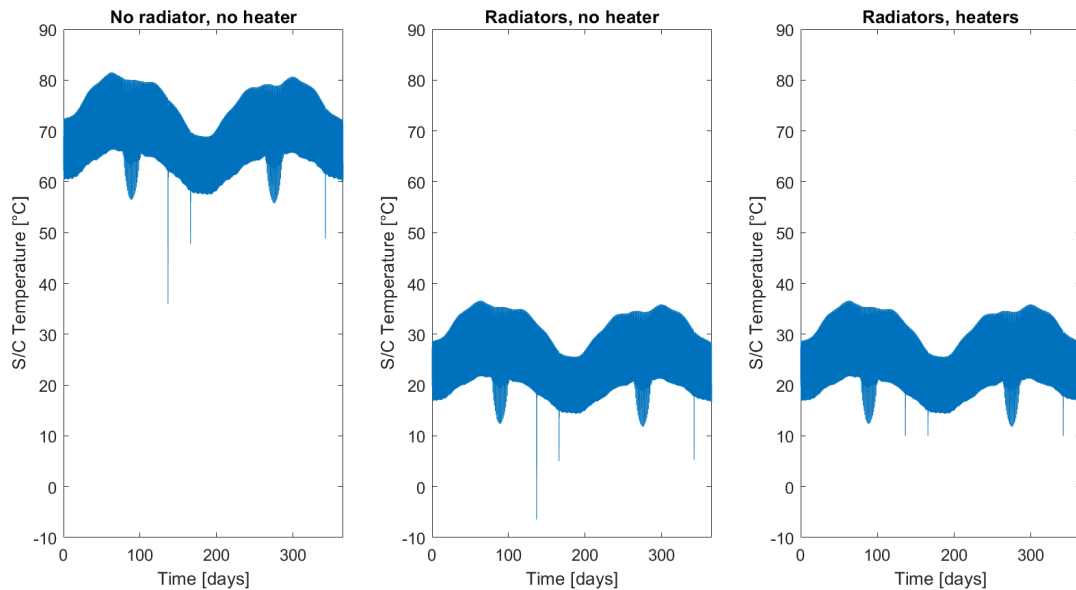


Figure 4.30: Temperature evolution of the spacecraft over one year.

Now that this temperature evolution is understood, the sizes of the radiators on the “Anti-sun”, “+Y”, “-Y” sides can be increased in order to reduce the satellite temperature. After some trials, a satisfactory evolution (figure 4.30 in the centre) is found for the following sizes of radiators: (a) 1 [m<sup>2</sup>] on the “Anti-sun” side, (b) 0,6 [m<sup>2</sup>] on the “+Y” side, (c) 0,6 [m<sup>2</sup>] on the “-Y” side.

As it can be noticed, the temperature of the spacecraft is between 10 [°C] and 37 [°C] throughout the whole year, except during Earth eclipses. Hence, it is decided to keep this design of radiators and to add heaters in order to cope with eclipses and to keep at all time the temperature higher than 10 [°C]. After some computation, 400 [W] are proven to be the required power during eclipses to avoid the temperature falling below 10 [°C] which is considered as the acceptable lower limit. The temperature evolution of the satellite in this final configuration (with radiators and heaters) is depicted in figure 4.30 (right).

### Conclusion of this global study

The preliminary sizing obtained by means of this global study is summarized in table 4.20. However, it should be noted that the sizes of the radiators and heaters obtained are most probably underestimated due to the assumptions made. They give a first interesting idea about their order of magnitude, but needs to be refined thanks to a more local model.

<b>Radiators</b>	Surface [m <sup>2</sup> ]
Anti-sun side	1
+Y	0.6
-Y	0.6
<b>Heaters</b>	Power [W]
	400

Table 4.20: Synthesis of the design yielded by the global model.

#### 4.6.6 Second model: local study

The previous model gives a first sizing of the radiators but does not give information about the local temperature variations. For this reason, the stability of the clocks temperature, which is one of the major constraints of the thermal control of the Pegasus satellites, cannot be demonstrated. This is the reason why a second model based on a nodal description of the thermal architecture has been used.

A node is defined as a group of equipment that have the same temperature. 8 thermal nodes are considered: the six faces of the satellite, the clocks and the solar panels. Clocks have been voluntarily excluded from the rest of the satellite to isolate them as much as possible from the other equipment, to avoid unwanted temperature variations due to thermal dissipation. Solar panels are considered as isolated due to the few thermal exchanges that they have with the rest of the satellite.

## Radiator Sizing

The thermal model for the clocks is based on the following assumptions:

- Transient effects are neglected.
- The 4 clocks have the same uniform temperatures.
- They are all linked by conduction to a radiator via a perfect thermal contact (no resistance of conduction). This implies that the temperature of the radiator is the same as the clocks temperature.
- There is no radiative nor conductive coupling between the clocks and the rest of the satellite, as well as no radiative coupling between the clocks and the external environment.
- The view factor of the radiator is assumed to be maximum ( $F = 1$ ).
- The clocks dissipate approximately 24 [W].

As explained before, the radiator for the clocks is placed on the Anti-Sun side to avoid as much as possible variations of the thermal constraints. The general idea is to solve the power budget equation 4.12 applied to the radiator, in order to size the radiator area  $A_{rad}$ , knowing the temperature  $T_{Clocks}$  imposed by the thermal tolerances. Given the assumptions presented previously, some simplifications and substitutions can be made in the thermal equation:

- The steady state solution is searched:  $\frac{dT_{Rad}}{dt} = 0$
- The thermal contact is perfect:  $T_{Clocks} = T_{Rad}$
- $A_s = A_e = A_{rad}$
- $Q_d = 24 W$
- $\alpha_s = \alpha_{rad} = 0.06$
- $\epsilon = \epsilon_{rad} = 0.83$
- The view factor is maximum:  $F = 1$ .
- $T_{Clocks} = 5 [^{\circ}C]$
- Incoming fluxes correspond to the flux received by the "Anti-Sun" side, depicted on figure 4.29d

Two successive calculations are then made: the first one is aimed at sizing  $A_{rad}$  imposing  $T_{Clocks}$  in the hot case (situation where the fluxes are maximum), the second one corresponds to the cold case (when fluxes are minimum) and is aimed at computing  $T_{Clocks}$  based on the previous calculated  $A_{rad}$ . This second calculation is necessary to check the whole temperatures range of the clocks.

The result of this analysis shows that a radiator of  $0.09 [m^2]$  located on the "Anti-Sun" side is sufficient to maintain the clocks between  $4.71 [^{\circ}C]$ , and  $4.74 [^{\circ}C]$ , which means that the temperature tolerances and the stability requirement are satisfied (maximum temperature variations of  $0.29 [^{\circ}C]$ ). This simple model could be improved by taking into consideration conductive effects between the clocks and the radiator as well as transient effects, but it gives a good first estimation of the required radiator area for the thermal control of the clocks.

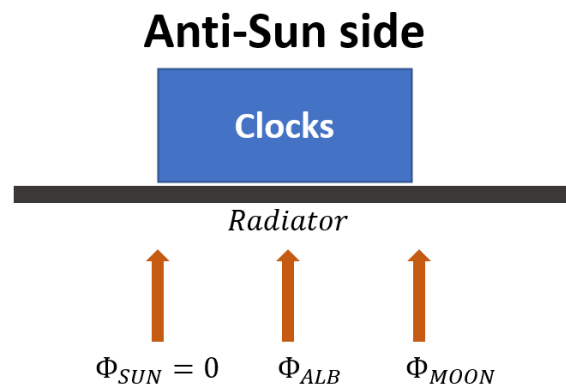


Figure 4.31: Thermal model of the clocks.

### Radiators, heat pipes and heaters sizing

6 new nodes are now considered, each of them corresponding to one face of the satellite. The following assumptions are made:

- The geometry presented in the first global model is kept for this second study, the satellite is a box of 2 [m] x 1 [m] x 1 [m]. MLI is used to cover specific areas of the satellite.
- The satellite faces have uniform temperatures noted respectively  $T_{Sun}$ ,  $T_{AntiSun}$ ,  $T_{Moon}$ ,  $T_{AntiMoon}$ ,  $T_{Y+}$ ,  $T_{Y-}$ .
- All equipment attached to the considered face is grouped into one single element that has the same temperature as the face (perfect thermal contact).
- Element linked to the different faces dissipates a constant power over the time. The total power dissipated is approximately 360 [W].
- Faces only exchange heat by radiative transfer with the external environment through radiators or MLI, radiative transfers with other faces are neglected. View factors are assumed to be maximum ( $F = 1$ ).
- Heat pipes are used to transfer heat between the different faces, other conductive transfers between them are neglected (no conduction through the edges of the faces). It is assumed that the power transferred by the heat pipes between two units does not depend on the temperature difference between the two units. This assumption is necessary to decouple the different equations, but induces a non-negligible error in the thermal behavior of the satellite.
- Radiators (OSR) are used to dissipate heat. Only a part of the "Anti-Sun" side is available for radiators, because of other external units installed on this face (radiator of the clocks, TMTC antenna and Laser Reflectors). The remaining available surface is 0.41 [m<sup>2</sup>].
- Thermal inertia and transient effects are neglected (only the steady solution is considered in this study).
- In a first approximation and excluding eclipses, the "hot case" of a given face (configuration for which the total incoming heat flux reaches its maximum in one year) corresponds to a "cold case" for the opposite face (minimum heat flux for the face).

To increase the heat rejection capacity of the radiators, it is better to place them on faces that receive low heat fluxes. The preferential faces for installing radiators are therefore the +Y and -Y sides and the already used Anti-Sun side. Indeed, fluxes for these faces are very low and do not vary a lot. As a consequence, a good stability of the thermal rejection is expected, which is certainly an advantage for the thermal control. It is chosen to install 3 radiators, one on the "+Y" side, one on the "-Y" side and one on the "Anti-Sun" Side, as it is depicted in black on the nodal representation of the model (figure 4.32).

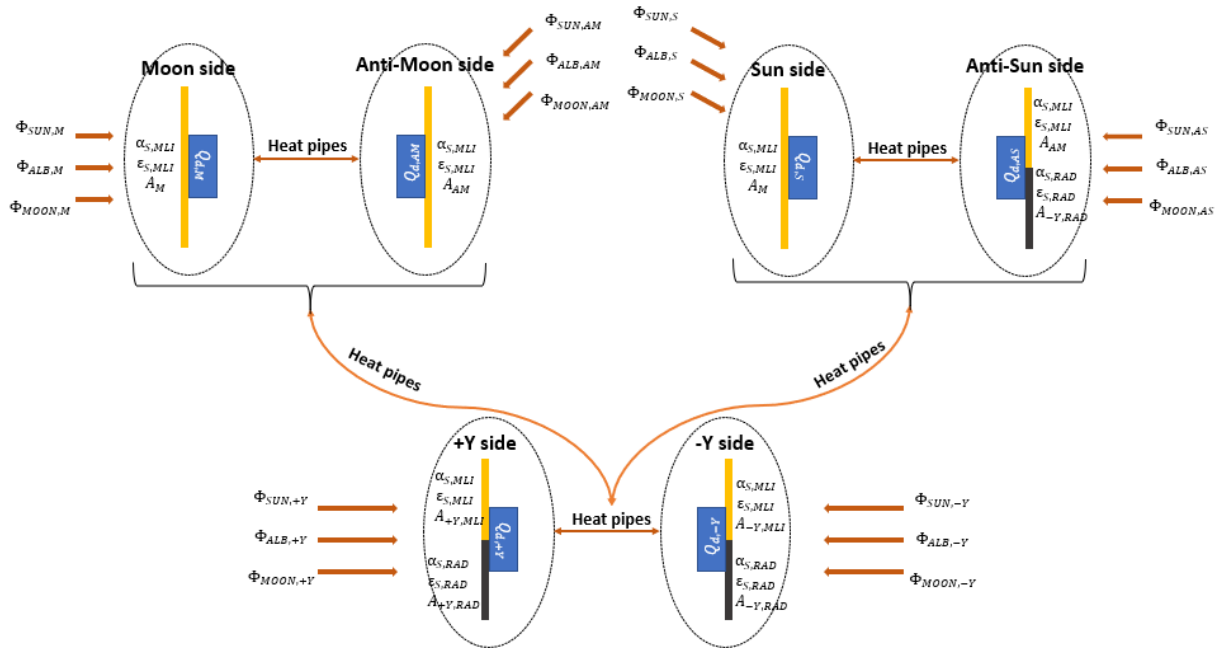


Figure 4.32: Nodal representation of the local thermal model.

As the hot case of a face corresponds to the cold case of the opposite one, the latter can be used as "heat dissipator": a thermal link is imagined between the two faces, and the excess heat from the hot face is used to maintain the cold face at a good temperature. In order to prevent the cold face from being too warm, the excess heat is then transferred through a heat pipe to a face that contains a radiator. In addition, heaters are added to prevent the temperatures from going outside the temperature tolerances during eclipses (cold case). To sum up, each node can receive heat fluxes from heaters, heat pipes, dissipative units and from the external environment, and can also provide heat power to another node through a heat pipe. In addition, the 3 nodes corresponding to the faces "+Y", "-Y" and "Anti-Sun" rejects heat via the radiators. The whole thermal model is depicted on figure 4.32.

Knowing the incoming and outgoing fluxes of each thermal nodes, the thermal budget 4.12 is solved for each node, either to calculate radiator surfaces or node temperatures. The sizing of the radiators is made for the worst case, that is to say when the power to dissipate is the maximum and during the hot case of the "+Y", "-Y" and "Anti-Sun" sides (in reality, there is no real hot or cold cases for these faces due to their very low incoming heat fluxes).

Calculated temperature ranges obtained with the nodal model are depicted in the table 4.22. Necessary radiators and heaters are listed in the table 4.21. Some comments can be made about

these results:

- The method used only provides the temperature of the 6 faces and does not allow to refine the temperature estimation at the equipment level. Knowing the 6 temperature ranges, the equipment must be then placed in accordance with their thermal constraints and their dissipation.
- Batteries are installed on the "-Y" face and need to have a minimum temperature of  $15^{\circ}$  to work properly during eclipses, that is why the "-Y" panel has a higher minimum temperature than the other nodes.
- The maximum temperature of the "Anti-Sun" side is intentionally kept low to limit temperature gradients between the face and the atomic clocks in order to reduce the conduction between them and therefore to limit temperatures variations of the clocks.
- The constraint on the minimum temperature of the Xenon Pressure Regulator is not respected, but as the propulsion unit is not used during Eclipses, this is not a problem.
- All other equipment of the table 4.18 can be placed on any face as the temperature variations of the faces respect the equipment temperature tolerances, including some margins. The latter cover the model errors and uncertainties. It is therefore concluded that the thermal requirements are respected with the configuration found.

### Solar Array Thermal Control

Regarding the solar array, it has been assumed that they were an independent system able to maintain on its own its temperature between the pre-defined limits of  $-170/120$  [ $^{\circ}\text{C}$ ]. Moreover, as it has been seen in section 4.4, the worst-case performance of the solar panels has been computed for a maximum temperature of  $60$  [ $^{\circ}\text{C}$ ]. This section aims thus at proving that the temperature of the solar array can be kept between  $-170/60$  [ $^{\circ}\text{C}$ ].

Therefore, the thermal budget of equation 4.12 is solved a last time with the minimum and maximum fluxes that can be perceived by the solar panels. The following considerations are used:

- The power budget is applied to a single panel which combines the two "physical" solar panels. The temperature of the panel is assumed to be uniform.
- Solar cells do not dissipate heat power.
- The conduction and the radiative transfer between the panel and the satellite are neglected.
- The conversion of solar flux into electrical energy by the cell is modeled by a reduction of the incoming solar flux. A cell efficiency of 30% is supposed.
- The surface of the panel considered is  $15$  [ $\text{m}^2$ ]. The effective surface covered by the cells is  $11$  [ $\text{m}^2$ ], the remaining being MLI.
- The backside of the panel is covered by a MLI working as a Secondary Surface Mirror (SSM).
- The optical properties of the solar cells and the SSM are listed in the table 4.23.



- Heaters are used to maintain the panel at a good temperature during eclipses.

After solving the thermal budget equation for the temperature of the solar panel, it is found that this temperature varies between  $-163^{\circ}$  and  $60^{\circ}$ , if a heater of  $100\text{ W}$  is used during the eclipse. This temperature range is in accordance with the operating tolerances of the solar cells, the choice of the thermal insulation is therefore validated.

### Local Study Synthesis

The final characteristics of the thermal hardware sized with the local study are presented in the table 4.21. The table 4.22 gives the calculated temperature ranges for each node.

<b>Radiators</b>	Surface [ $m^2$ ]
Anti-sun side	$0.09 + 0.41 = 0.5$
+Y	1.5
-Y	1.3
<b>Heaters</b>	Power [W]
Nominal Mode	
Main body	160
Eclipse Mode	
Solar panels	100
Main body	750
<b>Total</b>	850

Table 4.21: Synthesis of the design yielded by the nodal model.

<b>Thermal Node</b>	Min Temperature [ $^{\circ}\text{C}$ ]	Max Temperature [ $^{\circ}\text{C}$ ]
Clocks	4.71	4.74
+Y Face	6.44	34.01
-Y Face	16.6	28.21
Moon Face	5.13	33.29
Anti-Moon Face	5.12	33.29
Sun Face	5.12	30.39
Anti-Sun Face	6.92	12.85
Solar Panels	-163	60

Table 4.22: Calculated temperature ranges for each node



#### 4.6.7 Synthesis

As the global model seems to underestimate the size of the required radiators and of the heaters, it is decided to rely on the conclusion of the nodal model since it provides worst-case dimensions, masses and power consumption for the thermal control subsystem. Indeed, the worst cases considered during the second study is a combination of worst cases for the different faces that would probably never happen simultaneously. Moreover, as the satellite inertia has been neglected, the heater power used during eclipses is nearly 2 times higher than the result obtained in the global study.

Estimating and considering the satellite thermal inertia in the equations would be a possibility to reduce the estimation of the power required by the heaters. It is however decided to keep this omission as an additional margin, and to try to decrease the power needed by means of louvers. This system works as following: during the nominal mode, the louvers which are placed on top of a radiator are completely opened to increase as much as possible the radiator efficiency. During eclipses, they are closed and limit the heat rejection. This is an interesting solution in the present case, as the high emissivity of the radiators is a real problem during eclipses. This system is a passive hardware, which is controlled by temperature differences.

A last calculation was performed with 2 additional systems of louvers on top of the radiators of the "+Y" and "-Y" sides, to assess the interest of this technology. The total radiator surfaces obtained with the previous calculation have been kept, but in the thermal model, a part of these surfaces were replaced by the louvers. Optical properties of louvers are given in the table 4.23. By solving the thermal budget equation, it was then possible to adjust the heater power needed to maintain the same minimum temperature during eclipses as the ones obtained without louvers. As expected, due to the lower emissivity of the closed louvers, less power is needed to maintain the faces at an acceptable temperature: with 2 systems of louvers of 0.45 [m<sup>2</sup>] placed on top of the radiators of the "+Y" and "-Y" sides, only 490 [W] of power is required for the heaters. Adding the 100 W of power required to heat the solar panels, the final power consumption of the thermal subsystems during eclipses is thus 590 [W].

## Equipment choice

**Radiator** Regarding the thermal radiating systems installed on the satellite faces, it has been decided to rely on an efficient well-known technology: *Optical Solar reflectors* (OSRs). Such radiators consist of reflectively coated glass tiles, which enable them to combine a very low absorptivity and a very high emissivity. For the Pegasus satellites, a Swiss provider (RUAG) has been selected since it proposes very competitive solutions. The data sheet of the chosen OSR can be found in Appendix A.7 and its main properties are recalled here:  $\alpha_S \leq 0.06$ ,  $\epsilon \geq 0.83$ , area weight = 470 [g/m<sup>2</sup>] all inclusive, and temperature range limits = -70/+ 90 [°].

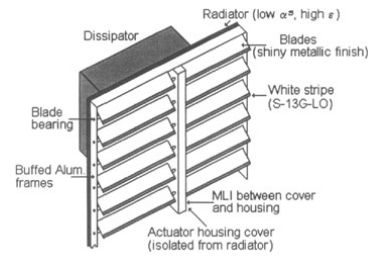


Figure 4.33: System of louvers used to reduce the heat rejection during eclipses [38]

Concerning the louvers, this technology enables to modify the emissivity of radiators by opening and closing flaps on them. Interestingly, the actuation of the flaps is passive since it relies on bimetallic springs that expand and retract depending on the radiator temperature. When the temperature is high, the flaps open in order to increase the emissivity, whereas they close when the temperature decreases. Besides, it should be noted that multiple springs are installed for ensuring inherent redundancy. It is noted that this technology has been used for some GPS satellites.

**Heat pipes** As it has been seen in the local thermal study, important thermal fluxes must be transferred from one side of the spacecraft to another. Therefore, a passive system relying on axial grooved heat pipes is chosen because of its high reliability and its relatively low cost. Such a system transfers heat thanks to fluid evaporation/condensation and then conveys it by means of capillary forces. Aboard the Pegasus satellites, a total of 13 [m] of AGHP-12.5 heat pipes provided by Iberespacio is mounted. The data sheet of this heat pipe can be found in Appendix A.7.

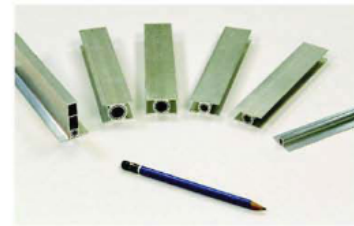


Figure 4.34: Several heat pipes profile.

**Miscellaneous items** Besides radiators, louvers, and heat pipes, several other equipment are needed for ensuring the thermal control of the Pegasus satellite. One can cite amongst others: interface filler for ensuring good conduction between elements, MLI and MLI tents for thermal decoupling (especially for isolating the clocks from the internal radiative environment), heaters for heat dissipation during cold cases, white paint for covering antennas, and so on. Moreover, since an active system of heaters is used, thermistors must be installed in order to monitor the temperature of critical elements and to control the activation of their heaters. Fortunately, all these items have a small mass, volume, and power consumption and it is assumed that they will be included in the considered margins.



## Summary of the Thermal Control subsystem

As a summary, here are the final specifications of the thermal subsystem of the Pegasus satellites.

Radiative Surface	Absorptivity	Emissivity
OSR	0.06	0.83
OSR - With Louvers Open	0.06	0.83
OSR - With Louvers Closed	/	0.08
MLI	0.25	0.05
Solar Cells	0.8	0.9
SSM (Backside Solar Panels)	0.5	0.8

Table 4.23: Synthesis of the optical properties of the radiative surfaces.

Face	OSR [ $m^2$ ]	OSR with Louvers [ $m^2$ ]	MLI [ $m^2$ ]	Solar cells [ $m^2$ ]	SSM [ $m^2$ ]	Total surface [ $m^2$ ]
+Y	1.05	0.45	0.5	0	0	2
-Y	0.85	0.45	0.7	0	0	2
Moon	0	0	2	0	0	2
Anti-Moon	0	0	2	0	0	2
Sun	0.5	0	0.5	0	0	1
Anti-Sun	0.5	0	0.5	0	0	1
Solar panels	0	0	4	11	0	15
Backside Solar panel	0	0	0	0	15	15

Table 4.24: Summary of the thermal covering areas in [ $m^2$ ] for the satellite external faces.

Unit	Quantity	Mass [kg]	Power [W]
			Nominal/Eclipse mode
Radiator Anti-Sun Side	1	0.235	0
Radiator +Y Side	1	0.71	0
Radiator -Y Side	1	0.61	0
Louvers	2	1.71	0
Heat Pipes	13	0.668	0
Heaters	N/A	$\approx 0$	160/590
Total	N/A	13.66	160/590

Table 4.25: Properties of the Thermal subsystem.

## 4.7 Structure

### 4.7.1 Introduction

The structure design of the S/C is a crucial milestone of the project. It encompasses the spacecraft's shape, external and internal structure, as well as the protection for all the subsystems regarding vibrations, stress, and radiation events occurring in stages such as launch or in-orbit configuration.

To match the constraint of launching the entire Pegasus constellation within one year, an additional requirement has been added regarding the structure: one full orbital plane of the constellation must be sent to the Moon per launch of Ariane 64. This implies that, counting the dispenser structure on which the satellites are going to be mounted inside the launcher, at least seven of them have to fit inside the fairing.

With these considerations the following initial limits have been made:

- Ariane 6's fairing can take up to 8.5 [tons] of payload for a Lunar Launch mission, thus each satellite's launch mass has to be less than one ton.
- The span must not be bigger than one of Galileo [39] with its 2.7 [m] x 1.1 [m] x 1.2 [m], to fit inside the fairing internal diameter of 4.5 [m] and 11.78 [m] usable height.

### 4.7.2 Satellite Platform

#### The use of composite for a Monocoque structure

For this lunar mission, the materials used for the anatomy of the satellite should meet the highest achievable performance in three different choice criteria: One must consider absolute values of tensile stress and strength, but also a material's ability to shield the subsystems inside the platform from cosmic and sun radiations. According to [40], the conventional repetition of frames involving aluminum made longerons and rails to assemble sandwich panels and support load undoubtedly works but comes with a heavy price in terms of the mass of this type of arrangement. The composition of this high number of frames in addition to the payload and the structure panels makes the structure design all the more complex. An example of this type of structure is presented on Figure 4.35.

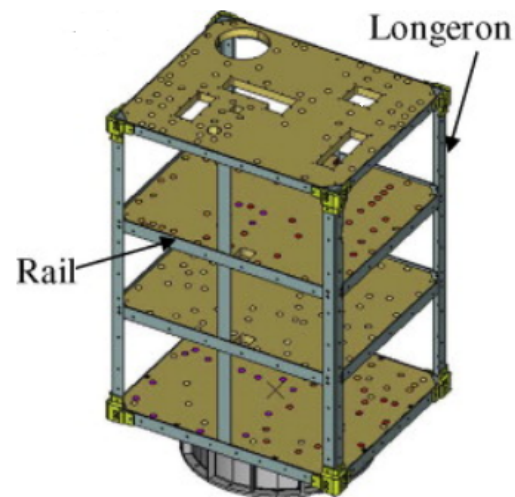


Figure 4.35: A conventional frame type structure – Science and Technology Satellite II, [40]

Composite materials have already been used in space applications for over two decades [41]. The change from mechanically fastened aluminum to bonded fiber-reinforced composite structures was first made by Gary Tremblay, Ed Boyce, and Toan Pham [42]. Because sandwich

panel arrangement is widely spread in the aerospace industry, a lot of investigation was done on how to maximize the joints of these panels, arriving at the T-shape joint. The study of [40] concludes that, after a Finite Element Analysis comparison with a aluminum honey-comb part, the composite sandwich panels assembled with T-shape joints using an I-shape side insert with a bolt hole were reliable and satisfied all the requirements deemed necessary for its application in space projects.

For similar requirements in the design of the Satellite III investigated in their paper, a mono-coque composite arrangement with the T-joints granted a gain of 14.8 [kg] compared to a conventional aluminum skin frame, while being cheaper to manufacture. The Pegasus satellites will use this method for the layout of their structure. The composite in question is a carbon epoxy composite (USN150). The panels will be composed of two carbon fiber/epoxy composite faces and an aluminum honeycomb core depicted in Figure 4.36.

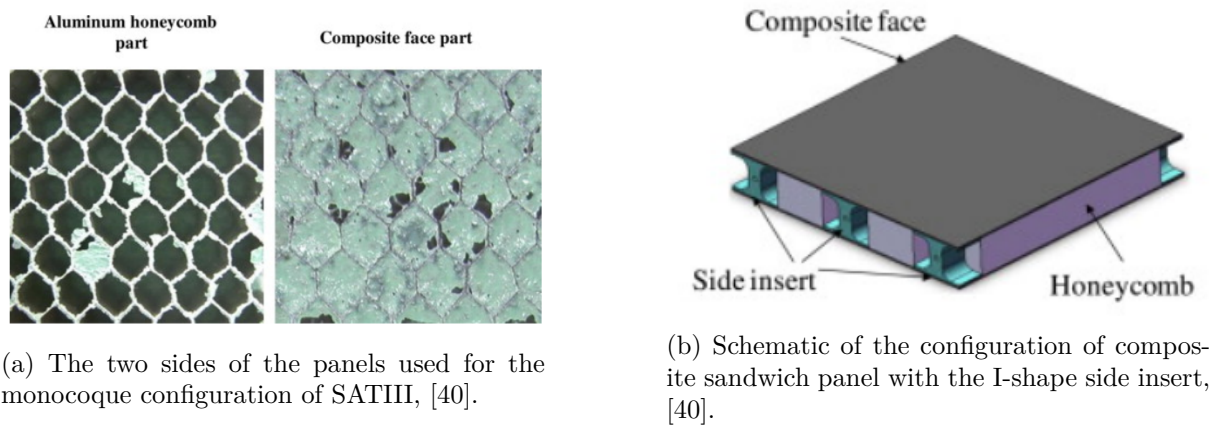


Figure 4.36: Material chosen for the monocoque structure configuration of Pegasus' satellites.

### Structure Mass

Knowing the exact dimensions of SATIII and the mass of its monocoque structure, it is possible to extract the area density of the panels used for this particular satellite. SATIII is 1024 [mm] x 1030 [mm] x 885 [mm] [43], meaning a total area of 5.74 [m<sup>2</sup>]. Having a structured weight of 31.9 [kg] [40], this means the panels used for SATIII have an area density of:

$$\frac{31.9}{5.74} = 5.55[kg/m^2] \quad (4.13)$$

Taking into consideration the assertions mentioned in section 4.7.1, the Pegasus satellites are estimated to be a “box-wing” type satellite of 2.0 [m] x 1.0 [m] x 1.0 [m], consisting of a central cubical structure, the “box”, and two rectangular solar arrays, the “wings”, attached to it.

Knowing now the dimension of one Pegasus satellite, it is possible to evaluate the overall panel weight of the monocoque structure. It is composed of six panels creating the box in addition to two inside floors for a total of 12 [m<sup>2</sup>]. Hence, using results from equation 4.13, the overall monocoque arrangement weights:

$$12 \times 5.55 = 66.6[kg]. \quad (4.14)$$

The satellite is henceforth endowed with a light, high-performing material as part of its structural design. Nevertheless, the ability of this structure to withstand cosmic and solar radiation must now be taken into account. The composite used for the panels is not suited to this task due to a low area density. Aluminum shielding is mostly used for this purpose. The thickness of Aluminium will be chosen about the received dose depicted in Figure 4.37, computed with the software OMERE with environmental constraints matching Pegasus' specifications.

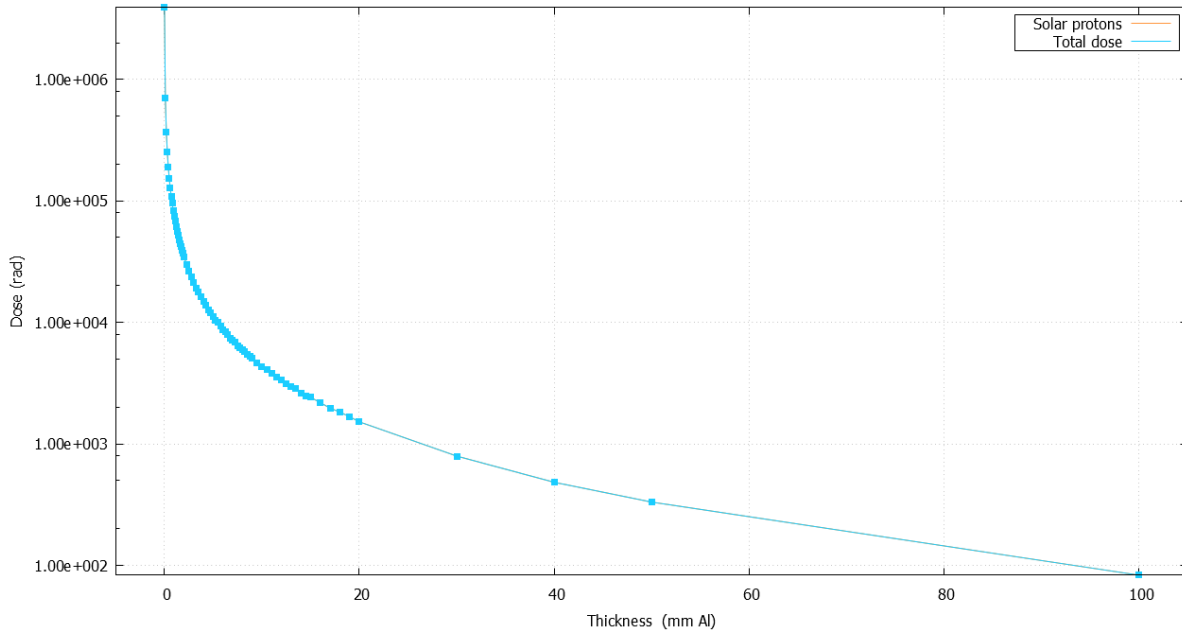


Figure 4.37: Evolution of Aluminium coating's thickness with received dose

As all equipment are qualified to withstand a precise amount of radiation dose, it is assumed that the satellite can receive a cumulative dose of 10 [krad] during the whole duration of the mission. According to the figure 4.37, the coating applied on Pegasus has to at least be 5.5 [mm]. It is decided that only the Sun, Moon, and anti-Moon sides of the satellite, being the most likely to receive the highest doses of radiation, will be protected by this shielding (see yaw steering law in section 4.3).

Those three faces together add up for a total of 5 [m<sup>2</sup>] of a 5.5 [mm] Aluminium coating. The rest of the panels, representing 5 [m<sup>2</sup>], will be equipped with a 1 [mm] Aluminium coating protection since they are less prone to receive high doses of radiation. Aluminum has a density of 2700 [kg.m<sup>-3</sup>]. Therefore, the coating protection weight is:

$$(2700 \times 0.0055 \times 5) + (2700 \times 0.001 \times 5) = 87.75[kg] \quad (4.15)$$

Hence, the final weight of the structure of the satellite taking into account the panels and the coating protection is:

$$87.75 + 66.6 = 154.35[kg] \quad (4.16)$$

Taking a 5% margin on the overall structure, this brings the structure weight to 162.07 [kg].

### 4.7.3 Mass budget

The summary of every subsystem mass, shown in its respective sections in this document is used to create a complete satellite mass budget. Every equipment mentioned composing these subsystems is taken into account for a total dry mass of the satellite, detailed on table 4.26. It also shows the mass with the mentioned margins applied as well as the percentage of the total mass that corresponds to every subsystem.

For practical reasons, hardware like the cables connecting the subsystems between each other is not included in the design process. However, they cannot be neglected for the computation of the mass budget of the satellite. For this reason, a 10% margin is taken for every subsystem's total mass, in addition to the 5% margin on every "off the shelf" piece of equipment selected.

Subsystem	Without margin [kg]	Including margin [kg]	[%] of total
Structure	154.35	162.07	18.85
E/P	160.04	176.44	20.52
Propulsion	86.1	94.71	11.0
TTC	62.65	68.91	8.0
T/C	13.66	15.03	1.75
Avionics	52.67	62.44	7.26
P/L: NS	93.1	102.41	11.91
P/L: EBS	26.39	29.03	3.37
Dry mass	648.96	711.04	82.7
Propellant	136	149.6	17.3
Wet mass	784.96	860.64	100

Table 4.26: Satellite Mass Budget.

The dry mass of the satellite adds up to 711.04 [kg]. Adding the mass of the Xenon propellant with a 10% margin as seen in section 4.2.4, the overall wet mass of the satellite reaches 860.64 [kg]. This means that the launch mass of the seven satellites will be:

$$860.64 \times 7 = 6024.48[kg] \quad (4.17)$$

With this budget, Pegasus complies with the weight requirement of fewer than 8.5 tons for the launch, still having a margin for the dispenser structure mass.

### 4.7.4 Satellite Design

The computer design of the satellite was made using IDM-CIC, a software developed by the French space agency, CNES. This software is used to serve as a technical reference during the early design phases of a satellite[44]. The final Phase B design of a Pegasus satellite is illustrated in figure 4.38.



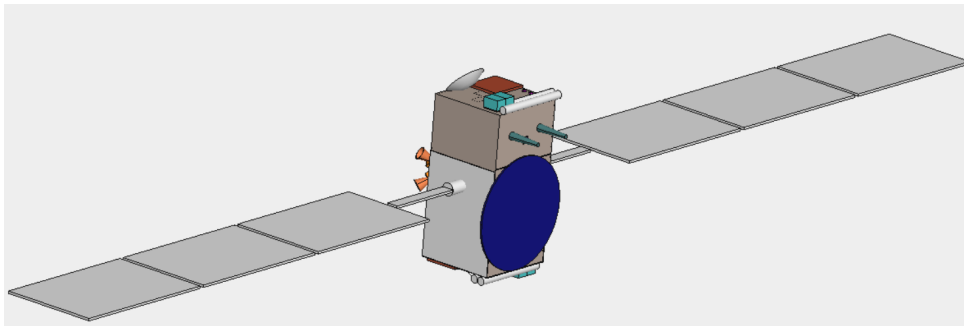
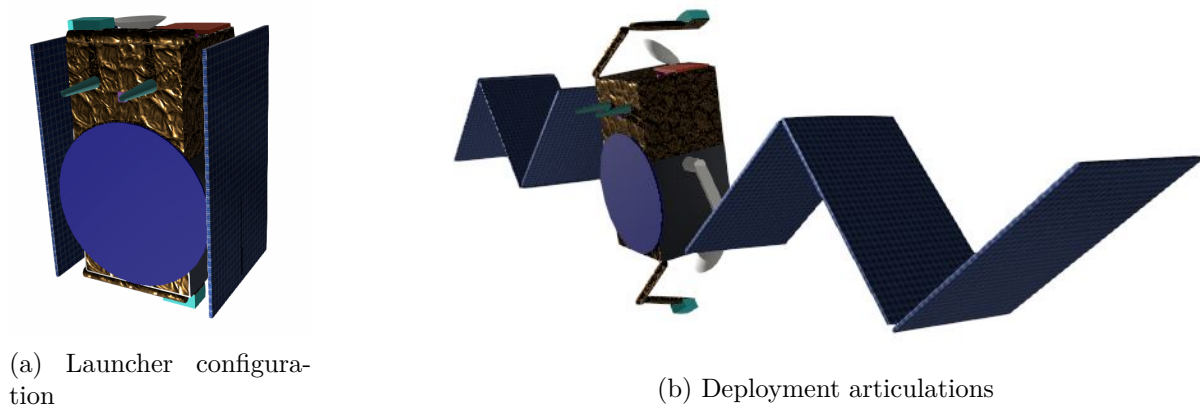


Figure 4.38: Perspective CAD view of a Pegasus spacecraft.

Apart from the outside structure design, all selected components are allocated inside two different categories: Platform and Payload, and then modeled, with their respective mass and consumption to aid with the mass and power budgets. The positioning of the equipment (Fig. 4.41) and the solar array deployment are thought off during the design. Figure 4.39a shows the launcher configuration with a "closed" satellite, and figure 4.39b demonstrates the articulations added to the solar panels and arm thrusters for the deployment.



(a) Launcher configuration

(b) Deployment articulations

Figure 4.39: External Pegasus configurations.

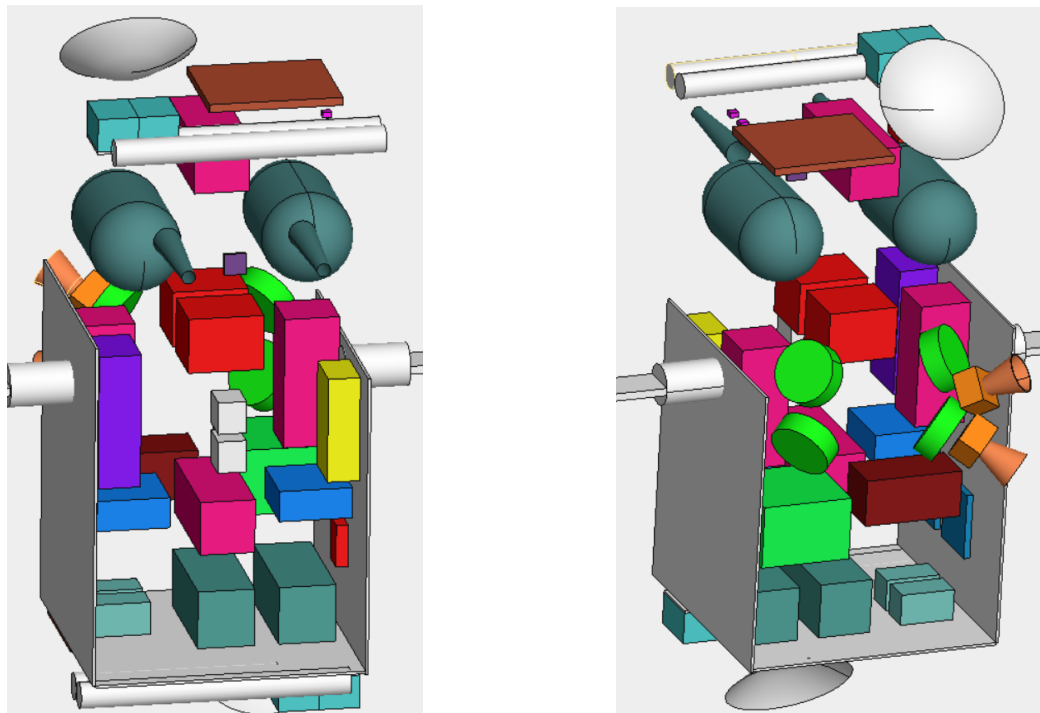
A more realistic view can be created using IDM-VIEW, the viewer of IDM-CIC, which allows computing the entire geometry of the satellite while adding material textures like MLI, and solar cells to the model. The "realistic" model of a Pegasus spacecraft is depicted in figure 4.40.



Figure 4.40: In orbit configuration, of a Pegasus satellite.

## Positioning of equipment

The inside configuration of the subsystems of the satellite is displayed in figure 4.41. An overall arrangement of the subsystems throughout the panels is done by taking into consideration the thermal requirements of each subsystem for them to perform nominally (Section 4.6.2), and their mass to compose the center of balance of the satellites. For an exhaustive overview of all equipment being carried out by the satellite, refer to the System Engineering report, to improve visibility of the equipment, the navigation antenna, and the two structure floors have been rendered invisible.



(a) Inside configuration, Moon side.

(b) Inside configuration, Anti-Moon side.

Figure 4.41: Inside configuration of a Pegasus satellite.

## Inside the spacecraft

- The clocks (air superiority blue) are the most sensitive to a temperature gradient and are then placed at the anti-sun side, the lowest floor on both figures, where they will be protected by the Yaw Law (Section 4.3.3).
- The anti-sun, moon, and anti-moon side covered by radiators (dark grey) to make sure the thermal dissipation of the clocks, as well as hardware such as the Power Control Unit (purple), the Li-ion battery (green box), and the two Spacecraft Monitoring Units (large red boxes) stay under control.
- The tanks are symmetrically placed near the sun side so that their heavy wet mass minimizes the effect on the center of gravity of the spacecraft.
- The reaction wheels (green cylinders) are placed on a pyramid configuration to make them redundant in three directions, the closest as possible to the center of the gravity of the spacecraft.

## Outside the spacecraft

- The EBS and Payload antennas are on the Moon-side, pointing towards the moon.
- The TTC antennas are pointing towards the earth on the sun and anti-sun side of the satellite, where the laser reflectors and the arms carrying the hall thrusters are mounted.
- For the AOCS, the sun sensors are placed on the sun side of the spacecraft while the star trackers lay on the anti-moon side.

## Launcher configuration

With all pieces of equipment placed, the overall dimensions of the satellite on its different views are portrayed in Figure 4.42.

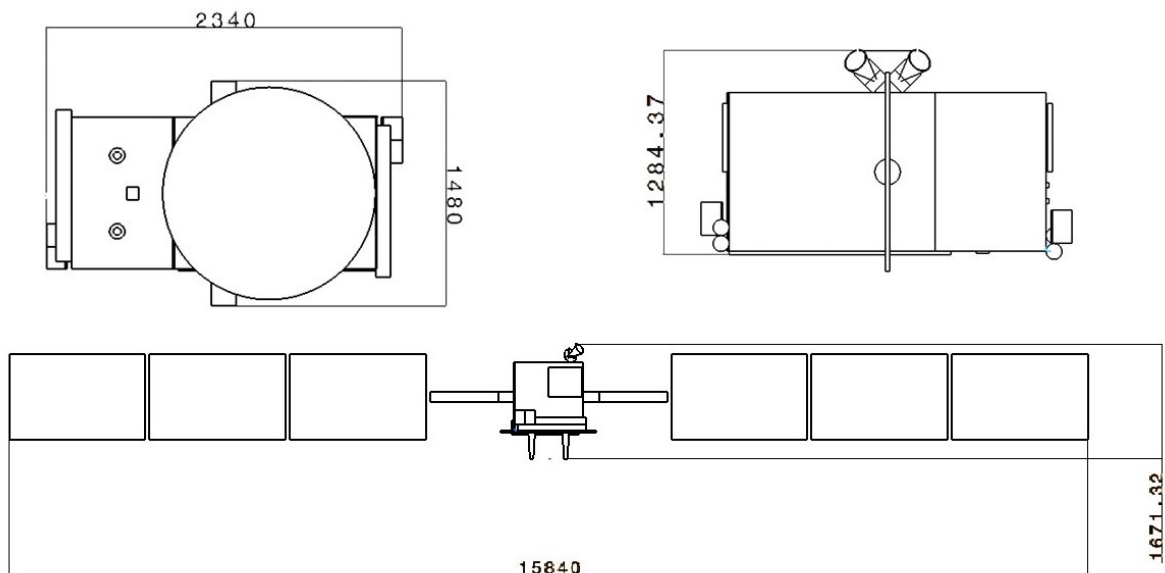


Figure 4.42: Final dimension of a Pegasus satellite in mm.

With these dimensions, it is possible to estimate if the constraint of fitting at least seven satellites of the constellation inside the fairing of Ariane 6 is satisfied. As explained in 4.7.1, Ariane 6's usable diameter is 4.5 [m] wide.

The preferred configuration of the satellites inside the Launcher is displayed in Figure 4.43, where the seven satellites of one Pegasus orbit are launched simultaneously. Following the chosen configuration of the satellite's dispenser, it is possible to estimate its maximum span inside the fairing.

This distance can be modeled as the hypotenuse of a right triangle where the adjacent and opposite sides are known. The adjacent side is equal to the distance between the tip of the two Solar Array Drive Mechanisms, which is 1.480 [m] (Fig. 4.42). The opposite side is equal to two times the distance between the folded helicoid uplink antennas and the star-trackers summed with the distance between the two SADMs, giving  $1.284 \text{ [m]} \times 2 + 1.480 = 4.048 \text{ [m]}$ .

The calculated diagonal using Pythagoras's theorem is:

$$4.048^2 + 1.480^2 = 18.57$$

$$\sqrt{18.57} = 4.31[m]$$
(4.18)

The 4.31 [m] of the maximum dispenser configuration span is inferior to the 4.5 [m] of usable diameter inside Ariane 6's fairing, and two times the height  $2.34 [m] \times 2 = 4.68 [m]$  (Fig. 4.42), is lower than the 11.78 [m] of the fairing (Appendix A.9), validating the strategy. Moreover, the weight constraint has been validated in the 4.26 section.

The seven satellites can be mounted with a first floor counting four spacecraft, and the second floor with an arrangement of three satellites spaced  $120^\circ$  so that the center of mass of the launch structure is not impacted (Fig. 4.43).

In simpler terms, the constellation is ready to be launched!

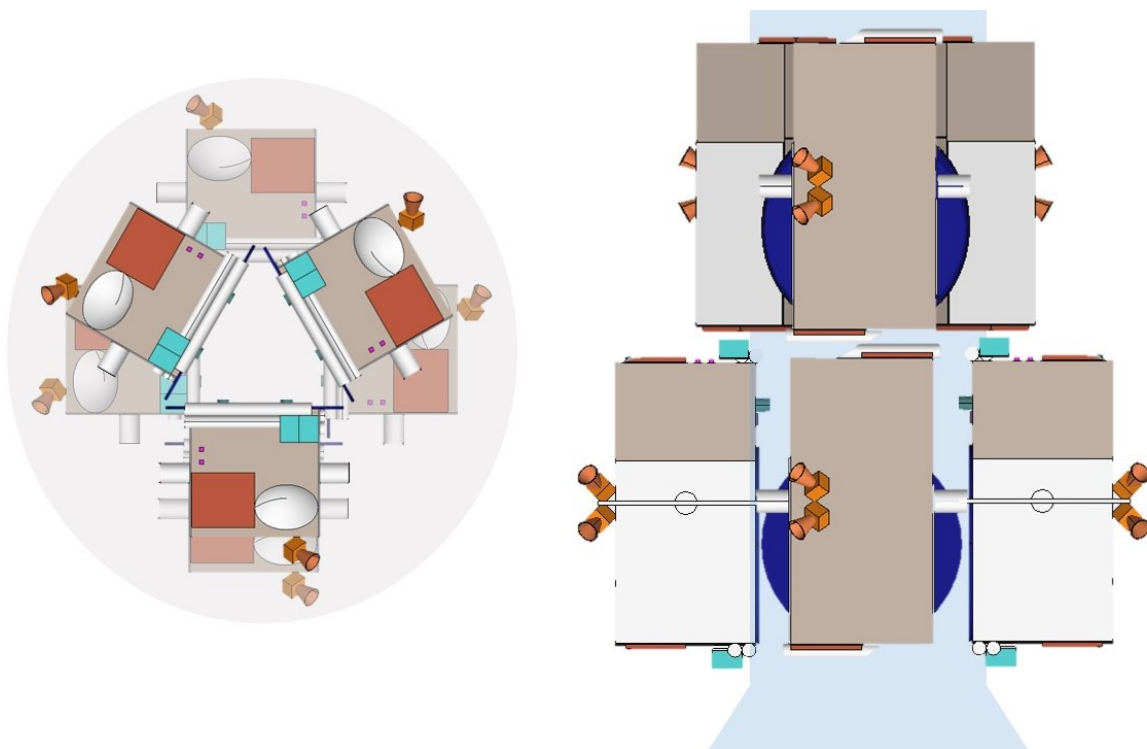


Figure 4.43: Configuration of a one of the three launch of the Pegasus constellation.

## Chapter 5

# Conclusion

The implementation of a GNSS constellation around the Moon has been investigated. The Pegasus constellation provides services with a 100% availability on the lunar surface and on LLO. The NS affords a position accuracy within less than 7 [m] at  $3\sigma$  and a time precision of 32 [ns]. The EBS allows to transmission up to 2 [kbytes] data per message.

To achieve this service level, each orbit is set at 10 000[km] of SMA,  $80^\circ$ . There are seven satellites distributed on three orbits, twenty-one S/Cs in total. These orbits come with thermal environment constraints which are being dealt with using a Yaw Steering Law, radiators, heat pipes, heaters. For the mission to operate 24/24, the subsystems are powered by a 50[V] PCU and 165 [Wh/kg] Li-on battery which will be recharged by 15 [m<sup>2</sup>] of solar panels.

The chosen core payload equipment is composed of four atomic clocks: two PHM clocks to be the master clocks of Pegasus S/Cs and two RAFS for additional reliability. To keep an accurate service, corrections have to be done regularly. The ephemeris corrections will be sent from Earth GS using LRR technique. The clock offset corrections are established synchronizing the whole constellation with the same Earth-based time reference every 12 hours.

To provide the navigation signal, a navigation isoflux antenna is used. The 2 [kBps] EBS channel is enabled by two L-band helix antennas uplink and one S-band down-link patch antenna. Finally, the TTC link with Earth is merged with the Earth-EBS link and received thanks to two S-band parabolic antennas.

To ensure the good operation of the system, the Pegasus's S/Cs is endowed with a pair of robotic arms with six degrees of freedom. On each arm is mounted two electric hall thrusters to perform, among other tasks, station-keeping for the well-being of the mission until the end-of-service. The EoL involves final maneuvers to crash on the lunar surface close to the North Pole, far from the lunar base.

The dimensions have been chosen in order for the constellation to be deployable in less than one year with three launches of Ariane64. One Pegasus S/C is 2.34 [m] long, 1.480[m] in width, and 1.284[m] in depth. In addition, the total dry mass of one S/C, including margin, is 711.04 [kg]. The mass of propellant computed for a 10 years mission being 150 [kg], hence the total wet mass is 860.64 [kg]. The total cost of the mission has been evaluated at 4.4 billion euros, it involves the definition, development, deployment, and operations of Pegasus.



# Appendix A

## Appendix

### A.1 Navigation data sheets

#### LRR & CRR data sheet

Size	49*43*3.0 cm
Diameter of corner cube	33 mm
Number of corner cube	90
Reflective area	770 cm <sup>2</sup>
Material	Fused silica
Dihedral offset	0.5"
Weight	4.85 kg



## Rubidium clock - data sheet

Specifications	Standard
Output Input	10 MHz and 10 MHz auxiliary n/a
Accuracy	$\leq 2E-10$ after launch & commissioning $\leq 1E-10$ under vacuum at delivery
Tempco Temp Aging	n/a -5 to 10C $< 1E-10$ /yr
Power (operating) Voltage Warm-up	$< 35W$ 28V $< 60W$
Size (WxHxL)	217x124x117mm   8.54x4.88x4.6"
Weight	3.4 Kg   7.49 lbs

## Passive Hydrogen Masers Clock - data sheet [6]


Mini PHM	
Output Frequency	10.00285741MHz (FH/142)
Output Level	+ 7dBm (main and auxiliary outputs)
Frequency Drift (/Day)	$\leq 1 \times 10^{-14}$ after 1 week $< 1 \times 10^{-15}$ after 30 days
Allan deviation (Is<t<10 <sup>4</sup> s)	$< 1 \times 10^{-12} \times t^{-1/2}$ max. $< 7 \times 10^{-15} \times t^{-1/2}$ typical
Freq. sensitivity to temperature	$< 1 \times 10^{-15}/^{\circ}C$
Freq. sensitivity to Main Bus Voltage	$\leq 3 \times 10^{-15}/V$
Dimensions	210 x 485 x 218mm
Mass	12Kg
Main Bus Voltage	50V $\pm$ 1V
Power consumption (W)	$\leq 54W$ at -5°C baseplate $\leq 47W$ at +10°C baseplate
Qualification Temperature Range	-15°C to +20°C
Lifetime (MEO Orbit)	>12 years



## A.2 SMS data sheets

### EBS & SMS S-Band Downlink Antenna from ANYWAVES [17]- data sheet 1

The constructor has designed a TTC antenna but we take it as a model for our EBS antenna.




# S-Band TT&C Antenna

Tx and Rx

Hemispherical coverage

HPBW > 90°

Size < 1U



### Space Heritage

- **CNES Advance Label** : material & processes used have French Space Agency heritage.
- **4 flight models in orbit since December 2019** : ANGELS (CNES Program, Hemeria 12U platform) EYESAT (CNES / CSUT JANUS Project, U-Space 3U platform).

### Benefits

- **Full Duplex Telemetry & Telecommand**
- Radome protection against harsh environment : temperatures & ESD
- **Acceptance Tests** (RF, Mechanical, Thermal) included :
  - Return loss
  - Z-axis random vibration
  - Thermal cycling
- ITAR Free


ANYWAVES, a CNES (French Space Agency) spin-off based in Toulouse, provides high-performance and high-quality antennas for satellite constellations.

Perfectly suited to LEO platforms, ANYWAVES S-Band antenna operates both in transmission for telemetry and in reception for telecommand.

Its wide beam coverage enables the best satellite availability for TT&C link.

**ANYWAVES**  
 2, Esplanade Compans Caffarelli - Bât. Toulouse 2000 Hall D  
 31000 Toulouse, France  
 +33 (0)7 67 04 63 49  
[anywaves.eu](http://anywaves.eu)

Waiver : Fact and figures herein are for information only and do not represent any warranty of any kind





## EBS & SMS S-Band Downlink Antenna from ANYWAVES - data sheet 2



**ANYWAVES**  
CONTROL MATERIAL TO MASTER WAVES

# S-Band TT&C Antenna

Tx and Rx

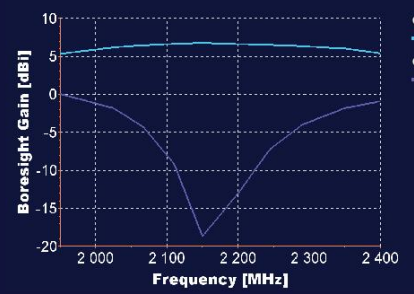
Hemispherical coverage

HPBW > 90°

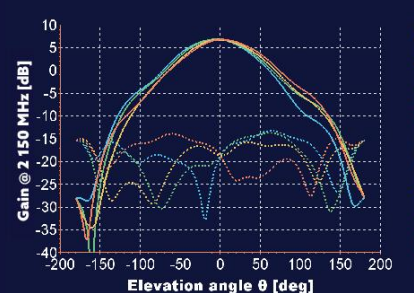
Size < 1U

### Measured performance









### Typical performance


<b>Frequency band</b>	From 2 025 MHz to 2 290 MHz
<b>Bandwidth</b>	> 265 MHz
<b>Polarization</b>	Left or Right Hand Circular Polarization
<b>Reflection coefficient</b>	< -15 dB (all frequency band)
<b>Half Power Beam Width</b>	> 90° (± 45° in all planes)
<b>Efficiency</b>	> 92%
<b>Gain @ 2 150 MHz</b>	Gain @ boresight > 6,5 dBi Gain @ ± 30° > 4,5 dBi Gain @ ± 60° > 0 dBi
<b>Axial Ratio @ 2 150 MHz</b>	< 3 dB from 0° to ± 30° < 5 dB from 0° to ± 60° < 8 dB from 0° to ± 90°

### Physical characteristics

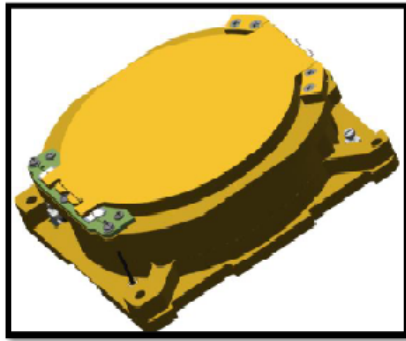
<b>Envelope size without connector</b>	L 79.8 x W 79.8 x H 12.1 mm <sup>3</sup> Protruding height : 6.25 mm
<b>Mass with connector</b>	132 g ± 2 g
<b>RF Power</b>	More than 3W
<b>Operational Temperature</b>	-120°C / + 120°C
<b>Radiation</b>	VESPEL Radome
<b>Electro Static Discharge</b>	ESD free; radome anti-ESD SG121FD white paint on Flight Models only
<b>Connector</b>	Coaxial SMA female (50 Ω)
<b>Mechanical interface</b>	4 x M3 (unthreaded hole)
<b>Acceptance Tests</b>	Performed on Flight Models only

Waiver : Fact and figures herein are for information only and do not represent any warranty of any kind

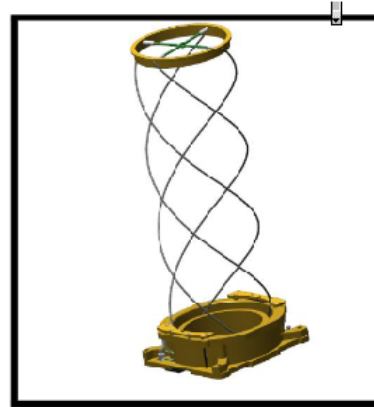
Designed by **AGENCEPURE** +33 (0)5 34 26 00 39 - 2020



## EBS & SMS Reception Helical Antenna from Helical Communication Tech



**STOWED**

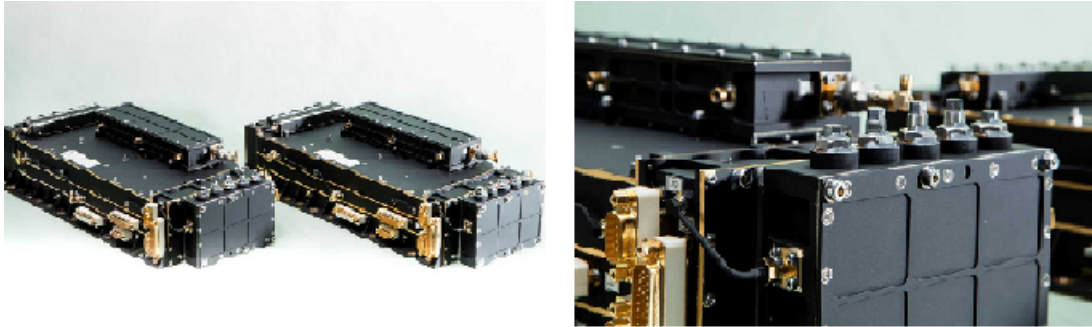


**DEPLOYED**

Mechanical Parameter	Nominal Value
Depth	~100mm
Width	~100mm
Height (400MHz Deployed)	<=270mm
Height (437MHz Deployed)	<=260mm
Height (Stowed)	<=40mm
Mass	<=180g
Thermal Knife Cord Material	50lb. test line
Housing Construction	Ultem 1000 with 18-8 stainless steel fasteners
Filar Construction	Super elastic Shape Memory Wire
Deployment Mechanism	Thermal Knife/Spring Loaded/Super-Elastic Filars
DC Connector	10-Pin Harwin Connector

RF Parameter	Nominal Value
Frequency	400 MHz or 437MHz
Gain	3.5dBi
-3dB Beamwidth	120° *Other beamwidths available
Axial Ratio	<2dB
VSWR	<1.5:1
Polarization	RHCP, LHCP
Transmit Power	10W
RF Connector	SMA (Straight/Right Angle) or SMP (Straight/Right Angle)

## EBS & Transponder Kongsberg data sheet [14]



### KEY FEATURES

- 406.05 MHz input w. LNA
- Selectable bandwidth, 50 or 90 kHz, or fixed 90kHz
- 1544-1545 MHz 5W output, compatible with MEOLUT or GEOLUT
- Internal (typical GEO) or external (typical MEO/Navigation) reference frequency

### HERITAGE

- 4 in orbit on Meteosat 8, 9, 10 and 11
- 4 MTG delivered for launch
- 22 Galileo in Orbit
- 12 Galileo in manufacturing or delivered for launch



## A.3 TTC data sheets

### TTC & Transponder STC-MS03 Honeywell data sheet 1

## Honeywell

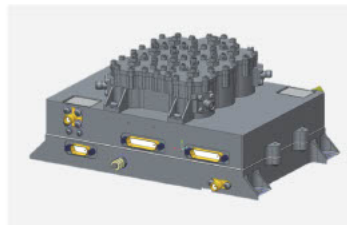
### S-Band TT&C Transceiver

STC-MS03

Honeywell introduces to the space market, our first TT&C transceiver qualified to fly on an ESA S-Class mission (CHEOPS). During many years of supplying equipment on numerous missions, Honeywell has developed an innovative, flight-qualified, digital TT&C Transponder, incorporating software defined radio techniques and utilising our well-known excellence in RF engineering.

#### Main Features

- In-flight configurable modulation, RF power output and data-rate
- Highly adaptable Software Defined Radio (SDR) architecture
- FPGA based design for fast customisation
- ITAR free equipment
- Low mass and low volume unit
- Independent BPSK and PM demodulators
- Supports BPSK (32k to 1024 Kbps), QPSK, OQPSK (up to 6.25 Mbps)
- Flexible RF frequencies and Tx power
- High efficiency GaN amplifier based design
- Fully space qualified equipment with flight heritage and multiple flight units integrated on numerous missions, both commercial and institutional (ESA)
- Established reliability for the most critical communications link to the ground infrastructure

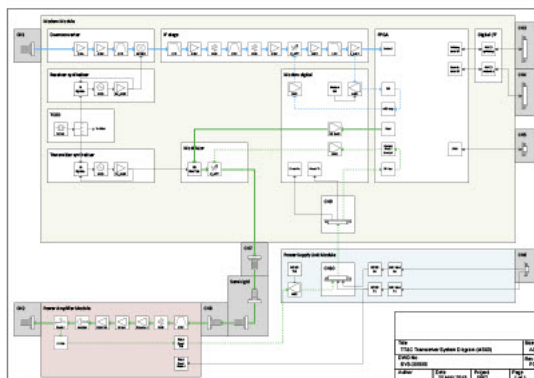


^ TT&C with optional diplexer/filter attached

#### S-Band TT&C Transceiver

The STC-MS03 is an integrated Telemetry, Tracking and Command (TT&C) transceiver which provides two-way radio communication between a spacecraft and ground infrastructure. It is based on a Software Design Radio (SDR) implemented on an FPGA and is designed to allow for fast customisation to accommodate customer requirements.

The critical role of the TT&C function, make it particularly difficult to miniaturise without compromising system reliability. The STC-MS03 is designed with specific attention to power and size in order to address the limited space and reduced battery capacity of small satellites. An extensive qualification campaign has been completed to establish full characterisation of performance in the operation environment.





## TTC & Transponder STC-MS03 Honeywell data sheet 2

### STC-MS03 S-Band TT&C Transceiver Technical Specifications

GENERAL	
EXPECTED LIFE	7 years
MASS	1kg (without diplexer or 1.25Kg with diplexer)
VOLUME	160 x 110 x 44mm
DC POWER CONSUMPTION	18 W typical (Total at 34.4 dBm output power)
SUPPLY VOLTAGE	28V ± 6 V
DATA INTERFACES	Dual RS-422
OPERATING TEMPERATURE RANGE	-20°C to +60°C
RADIATION TOLERANCE	10 KRad

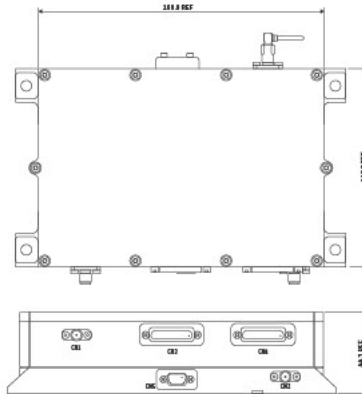
S-BAND RECEIVER	
Rx FREQUENCY RANGE	2025 to 2120 MHz
MODULATION FORMAT / DATA RATES	PCM (NRZ-L)/PSK/PM 8kHz (0.5, 1.2 Kbps) & 16kHz SC (1.24 Kbps) PCM (NRZ-L)/BPSK (8 to 1024 kbps)
MODULATION INDEX TC	0.2 to 1.5 rad
RECEIVER NOISE AND IMPLEMENTATION LOSS	2 dB typical
RECEIVER POWER CONSUMPTION	< 4 W
INPUT POWER RANGE	-135 to -40 dBm
CARRIER ACQUISITION THRESHOLD	-120 dBm
CARRIER ACQUISITION SWEEP RATE	±32 kHz/s
CARRIER TRACKING RANGE	±150 kHz

Optional peripherals that can be supplied include:

- Rx and Tx filters for separate Rx and Tx antennas
- Diplexer for sharing Rx/Tx Antenna
- Hybrids
- Switch
- RF Harness

S-BAND TRANSMITTER	
Tx FREQUENCY RANGE	2200 to 2290 MHz
Tx POWER CONSUMPTION	Less than 14W at 34.4 dBm RF-out
OUTPUT POWER RANGE	0.2 to 3.16W (23 to 35 dBm)
TM MODULATION FORMATS	QPSK, OQPSK, BPSK
DATA MODULATION FORMATS	BPSK (O)QPSK SRRC filter, NRZ/BPSK/PCM, SP-L
DATA RATE	32 to 1024 kbps BPSK 1024 to 6250 kbps QPSK/OQPSK
ENCODING	Convolutional 1/2, NRZ-M, NRZ-L, PCM

DIMENSIONS	
LENGTH	6.29" (160 mm)
WIDTH	4.33" (110 mm)
HEIGHT	1.74" (44.3 mm)



Dimensions in mm



**For more information**  
Please contact Iraklis Hatzithanasiou  
+44 1296 616418  
iraklis@honeywell.com

**Honeywell Aerospace**  
Triangle Business Park,  
Stoke Mandeville, Aylesbury  
HP22 5SX  
United Kingdom  
aerospace.honeywell.com

N61-1603-000-000 | 07/16  
© 2016 Honeywell International Inc.

**Honeywell**

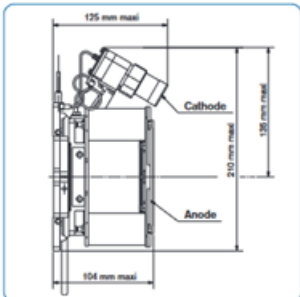


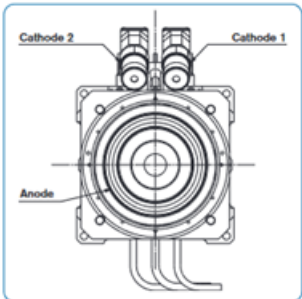
## A.4 Propulsion data sheets

### PPS-1350 thruster data sheet [45]

Performance specifications	
• Power (nominal)	1,500 W
• Thrust	92 mN
• Specific impulse	1,800 sec.
• Specific power	16.3 W/mN
• Minimum impulse delivered	<3 N.s
• Total impulse delivered	2.10 <sup>6</sup> N.s
• Number of cycles	7,800
• Discharge current	4.28 A
• Efficiency	55%
• Supply voltage	300 to 350 V
• Xenon feed pressure	2.5 to 2.8 bar
• Xenon class	high purity
• Mass (including 2 Xe flow control systems)	5.3 kg





### ETS VIII xenon tank data sheet [24]

PARAMETERS	REQUIREMENTS
Maximum Expected Operating Pressure (MEOP)	150 bar (2175 psi), 50 cycles minimum
Proof Pressure	187.5 bar (2719 psi), 5 cycles minimum
Burst Pressure	225 bar (3264 psi) minimum
Collapse Pressure	-1 bar (-14.7 psi), 20 cycles minimum
Propellant Weight	89 kg (196 lb) Xenon gas
Size	336.7 mm Ø x 682.8 mm long, (13.26" Ø x 26.9" long), boss to boss
Overall Length	841.8 mm (33.14 inches) nominal
Tank Weight	7 kg (15.4 lb) maximum
Tank Capacity	50 liters (3050 in <sup>3</sup> ) minimum, unpressurized
Natural Frequency	>100 Hz
Compatibility	Xenon, Argon, IPA, Helium, Nitrogen, PF 5060, and DI water
Shell Leakage	<1x10 <sup>-6</sup> std cc/sec He @ MEOP
Failure Mode	Leak-before-burst
Operating Temperatures	5°C to 55°C (41°F to 131°F)



## XPRFS data sheet [21]

Xenon Pressure Regulator Characteristics	
Regulator Type	"Bang-bang" type regulator (pulsing valves) with two parallel redundant regulation branches, each branch being twice redundant.
Flow Control	The maximum possible flow rate is limited by upstream pressure and smallest diameter in the system's flow path. The actual flow is controlled by regulation of the pressure within the plenum.
Inlet Pressure	3 to 120 bar
Outlet Pressure	2.65 bar $\pm$ 0.2 bar
External Leakage	< 1x10 <sup>-6</sup> scc/s GHe
Internal Leakage	< 2x10 <sup>-4</sup> scc/s GHe
Flow Rate	> 6 mg/s gaseous xenon
Flow Restrictor	46800 Lohms
Total propellant throughput	300 kg max
Mass	< 5.9 kg
Dimensions	443,5 mm x 278 mm x 228 mm (plenum)
Temperature Range	27 C° to 45 C° (operating)
Design Life	15 years
Cycle Life	1,000,000 qualified
Reliability	> 0.998

## PPU Mk1 data sheet [25]

### Power Processing Unit Mk1

Mass	10.9 kg
Dimensions	<u>390x190x186 mm<sup>3</sup></u>
P anode	<b>1 500 W</b>
Input power bus	<b>50V</b> or 100V
Efficiency at nominal conditions	91.6% (50V) 92.4% (100V)
Reliability for one PPU + TSU	2996 fits
Operating up to pressure of	200 mPa
TC/TM plug-in module	Mil-Std-1553 OBDH-RS485 (RUBI) ML16/DS16
Thrusters	<b>SPT-100</b> PPS1350-G



## A.5 AOCS data sheets

### Sun Sensors data sheet [28]

	NCSS-SA05	NFSS-411
<b>FUNCTIONAL CHARACTERISTICS</b>		
Field of view	114°	140°
Update rate	>10 Hz (limited by customer ADC)	5 Hz typical
Accuracy	<0.01° RMS error over FOV	≤0.1° RMS error over 120° FOV
<b>PHYSICAL CHARACTERISTICS</b>		
Dimensions	33 mm x 11 mm x 6 mm	34 mm x 40 mm x 20 mm
Mass	<5 g	<35 g
Power	<10 mA @ 5 V	Idle: <3mA [15mW], bootloader mode <8mA [40mW], application mode Active: <30mA [150mW]
<b>ENVIRONMENTAL CHARACTERISTICS</b>		
Thermal (acceptance/operational)	-25 °C to +70 °C	-25 °C to +70 °C
Mechanical Tests (qualification)	16 g <sub>rms</sub> (random), 20g (sin)	17.25g rms (random), 26.25g (sin), 1600 g shock
Radiation (TID) (qualification)	n.a.	20 krad (component level)
<b>INTERFACES</b>		
Power supply	5 V <sub>DC</sub>	5 V <sub>DC</sub> to 50 V <sub>DC</sub> (5 V <sub>DC</sub> nominal)
Data	5 analogue channels	RS-485 UART
Connector	9-way female Nano-D	9-way socket Micro-D
Mechanical	3 x M2 threaded holes	4 x M2 clearance holes
<p><b>ACCEPTANCE TESTING:</b> All FM parts undergo random vibration (10 rms) as well as thermal cycling (four cycle ambient pressure) to five degrees beyond operation of thermal specifications. However, NewSpace can perform additional environmental testing if required by a client.</p> <p><b>CONFIGURATION MANAGEMENT:</b> Specifications are subject to change. Please refer to latest version.</p>		



## Star Tracker data sheet [29]

CHARACTERISTICS	A-STR	AA-STR
Detector	MPP CCD	HAS APS
FOV	16.4 x 16.4°	20 x 20°
Dynamic range	1.5M <sub>i</sub> to 5.5M <sub>i</sub>	1.5M <sub>i</sub> to 5.5M <sub>i</sub>
Number of Tracked Stars	Up to 10	Up to 15
Tracking rate	Up to 2°/sec	Up to 2°/sec
Acquisition time (from Lost in Space)	Lower than 6 sec.	Lower than 9 sec.
SEU Tolerance	up to 17000 protons/cm <sup>2</sup> /sec (depending on SW settings)	up to 170000 protons/cm <sup>2</sup> /sec (depending on SW settings)
Update rate	10Hz, 4Hz	10Hz, 8Hz, 5Hz, 4Hz
ACCURACY (SSIGMA; EOL; FULL TEMPERATURE RANGE; 10HZ UPDATED RATE)		
Bias (Gaussian distribution)	8.25 arcsec (pitch/yaw) 11.1 (roll)	8.25 arcsec (pitch/yaw) 11.1 (roll)
Low Frequency Error (FOV error)	<3.6 arcsec (pitch & yaw) <21 arcsec (roll)	<3.5 arcsec (pitch & yaw) <15.6 arcsec (roll)
NEA (random error) @0.7°/sec tracking rate	<6 arcsec (pitch & yaw) <6.3 arcsec (roll)	<6 arcsec (pitch & yaw) <49.4 arcsec (roll)
NEA (random error) @0.5°/sec tracking rate	<7.5 arcsec (pitch & yaw) <7.8 arcsec roll	<8.4 arcsec (pitch & yaw) <68.2 arcsec (roll)
NEA (random error) @ 2°/sec tracking rate	<25 arcsec (pitch & yaw) <230 arcsec roll	<34 arcsec (pitch & yaw) <288 arcsec (roll)
DATA INTERFACES		
Telecommand & Telemetry	MIL-STD-1553B; RS 422	MIL-STD-1553B; RS 422
Interface for EGSE	Custom	Custom
MECHANICAL INTERFACES		
Size (L x W x H)	195mm x 175mm x 290.5mm (40 deg SEA baffle)	164mm x 166mm x 348mm (25 deg SEA baffle)
Mass	3.55kg with 40° SEA baffle GEO orbit radiation shielding	2.6kg with 26° SEA baffle GEO orbit radiation shielding
ELECTRICAL INTERFACES		
Power Supply	20V to 50V	60V to 110V, 20V to 52V
Power consumption	8.9W @ 20°C 13.5W @ 60°C	5.6W @ 20°C 12.6W @ 60°C
ENVIRONMENTAL CONDITIONS		
Operational temperature	-30°C to +60°C	-30°C to +60°C
Storage temperature	-35°C to +70°C	-35°C to +65°C
Pressure	Ambient or space vacuum	Ambient or space vacuum
Vibrations levels	Design level Higher than 22g rms Qualification level 17.5g rms all axis Shock: 2000g	Design level Higher than 22g rms Qualification level 17.03g rms all axis Shock: 2000g
Lifetime	18 years in GEO orbit	18 years in GEO orbit
Reliability	1346 fits with Level 1 parts	850 fits with Level 1 parts



## Reaction Wheel data sheet [30]

Main technical data	RSI 4-75/60	RSI 12-75/60
Angular momentum at nominal speed	4 Nms	12 Nms
Operational speed range	± 6,000 rpm	± 6,000 rpm
Speed limiter (EMF)	< 7,000 rpm	< 7,500 rpm
Motor torque at nominal speed	75 mNm	75 mNm
Loss torque (max.)	< 20 mNm	< 20 mNm
Dimensions		
Diameter	222 mm	247 mm
Height	85 mm	85 mm
Mass	< 3.7 kg	< 4.85 kg
Power consumption		
Steady state at nominal speed	< 20 W	< 20 W
Maximum torque at nominal speed	< 90 W	< 90 W
Power interface		
Supply voltage	24 to 51 VDC	24 to 51 VDC
Input current	< 3.75 A	< 3.75 A
Galvanic isolation between primary return and secondary return	Yes	Yes
Preceding stage	Yes	Yes
On/off relay	Yes	Yes
Signal interface		
Torque command and direction	Analog/bi-level	Analog/bi-level
Speed measurement and direction	Analog/bi-level	Analog/bi-level
Motor torque (current)	Analog	Analog
Bearing temperature	Analog (thermistor)	Analog (thermistor)
On/off status	Bi-level	Bi-level
On/off command	Pulses	Pulses
Environmental conditions		
Qualification/protoflight temperature	-10 to +55 °C (mineral oil), -25 to +75 °C (synthetic oil)	-10 to +55 °C (mineral oil), -25 to +75 °C (synthetic oil)
Operating temperature	-5 to +50 °C (mineral oil), -20 to +70 °C (synthetic oil)	-5 to +50 °C (mineral oil), -20 to +70 °C (synthetic oil)
Survival/Non-operating Temperature	-20 to +60 °C (mineral oil), -40 to +75 °C (synthetic oil)	-20 to +60 °C (mineral oil), -40 to +75 °C (synthetic oil)
Lifetime	> 15 years (in orbit)	> 15 years (in orbit)



## SADM data sheet [31]

DESIGN CHARACTERISTICS				
<b>Mechanism</b>				
Drive direction	Forward and reverse rotation (endless rotation)			
Speed range	0 to 1 rev / 15 min			
Maximum rotation speed	0.4°/s			
Qualified life span	12 years in orbit + 5 year storage (2 years Integrated on Satellite)			
Qualification sequence	21000 sweeps			
<b>Actuator</b>				
Winding resistance (at 20°C)	82.9 $\Omega$ ±5%			
Number of steps per revolution of motor	360			
Gear ratio options	1:486.667 or 1:184			
Stable positions (motor is unpowered)	175200 or 66240 steps			
1 step corresponds to (at output)	0.002065° or 0.0054°			
SA holding torque (unpowered motor)	≥ 20 Nm			
SA average torque (powered motor)	≥ 10 Nm			
SA repeated peak torque (powered motor)	≥ 14 Nm (starting and stop)			
SA momentary peak torque (powered motor)	≥ 20 Nm (exceptional peak torque)			
<b>Power Transfer (forward and reverse line)</b>				
Number of power transfers	10 (with 5 „win’ returns)			
Current	4.0 A <sub>RMS</sub>			
Voltage	Nom. 55 V			
Power transfer	2.2 kW			
Insulation	≥ 10 M $\Omega$			
Noise	10 mV <sub>RMS</sub> /A			
<b>Signal Transfer forward or reverse line)</b>				
Signal transfer number	8			
Current	1 A <sub>RMS</sub>			
Voltage	55 V			
Insulation	≥ 10 M $\Omega$			
Noise	10 mV <sub>RMS</sub> /A			
<b>Position Measurement</b>				
Potentiometer resistance	10 k $\Omega$ ± 10%			
Potentiometer accuracy	±0.5° resp. ( $\pm 8.73 \times 10^{-5}$ rad)			
Potentiometer linearity	±0.15%			
Alternative optical position sensor	10 bit, RS-422 Interface, dual 5 V and 12 V supply			
Reference position sensor	Active-low OC signal, 0.1° repeatability, 5...9 V supply			
<b>Dimensions</b>				
External diameter	140 mm to 160 mm			
Total length (from SA Interface flange to rear part)	240 mm			
Mass without external leads and connectors	M ≤ 4.0 kg			
Mass with external leads and connectors	M ≤ 4.25 kg			
<b>Mechanical Interface</b>				
	PF Interface		SA Interface	
	See Figures 2 to 5		See Figures 2 to 5	
<b>Power Consumption (worst case)</b>				
	V <sub>BUS</sub>	P <sub>POWER</sub>	P <sub>SADM</sub>	Total Power
Maximum conditions	28 V	4.6 W	N/A	< 4.6 W
<b>Qualified Temperatures</b>				
	T <sub>min</sub>	T <sub>Ambient</sub>	T <sub>max</sub>	
Ground Storage	+ 10°C	+22°C	+ 40°C	
In orbit non operational	- 40°C		+ 75°C	
Cold start-up limit	- 25°C			
In orbit operational (note: SA Interface at -60°C/+110°C)	- 25°C	+22°C	+ 70°C	



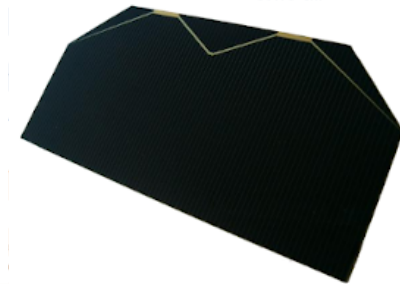


SAFT VES180 battery cells data sheet [46]

	VES 180
Guaranteed capacity (Ah)	48
Mean voltage at C/1.5	3.6
End of charge voltage (V)	4.1
Energy (Wh)	175
Specific energy (Wh/kg)	165
Height (mm)	250
Diameter (mm)	54
Weight (kg)	1.11
Power capability current pulses A	
Main application	GEO, MEO



## AZUR SPACE 3G30-C data sheet [35]



### 30% Triple Junction GaAs Junction Solar Cell Type: TJ Solar Cell 3G30C - Advanced



#### Design and Mechanical Data

Base Material	GaInP/GaAs/Ge on Ge substrate
AR-coating	TiO <sub>2</sub> /Al <sub>2</sub> O <sub>3</sub>
Dimensions	40 x 80 mm ± 0.1 mm
Cell Area	30.18 cm <sup>2</sup>
Average Weight	≤ 86 mg/cm <sup>2</sup>
Thickness (without contacts)	150 ± 20 μm
Contact Metallization Thickness (Ag/Au)	4 – 10 μm
Grid Design	Grid system with 2 contact pads



#### Electrical Data

		BOL	2,5E14	5E14	1E15
Average Open Circuit V <sub>oc</sub>	[mV]	2700	2616	2564	2522
Average Short Circuit I <sub>sc</sub>	[mA]	520.2	518.5	514.0	501.9
Voltage at max. Power V <sub>mp</sub>	[mV]	2411	2345	2290	2246
Current at max. Power I <sub>mp</sub>	[mA]	504.4	503.2	500.6	486.6
Average Efficiency η <sub>bare</sub> (1367 W/m <sup>2</sup> )	[%]	29.5	28.6	27.8	26.5
Average Efficiency η <sub>bare</sub> (1353 W/m <sup>2</sup> )	[%]	29.8	28.9	28.1	26.8

Standard: CASOLBA2005 (05-20MV1, etc); Spectrum: AM0 WRC = 1367 W/m<sup>2</sup>; T = 28 °C

@fluence 1MeV [e/cm<sup>2</sup>]

#### Acceptance Values

Voltage V <sub>op</sub>	2350 mV
Min. average current I <sub>op avg</sub> @ V <sub>op</sub>	505 mA
Min. individual current I <sub>op min</sub> @ V <sub>op</sub>	475 mA



#### Temperature Gradients

		BOL	2,5E14	5E14	1E15	
Open Circuit Voltage	ΔV <sub>oc</sub> /ΔT ↑	[mV/°C]	- 6.2	- 6.5	- 6.6	- 6.7
Short Circuit Current	ΔI <sub>sc</sub> /ΔT ↑	[mA/°C]	0.36	0.33	0.35	0.38
Voltage at max. Power	ΔV <sub>mp</sub> /ΔT ↑	[mV/°C]	- 6.7	- 6.8	- 7.1	- 7.2
Current at max. Power	ΔI <sub>mp</sub> /ΔT ↑	[mA/°C]	0.24	0.20	0.24	0.28

@fluence 1MeV [e/cm<sup>2</sup>]



#### Threshold Values

Absorptivity	≤ 0.91 (with CMX 100 AR)
Pull Test	> 1.6 N at 45° welding test (with 12.5μm Ag stripes)
Status	Qualified

## PCU 50V Airbus data sheet [32]



### KEY FEATURES

- Generates a precise and fully regulated 50V bus ( $\pm 0.5\%$ ), with a maximum ripple up to 0.25V peak to peak, during sunlight and eclipse and under all spacecraft operating conditions
- Modular concept providing power outputs ranging from 2kW to 6kW in 1000W steps
- Implements a centralised low impedance point for power distribution (Platform and Payload)
- Fully autonomous operation without support from any other satellite subsystems under all mission operational conditions including contingency situations
- Single Point Failure Free architecture
- Battery connection / disconnection through Solid State Switches in the Battery Discharge Regulator (BDR)
- Autonomous battery disconnection in the event of an over discharge
- Capability to operate with either one or two independent batteries. In the case of two batteries, specific control electronics guarantee balanced battery discharge even after one failure
- Power Modules include 3 Sequential Switching Shunt Regulators (S3R) sections plus 1 BDR to optimise thermal dissipation and control
- Li-Ion battery charge / discharge control via a fully autonomous hardware control loop
- Communication with the OBC via MIL STD 1553 Bus
- Compatible with Multi Junction High Capacitance Ga-As Solar Cells

### CUSTOMERS / APPLICATION

- Telecommunications, SGEO Platform

### INTERFACES

- Power bus: 50V  $\pm 0.5\%$
- Battery: Li-Ion
- Dialog: MIL STD 1553

### ENVIRONMENTS

- Thermal: -15°C to +60°C (operating), -25°C to +60°C (non operating), -25°C (start-up)
- Radiation: total dose (15 years GEO orbit), SEU, latchup immune
- Lifetime: 15 years

### MAIN APPLICATION FIELDS

- All GEO applications

### DEVELOPMENT STATUS

- 5kW version qualified in March 2012
- First FM delivery by end 2012

### BUDGETS

- Mass: 25kg @ 5.5kW
- Volume: 480 to 505 x 260 x 265mm<sup>3</sup>
- Power: 2kW to 6kW @ 50V Fully Regulated
  - > 96% BDR efficiency @ 5kW, 36V battery voltage
  - > 97% BCR efficiency @ 14A battery charge, 36V battery voltage
  - > 98.9% S3R efficiency

### Main performances of the PCU

#### Solar array Power Control S3R

- Switching Shunt Regulator: Up to 24 sections, 7A per section
- 20A maximum Solar Array peak current even after one failure
- No power loss after a failure
- Compatible with Multi Junction Solar Array cells up to 1.5 $\mu$ F per 7A section (7 $\mu$ F/A per 3J Ga-As cell)

#### Battery Discharge Regulator, BDR

- Weinberg topology
- Up to 1000W per module
- Independent solid state battery isolation device per BDR module
- 27.5V to 48V battery voltage I/P range
- 3% BDR output current matching

#### Battery Charge Regulator, BCR

- Low ripple buck topology
- 14A maximum output current
- Independent solid state battery isolation device per BCR module
- 27V to 48V battery voltage O/P range
- Charge Method: Taper Charge (Constant Current/Constant Voltage)

#### Main Error Amplifier, MEA

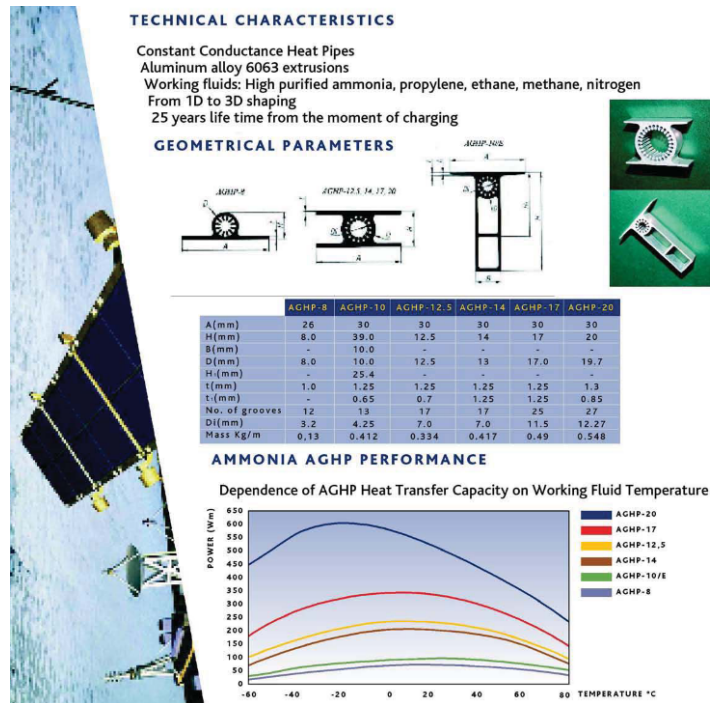
- Bus regulation better than 0.5%
- Bus ripple better than 0.5% peak-peak, compatible with last generation telecom loads
- Compatible with TDMA load mode
- Compatible with 6.6kW peak consumption @ electric propulsion operation





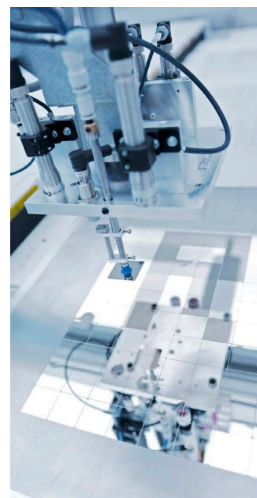
## A.7 Thermal data sheets

### Iberespacio heat pipes data sheet [47]



### Ruag OSR data sheet [48]

Characteristics	
Materials	Borosilicate glass Optical Solar Reflector (OSR) with reflective back coating
Available glass finishes	Plain surface Electrically conductive coating (ITO) Low UV absorbance coating
Area Weight	470 g/m <sup>2</sup> all inclusive (using 150 μm thick OSR)
No silicone contamination	
Temperature range	-70 °C to +90 °C
Thermo-Optical	$\alpha_s \leq 0.06 / \epsilon_{IR} \geq 0.83$  (OSR with ITO and low UV coating)
Front to back resistance	<200 kΩ

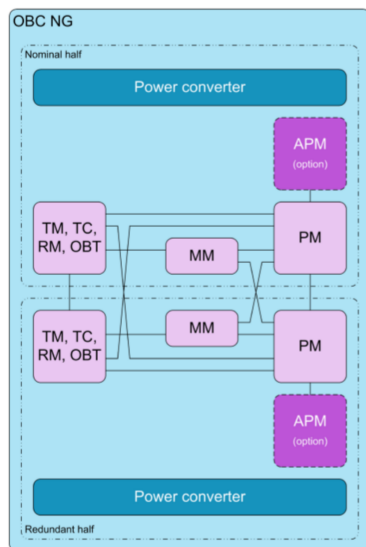




## A.8 OBDH data sheets

### On Board Computer data sheet [49]

#### Block Diagram



#### Software and Development Environment

- Eclipse integrated software development environment
- GNU cross compiler (GCC) suite
- Boot Software and Hardware Driver Software
- RTEMS operating system Board Support Package
- LEON Tools utilizing the advanced on-chip Debug Support Unit
  - LEONmon allowing source code level debugging using gdb and eclipse
  - xLoader for loading non-volatile SW image storage
  - BackTracker for software execution history analysis
  - Trace for real-time software execution trace dump
  - Inspector for real-time non-intrusive inspection of target
  - Shell for scripting of common tasks or tests
  - Broker management for LEON Tools and target management

#### Processing Function

- SPARC V8 LEON FT
- 110 DMIPS @ 87.5 MHz
- 32 Kbytes instruction cache
- 16 Kbytes data cache
- 512 MiB processing memory
- 32 KiB Boot PROM
- 8 MiB SW Image Storage
- Gigabit Ethernet Debug Link
- Real-Time Processor Trace Dump
- Hardware Driver Software

#### Interfaces

- 2 x 7 SpaceWire interfaces
- 2 x 2 Control Area Network (CAN) buses
- 2 x 2 Redundant MIL-STD-1553B buses
- 2 x 2 Pulse Per Second (PPS) inputs
- 2 x 16 Synchronisation Pulse outputs
- 2 x 8 Alarm inputs
- 2 x 3 Separation Strap inputs
- 2 x 4 TM serial outputs up to 20 Mbps
- 2 x 2 TC serial inputs up to 2048 kbps
- 2 x 30 Essential TM status inputs
- 2 x 128 Pulse Command outputs
- External USO input (optional)
- Primary power supply: 28V, 50V or 100V

#### Budgets

Unit Size	208 x 242 x 278 mm
Mass	6.5 kg
Power Consumption	< 23 W
Reliability	0.99
In-Orbit Life Time	up to 20 years
Processing memory	512 MiB w EDAC
File/Data storage	2 x 374 Gbit w EDAC

#### Heritage

- >2900 failure free equipment years in orbit
- >300 Launcher On-Board Computers
- >120 Satellite Data Handling Systems
- EDRS-C, MTG, ExoMars Rover, Hispasat 36W-1, SARah, Electra, Euclid, JUICE

RUAG Space | Product Group Electronics  
sales.electronics.usa@ruag.com  
sales.electronics.europe@ruag.com  
www.ruag.com/space

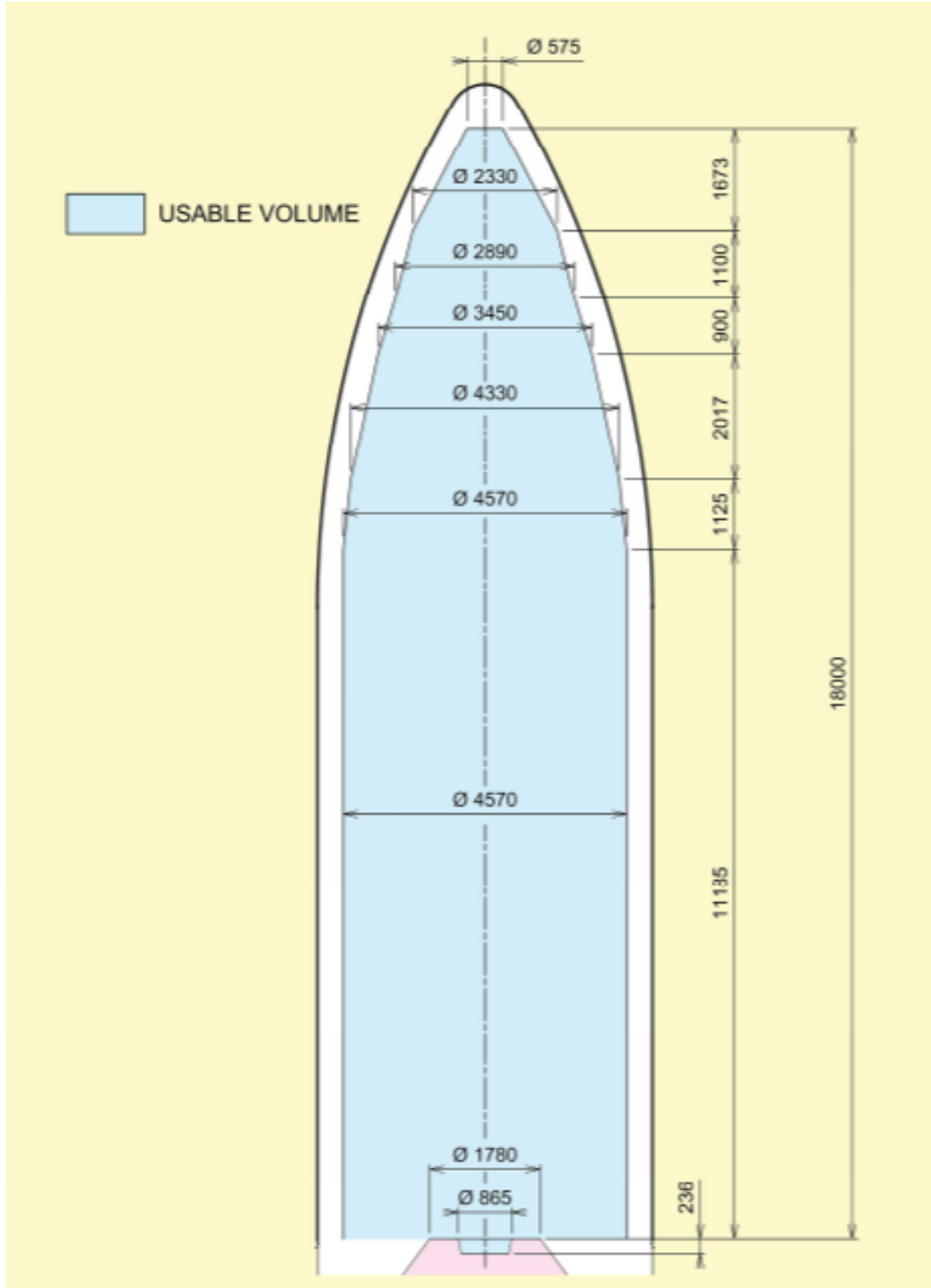


R-COMM-HOT-1238507-16E

05/19

## A.9 Structure data sheets

Ariane 6 faring [50]





# Bibliography

- [1] GSC, *Orbital and technical parameters*, <https://www.gsc-europa.eu/system-service-status/orbital-and-technical-parameters>, Accessed: 2021-04-13, 2021.
- [2] G. Mingotti, F. Topputo, and F. Bernelli-Zazzera, “Low-energy, low-thrust transfers to the moon,” *Celestial Mechanics and Dynamical Astronomy*, vol. 105, pp. 61–74, Nov. 2009. DOI: 10.1007/s10569-009-9220-7.
- [3] M. List, S. Bremer, B. Rievers, and H. Selig, “Modelling of solar radiation pressure effects: Parameter analysis for the MICROSCOPE mission,” *International Journal of Aerospace Engineering*, vol. 2015, pp. 1–14, 2015. DOI: 10.1155/2015/928206. [Online]. Available: <https://doi.org/10.1155/2015/928206>.
- [4] E. Batori, N. Almat, C. Affolderbach, and G. Mileti, “Gnss-grade space atomic frequency standards: Current status and ongoing developments,” *Advances in Space Research*, Oct. 2020. DOI: 10.1016/j.asr.2020.09.012.
- [5] *Spectratime rafs*, <https://www.oroia.com/products/atomic-clocks-oscillators/rafs>, NIST.
- [6] C. Leonardo, *Passive hydrogen maser*, [https://www.leonardocompany.com/documents/20142/3150113/Passive\\_Hydrogen\\_Maser\\_LQ\\_mm07688\\_.pdf?t=1538987567626](https://www.leonardocompany.com/documents/20142/3150113/Passive_Hydrogen_Maser_LQ_mm07688_.pdf?t=1538987567626), Accessed: 2021-04-17, 2017.
- [7] G. Bawden, *Coordination and prioritization of laser ranging on retroreflector equipped gnss*, <https://www.unoosa.org/documents/pdf/icg/2017/wgd/wgd3-05.pdf>, Accessed: 2021-04-16, 2017.
- [8] T. Jr, E. Adelberger, J. Battat, C. Hoyle, N. Johnson, R. Mcmillan, C. Stubbs, and H. Swanson, “Apollo: Millimeter lunar laser ranging,” *Classical and Quantum Gravity*, vol. 29, pp. 184005–11, Aug. 2012. DOI: 10.1088/0264-9381/29/18/184005.
- [9] ESA, *Galileo: Reflector information*, [https://ilrs.gsfc.nasa.gov/docs/IOV\\_LRA\\_2009-12-14.pdf](https://ilrs.gsfc.nasa.gov/docs/IOV_LRA_2009-12-14.pdf), Accessed: 2021-04-16, 2006.
- [10] J. A. Stone and J. H. Zimmerman, *Index of refraction of air*, <https://emtoolbox.nist.gov/Wavelength/Documentation.asp>, NIST.
- [11] J. Subirana, J. Zornoza, and Hernandez-Pajares, *Galileo navigation message*, [https://gssc.esa.int/navipedia/index.php/Galileo\\_Navigation\\_Message](https://gssc.esa.int/navipedia/index.php/Galileo_Navigation_Message), Accessed: 2021-04-14, 2011.
- [12] S. Arenas, F. Monjas, A. Montesano, C. Montesano, C. Mangenot, and L. Salghetti, “Performances of galileo system navigation antenna for global positioning,” in *Proceedings of the 5th European Conference on Antennas and Propagation (EUCAP)*, 2011, pp. 1018–1022.



- [13] F. Gonzalez, S. M, and S. E, *Phase centre calibration of the galileo satellite navigation antenna*, [http://navigation-office.esa.int/attachments\\_17858812\\_1\\_Gonzalez\\_IGS\\_WS\\_2017.pdf](http://navigation-office.esa.int/attachments_17858812_1_Gonzalez_IGS_WS_2017.pdf), Accessed: 2021-04-17, 2017.
- [14] Kongsberg, <https://www.kongsberg.com/fr/kda/products/space/products/on-board-electronics/search-and-rescue-transponders/>, Accessed: 2021-04-17.
- [15] Teledyne, <https://www.teledyne.com/en-us>, Accessed: 2021-04-17.
- [16] Wikipedia, “Phase-shift keying,” en, *Wikipedia*, Apr. 2021.
- [17] Anywaves, *S-band ttc antenna*, <https://anywaves.eu/products/s-band-ttc-antenna/>, Accessed: 2021-03-27, 2020.
- [18] H. C. Technologies, <https://www.cubesatshop.com/vendor-information/hct-helical-communication-technologies/>, Accessed: 2021-04-17.
- [19] ESA, *Snecma pps-1350 ion engine will provide smart-1’s primary propulsion*, [https://www.esa.int/ESA\\_Multimedia/Images/2003/07/SNECMA\\_PPS-1350\\_ion\\_engine\\_will\\_provide\\_SMART-1\\_s\\_primary\\_propulsion](https://www.esa.int/ESA_Multimedia/Images/2003/07/SNECMA_PPS-1350_ion_engine_will_provide_SMART-1_s_primary_propulsion), Accessed: 2021-04-12.
- [20] K. Herbert, *Eutelsat 172b satellite with all-electric propulsion*, <https://directory.eoportal.org/web/eoportal/satellite-missions/e/eutelsat-172b>, Accessed: 2021-04-13, 2002.
- [21] ArianeGroup, *Pressure regulator for ion space propulsion systems*, <https://www.space-propulsion.com/spacecraft-propulsion/valves/pressure-regulator.html>, Accessed: 2021-04-12, 2020.
- [22] T. Collard, J. Sheehan, and A. Gallimore, “Pressurized xenon propellant management system for the cubesat ambipolar thruster,” Jul. 2015.
- [23] E. Conti, *Enrico conti’s liquid xenon page*, <https://userswww.pd.infn.it/~conti/LXe.html>, Accessed: 2021-04-12, 2019.
- [24] W. Tam, A. Jackson, E. Nishida, Y. Kasai, A. Tsujihata, and K. Kajiwara, “Design and manufacture of the ets viii xenon tank,” Jul. 2000. DOI: 10.2514/6.2000-3677.
- [25] E. Bourguignon, S. Fraselle, T. Scalais, and J.-M. Defise, “Power processing unit activities at thales alenia space belgium (etca),” Jul. 2015.
- [26] K. Ebert, “Dynamic yaw steering method for spacecraft,” Apr. 2005, p. 36.
- [27] B. Wie, “Solar sail attitude control and dynamics, part 1,” *Journal of Guidance, Control, and Dynamics*, vol. 27, no. 4, pp. 526–535, 2004. DOI: 10.2514/1.11134. eprint: <https://doi.org/10.2514/1.11134>. [Online]. Available: <https://doi.org/10.2514/1.11134>.
- [28] NewSpace, *Nss fine sun sensor*, <https://www.cubesatshop.com/product/digital-fine-sun-sensor/>, Accessed: 2021-03-27, 2007.
- [29] L. S. Company, *Autonomous star tracker*, <https://www.leonardocompany.com/en/products/aastr?f=/all-products>, Accessed: 2021-03-27, 2018.
- [30] RockwellCollins, *Rockwell collins : Rsi 12 momentum and reaction wheels 4 – 12 nms with integrated wheel drive electronics*, [http://www.electronicnote.com/media/downloads/RSI%2012\\_A4.pdf](http://www.electronicnote.com/media/downloads/RSI%2012_A4.pdf), Accessed: 2021-03-27, 2007.
- [31] RUAGSpace, *Ruag space: Septa 33 solar array drive mechanism (sadm)*, [https://www.ruag.com/system/files/2016-12/2012\\_Septa33.pdf](https://www.ruag.com/system/files/2016-12/2012_Septa33.pdf), Accessed: 2021-03-27, 2021.
- [32] Airbus, *Power*, en, <https://www.airbus.com/space/spacecraft-equipment/power.html>, 2021.



- [33] Saftbatteries, *Rechargeable lithium battery: Ves 180 - very high specific energy space cell*, Doc No 33019-2-060, 2008.
- [34] W. Guter, F. Dunzer, L. Ebel, K. Hillerich, W. Köstler, T. Kubera, M. Meusel, B. Postels, and C. Wächter, “Space solar cells – 3g30 and next generation radiation hard products,” *E3S Web of Conferences*, vol. 16, p. 03 005, Jan. 2017. DOI: 10.1051/e3sconf/20171603005.
- [35] AZURSPACE, *SPACE Solar Cells - AZUR SPACE Solar Power GmbH*, <http://www.azurspace.com/index.php/en/products/products-space/space-solar-cells>, 2021.
- [36] OBD, *European satellite navigation system (space segment)*, [https://www.ohb.de/fileadmin/ohb/Downloads/190603\\_OHB-System\\_Galileo\\_FOC-Satellites\\_2019-05.pdf](https://www.ohb.de/fileadmin/ohb/Downloads/190603_OHB-System_Galileo_FOC-Satellites_2019-05.pdf), Accessed: 2021-04-16, 2019.
- [37] ECSS, *Home*, 2008. [Online]. Available: <https://ecss.nl/standard/ecss-e-st-31c-thermal-control/>.
- [38] R. D. Karam, *Satellite Thermal Control for Systems Engineers*. American Institute of Aeronautics and Astronautics, 1998.
- [39] ESA, *Esa-galileo*, [https://www.esa.int/Applications/Navigation/Galileo/Galileo\\_satellites](https://www.esa.int/Applications/Navigation/Galileo/Galileo_satellites), Accessed: 2021-04-16.
- [40] B. J. Kim and D. G. Lee, “Characteristics of joining inserts for composite sandwich panels,” *Composite Structures*, vol. 86, no. 1, pp. 55–60, 2008, Fourteenth International Conference on Composite Structures, ISSN: 0263-8223. DOI: <https://doi.org/10.1016/j.compstruct.2008.03.020>. [Online]. Available: <https://www.sciencedirect.com/science/article/pii/S0263822308000652>.
- [41] C. I. Grastataro, T. A. Butler, B. G. Smith, and T. C. Thompson, “Development of a composite satellite structure for forte,” Apr. 1995. [Online]. Available: <https://www.osti.gov/biblio/62626>.
- [42] G. Tremblay, E. Boyce, and T. Pham, “Demonstrated technology for affordable, high performance polymer composite spacecraft structures,” *Space Programs and Technologies Conference*, 1996. DOI: 10.2514/6.1996-4312.
- [43] H. J. Kramer, *Sat<sub>i</sub>ii*, <https://directory.eoportal.org/web/eoportal/satellite-missions/s/stsat-3>, Accessed: 2021-04-16, 2002.
- [44] L. Gal, “IDM-CIC and SIMU-CIC applications for setting up a technical reference during design phases of a satellite,” NA. [Online]. Available: [https://logiciels.cnes.fr/sites/default/files/attached\\_doc/IDM-CIC%5C%20and%5C%20SIMU-CIC%5C%20applications\\_SECESA2020.pdf](https://logiciels.cnes.fr/sites/default/files/attached_doc/IDM-CIC%5C%20and%5C%20SIMU-CIC%5C%20applications_SECESA2020.pdf).
- [45] SNECMA, *Pps 1350 datasheet*, <https://satsearch.co/products/snecma-pps-r-1350>, Accessed: 2021-04-12.
- [46] Saftbatteries, *Saft battery solutions for space: Reliability and performance for over 50 years*, Doc No 54085-2-0216, Edition: May 2019, 2019.
- [47] Iberespacio, *Axial grooved heat pipes*, 2010. [Online]. Available: <https://iberespacio.es/wp-content/uploads/2015/07/aghp.pdf>.
- [48] Ruag, *Thermal control*, 2019. [Online]. Available: <https://www.ruag.com/fr/produits-prestations/espace/structures-et-mecanisme-de-satellites/systemes-thermiques>.



- [49] RUAG, *Next generation on board computer*, Accessed: 2021-04-21, 2019. [Online]. Available: %5Curl%7Bhttps://www.ruag.com/system/files/media\_document/2020-12/Datasheet\_Next%5C%20Generation%5C%20n%5C%20Board%5C%20Computer\_Dec%5C%202020.pdf%7D.
- [50] ArianeSpace, *Ariane 6's user manual*, [https://www.arianespace.com/wp-content/uploads/2018/04/Mua-6\\_Issue-1\\_Revision-0\\_March-2018.pdf](https://www.arianespace.com/wp-content/uploads/2018/04/Mua-6_Issue-1_Revision-0_March-2018.pdf), Accessed: 2021-04-16, 2018.